

See discussions, stats, and author profiles for this publication at: <https://www.researchgate.net/publication/268520073>

Novel single-source surface integral equations for scattering on 2-D penetrable cylinders and current flow modeling in...

Thesis · May 2014

CITATIONS

0

READS

73

1 author:



[Anton Menshov](#)

University of Texas at Austin

16 PUBLICATIONS 24 CITATIONS

[SEE PROFILE](#)

Novel Single-Source Surface Integral Equations for
Scattering on 2-D Penetrable Cylinders and
Current Flow Modeling in 2-D and 3-D Conductors

by

Anton Menshov

A Thesis submitted to the Faculty of Graduate Studies of
The University of Manitoba
in partial fulfilment of the requirements of the degree of

MASTER OF SCIENCE

Department of Electrical and Computer Engineering
University of Manitoba
Winnipeg, Manitoba, Canada

Copyright © 2014 by Anton Menshov

Abstract

Accurate modeling of current flow and network parameter extraction in 2-D and 3-D conductors has an important application in signal integrity of high-speed interconnects. In this thesis, we propose a new rigorous single-source Surface-Volume-Surface Electric Field Integral Equation (SVS-EFIE) for magnetostatic analysis of 2-D transmission lines and broadband resistance and inductance extraction in 3-D interconnects. Furthermore, the novel integral equation can be used for the solution of full-wave scattering problems on penetrable 2-D cylinders of arbitrary cross-section under transverse magnetic polarization.

The new integral equation is derived from the classical Volume Electric Field Integral Equation (V-EFIE) by representing the electric field inside a conductor or a scatterer as a superposition of the cylindrical waves emanating from the conductor's surface. This converts the V-EFIE into a surface integral equation involving only a single unknown function on the surface. The novel equation features a product of integral operators mapping the field from the conductor surface to its volume and back to its surface terming the new equation the Surface-Volume-Surface EFIE.

The number of unknowns in the proposed SVS-EFIE is approximately the square root of the number of degrees of freedom in the traditional V-EFIE; therefore, it allows for substantially faster network parameter extraction and solutions to 2-D scattering problems without compromising the accuracy. The validation and benchmark of the numerical implementation of the Method of Moment discretization of the novel SVS-EFIE has been done via comparisons against numerical results obtained by using alternative integral equations, data found in literature, simulation results acquired from the CAD software, and analytic formulas.

Acknowledgments

I would like to express my deepest gratitude and respect to Dr. Vladimir Okhmatovski for his utmost contribution to my Master's degree and this thesis in particular, as well as for his exceptional professionalism and remarkable teaching skills. I highly appreciate his continuous support throughout the entire program and feel honoured for having the opportunity to work under his guidance.

I am very grateful to my committee members – Dr. Ian Jeffrey, Dr. David Swatek, and Mr. Pei Wang, whose genuine interest and invaluable participation made this work come to life.

I would like to thank all my friends for being around during these years, for sharing my university life, and enriching my cultural experience. Specifically, I wish to acknowledge the two people – Alexander Krylov and Oleksandr Maizlish, whose role in my current degree is tremendous, as they were who initially helped me to meet my advisor and come to Canada. Furthermore, I am grateful to my university colleagues – Mohammad Shafieipour, Jon Aronsson, Nozhan Bayat, and Bozhou Du, for their considerable input in my academic growth and proficiency.

Many words of thanks I say to my family – my dearest parents and beloved fiancé. It was their strong encouragement and sincere belief in me, which have always been my great motivation to move forward and never give up.

I wish to express my gratitude to my employers – University of Manitoba and Manitoba Hydro. They have provided me with unique opportunities and invaluable experience of working and developing my ideas in the field of electromagnetics. In particular, I value much the fact that part of my project related to the current flow modeling in 2-D conductors was funded by Manitoba Hydro and MITACS Accelerate.

“Through our scientific genius, we have made this world a neighborhood; now, through our moral and spiritual development, we must make it a brotherhood.”

— Martin Luther King, Jr., Peace Nobelist (1964)

Dedicated to Hope

Publications

The author contributed to the following publications while working towards the M.Sc. degree

Papers in International Journals

- A. Menshov and V. Okhmatovski, “RL Extraction in Complex Interconnects Taking Advantage of the Matrix Sparsity in Moment Method Solution of Surface-Volume-Surface EFIE,” *IEEE Transactions on Magnetics* (to be submitted).
- A. Menshov and V. Okhmatovski, “Surface-Volume-Surface Electric Field Integral Equation of Magneto-Quasi-Static Electromagnetic Analysis of Complex 3-D Interconnects,” *IEEE Transactions on Microwave Theory Techniques* (submitted).
- A. Menshov and V. Okhmatovski, “New Single-Source Surface Integral Equations for Scattering on Penetrable Cylinders and Current Flow Modeling in 2-D Conductors,” *IEEE Transactions on Microwave Theory Techniques*, Vol. 61, No. 1, pp. 341-350, Jan. 2013.

Papers in Conference Proceedings

- A. Menshov and V. Okhmatovski, “Novel Single-Source Surface Integral Equation for Broadband RL Extraction in 3-D Interconnects,” *IEEE 17th Workshop on Signal and Power Integrity (SPI)*, pp. 1–2, May 2013.
- A. Menshov and V. Okhmatovski, “Novel surface integral equation formulation for accurate broadband RL extraction in transmission lines of arbitrary cross-section,” *IEEE MTT-S International Microwave Symposium Digest (MTT)*, pp. 1-3, 17–22 June 2012.
- A. Menshov and V. Okhmatovski, “Method of moment solution of Surface-Volume-Surface Electric Field Integral Equation for two-dimensional transmission lines of complex cross-sections,” *IEEE 16th Workshop on Signal and Power Integrity (SPI)*, pp. 31–34, 13–16 May 2012.

Conference Abstracts

- A. Menshov and V. Okhmatovski, “Fast Extraction of Resistance and Inductance in Complex 3D Interconnects using Surface-Volume-Surface Electric Field Integral Equation,” *IEEE Symposium on Antennas and Propagation and URSI Radio Science Meeting*, July 2014 (in print).
- A. Menshov and V. Okhmatovski, “Well-Posed Microwave Imaging in Focusing Media: 2D Generalization and Impact on Convergence of the Contrast Source Inversion Method,” *IEEE Symposium on Antennas and Propagation and URSI Radio Science Meeting*, July 2014 (in print).
- A. Menshov and V. Okhmatovski, “Novel single-source integral equation for accurate quasi-magneto-static modeling of current flow in 3D conductors,” *IEEE Symposium on Antennas and Propagation and URSI Radio Science Meeting*, p. 110, 7–13 July 2013.

Contents

List of Figures	xi
List of Tables	xv
1 Introduction	1
1.1 Motivation and Current State of the Art	1
1.2 Thesis Research Scope and Contributions	4
2 Volume Electric Field Integral Equations	6
2.1 Maxwell's Equations	6
2.2 Magneto-Quasi-Static Approximation	7
2.3 Volume Electric Field Integral Equations	8
2.3.1 Volume Electric Field Integral Equation for Magneto-Quasi- Statics	8
2.3.2 Volume Electric Field Integral Equation for Scattering under Transverse Magnetic Polarization	10
3 Novel Surface Integral Equation Formulation for Accurate Broad- band RL Extraction in Transmission Lines of Arbitrary Cross-Sec- tion	14
3.1 Introduction	16
3.2 Novel Surface Integral Equation Formulation	17
3.3 Method of Moments Discretization	18
3.4 Numerical Results	20
3.5 Conclusion	25
4 Method of Moment Solution of Surface-Volume-Surface Electric Field Integral Equation for Two-Dimensional Transmission Lines of Com- plex Cross-Sections	27
4.1 Introduction	28
4.2 Surface-Volume-Surface EFIE and MoM Discretization	30
4.2.1 Integral Equation	30

4.2.2	Surface and volume meshes	31
4.2.3	MoM discretization of SVS-EFIE's surface-to-volume operator	32
4.2.4	MoM discretization of SVS-EFIE's volume-to-surface operator	34
4.2.5	MoM discretization of SVS-EFIE's surface-to-surface operator	35
4.2.6	Matrix form of MoM discretized SVS-EFIE	36
4.3	Numerical Results	38
4.4	Conclusions	41
5	New Single-Source Surface Integral Equations for Scattering on Penetrable Cylinders and Current Flow Modelling in 2-D Conductors	43
5.1	Introduction	45
5.2	Novel Single-Source Surface-Volume-Surface Integral Equation Formulation	48
5.2.1	Magnetostatics Formulation	48
5.2.2	Full-Wave Formulation	51
5.3	Method of Moments Discretization	54
5.3.1	MoM discretization of SVS-EFIE's surface-to-volume operator	56
5.3.2	MoM discretization of SVS-EFIE's volume-to-surface operator	58
5.3.3	MoM discretization of SVS-EFIE's surface-to-surface operator	60
5.3.4	Matrix form of MoM discretized SVS-EFIE:	61
5.4	Numerical Studies	65
5.5	Conclusion	75
6	Surface-Volume-Surface Electric Field Integral Equation for Magneto-Quasi-Static Electromagnetic Analysis of Complex 3-D Interconnects	81
6.1	Introduction	83
6.2	Single-Source SVS-EFIE for Current Flow Modeling in 3-D	86
6.3	Method of Moments Discretization	90
6.3.1	Method of Moments discretization of the contour-to-volume operator	93
6.3.2	Method of Moments discretization of the volume-to-contour operator	94
6.3.3	Method of Moments discretization of the contour-to-contour operator	96
6.3.4	Matrix form of the MoM discretized SVS-EFIE	97
6.3.5	Nodal Analysis	98
6.4	Numerical Results	101
6.5	Conclusion	107
7	Application of the Novel Surface-Volume-Surface EFIE to Power Cables Parameter Extraction	112

8 Conclusions and Future Work	122
8.1 Conclusions	122
8.2 Future Work	124
Bibliography	125

List of Figures

1.1	Three conductor co-axial power cables cross-sections with round and sectorial inner conductors.	2
3.1	Normalized distribution of the volumetric current density j_z across aluminum circular conductor of radius $\rho_0 = 0.025\text{ m}$	22
3.2	Surface (dot markers) and volume meshes utilized in MoM discretization (3.8) – (3.13). Cross-sectional distribution of the volumetric current density obtained via MoM solution (3.10) for the SVS-EFIE (3.3) at 60 Hz. The relative error with respect to the volumetric MoM solution of the V-EFIE (3.1) does not exceed 2.7%.	23
3.3	Resistance and inductance of circular conductor extracted with MoM solution (3.10) of the proposed SVS-EFIE (3.3) and volumetric MoM solution of the V-EFIE (3.1) for 6-sided and 20-sided polygonal approximation of the circular cross-section.	24
3.4	Cross-sectional distribution of the volumetric current density in two conductors obtained via MoM solution (3.10) for the SVS-EFIE (3.3) at 60 Hz. The relative error with respect to the volumetric MoM solution of the V-EFIE (3.1) does not exceed 1.8%.	24
4.1	Volume and surface meshes utilized in MoM discretization of the SVS-EFIE (4.2).	31
4.2	Matrix form (4.13) of the SVS-EFIE (4.2) discretized with the Method of Moments utilizing volume and surface meshes depicted in Fig. 4.1.	37
4.3	Surface (blue dot markers) and volume meshes utilized in MoM discretization (4.5) – (4.13). Volumetric current density obtained via MoM solution (4.13) for SVS-EFIE (4.2) at 400 kHz. The relative error of the V-EFIE (4.1) and the SVS-EFIE MoM solutions does not exceed 1.5%.	39
4.4	Resistance and inductance of circular co-axial conductor extracted with MoM solution (4.13) of the proposed SVS-EFIE (4.2) and volumetric MoM solution of the V-EFIE (4.1) for 6-sided and 20-sided polygonal approximation.	40

5.1	Volume and surface meshes utilized in the MoM discretization of the SVS-EFIE (5.13).	55
5.2	Matrix form (5.33) of the SVS-EFIE (5.13) discretized with the MoM utilizing depicted volume and surface meshes.	62
5.3	Distribution of the electric field inside $E_z^{(1)}$ and outside $E_z^{(2)}$ the dielectric cylinder obtained via MoM solution (5.33). The relative error of the latter (center plot) and the MoM solution of the PMCHWT surface IE solution (right plot) with respect to the volumetric MoM solution of the V-EFIE (5.11). Points A–F correspond to the points in the Fig. 5.4.	66
5.4	Equivalent electric and magnetic surface current densities (J_z^e , J_t^m on the left) obtained with the MoM solution of PMCHWT surface IE and the auxiliary surface current density (J_z on the right) obtained with the MoM solution of the proposed SVS-EFIE (5.13) for TM_z wave scattering from a single dielectric cylinder. Points A–F correspond to the points in the Fig. 5.3.	67
5.5	Condition number of the matrix (5.33), mean and standard deviation of the relative error of the cross-sectional distribution of the E-field inside the dielectric cylinder obtained via MoM solution (5.33) with respect to the volumetric MoM solution of the V-EFIE (5.11) as a function of surface and volume mesh refinement. Optimal volume/surface elements ratio $M = \sqrt{N/16}$	70
5.6	The condition number of the matrix (5.33) and impedance matrix for PMCHWT [10] surface IE, required number of CG-iterations, mean value and standard deviation of the relative error of the MoM solutions (5.33) and PMCHWT surface IE for 6-sided polygonal approximation of the circular cross-section with radius $\rho_0 = 25$ mm due to plane-wave incidence at 2 GHz.	73
5.7	Electric field distribution in circular dielectric cylindrical shell with plane-wave incident. The MoM solution (5.33) and numerical results from [23].	74
6.1	(a) Interconnect formed by two piecewise-straight conductor segments. (b) Segment 1 directed along the vector $\hat{\ell}_1$ with depicted volume and contour meshes utilized in the MoM discretization of the SVS-EFIE (6.8).	91

6.2 Distribution of the volumetric current density \mathbf{j} inside the conductors constituting the depicted twelve-conductor package. Conductor A is driven by 1A current source at 1 GHz frequency, other conductors are left floating. The package has two planes of symmetry shown with dashed lines. Geometric locations of the terminal points at the axes of the conductor segments are given for four conductors A – D in μm .(a) Volumetric current density j inside the cross-section of the “aggressor-conductor” A obtained via the MoM solution (6.38) of the proposed SVS-EFIE (6.8) and traditional V-EFIE (6.1), and their relative error. (b) Volumetric current density j inside the cross-section of the “victim-conductor” B obtained via the MoM solution (6.38) of the proposed SVS-EFIE (6.8) and traditional V-EFIE (6.1), and their relative error.	103
6.3 Resistance R_A , self-inductance L_{AA} , and mutual inductance L_{AB} of conductors A and B in the twelve-conductor package depicted in Fig. 6.2. The results are first obtained under the two samples per skin-depth MoM discretization of the SVS-EFIE (6.8) and compared against the FastHenry reference solution [28]. The relative error does not exceed 4% for resistance and 0.2% for inductance at frequencies from 10 MHz to 10 GHz.	104
6.4 Relative error of the MoM solution (6.38) of the novel SVS-EFIE (6.8) with respect to the FastHenry reference solution [28] for resistance R_A and self-inductance L_{AA} in the twelve-conductor package depicted in Fig. 6.2 as a function of mesh refinement – number of samples per skin-depth (6.5) at 1 GHz.	105
7.1 Circular co-axial cable with lead sheath (1) and copper inner conductor (2).	114
7.2 Extracted resistance (7.1) of the circular co-axial cable depicted in Fig. 7.1 for the frequency sweep from 10 mHz to 10 kHz.	115
7.3 Extracted inductance (7.2) of the circular co-axial cable depicted in Fig. 7.1 for the frequency sweep from 10 mHz to 10 kHz.	116
7.4 Square co-axial cable with lead sheath (1) and copper inner conductor (2).	117
7.5 Extracted resistance (7.1) of the square co-axial cable depicted in Fig. 7.4 for the frequency sweep from 10 mHz to 10 kHz.	118
7.6 Extracted inductance (7.2) of the square co-axial cable depicted in Fig. 7.4 for the frequency sweep from 10 mHz to 10 kHz.	118
7.7 Three-conductor round co-axial cable with lead sheath and copper inner conductors (Pirelli 35 KV 3 conductor round paper insulated cable 4/0 American Wire Gauge (AWG)).	120

7.8 Three-conductor sectorial co-axial cable with lead sheath and copper inner conductors (Pirelli 35 KV 3 conductor sectorial paper insulated cable 500 MCM)	121
---	-----

List of Tables

5.1	Computational Complexity Comparison for Direct and Iterative Solution of the V-EFIE (5.11), SVS-EFIE (5.13), and PMCHWT [10] Equations.	64
5.2	Computational Time and Memory for the Solution of the V-EFIE, SVS-EFIE, and PMCHWT Equations in Mathcad.	69
6.1	Computational Time and Memory for the Solution of the V-EFIE and SVS-EFIE for the twelve-conductor package.	106
7.1	Extracted resistance (7.1) and inductance (7.2) of the circular co-axial cable depicted in Fig. 7.1 at 60 Hz.	115
7.2	Extracted resistance and inductance of the three-conductor round co-axial cable depicted in Fig. 7.7 at 60 Hz.	120
7.3	Extracted resistance and inductance of the three-conductor sectorial co-axial cable depicted in Fig. 7.8 at 60 Hz.	121

Chapter 1

Introduction

1.1 Motivation and Current State of the Art

The importance of computer-aided design (CAD) tools has grown significantly over the past decades. In a vast number of fields, the use of accurate numerical simulations can reduce fabrication expenses and drastically enhance design efficiency.

Accurate modeling of current flow and network parameter extraction in 2-D and 3-D conductors has an important application in signal integrity analysis of high-speed interconnects [You01, Mor04, KTW94] and simulation of the power delivery systems [WW73, BKB09]. Electromagnetic-based modeling of current flow that takes into account the proximity and skin-effect [You01] is foundational for obtaining per-unit-length and terminal characteristics of transmission lines [Poz97], which can be used to generate lump circuit models [AN01]. Similarly, in the areas of microwave imaging [ML10], remote sensing [CJMS01], and design of radar absorber materials [Cad09, Ser03], the solution of full-wave scattering problems is commonly required. Virtual prototyping of such systems allows to reduce the number of fabrication cycles, thus lowering financial, human, and timing costs.

Such problems can be formulated as various differential [Jin02] and integral equations [PRM98], solutions of which are equivalent to the solution of the Maxwell equations [Str41]. The integral equation methods often lead to discretized problems of a substantially smaller size [CJMS01], as the discretization of the entire space is not required. In the case of electromagnetic characterization by integral equations, only conductors and scatterers are discretized, whereas differential equation formulations also require the discretization of the space surrounding conductors or scatterers. The volume electric field integral equation (V-EFIE) [Che95] has been traditionally used for a solution of the aforementioned problems. The V-EFIE under the magneto-quasi-static approximation [Not10] is foundational to the electromagnetic characterization of transmission lines in both 2-D and 3-D.

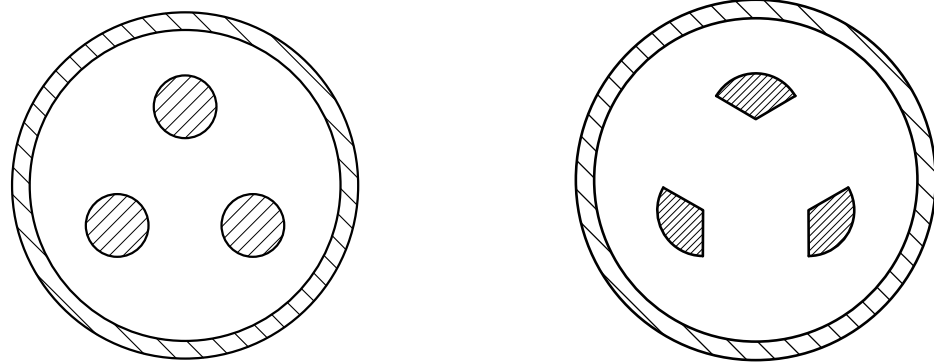


Figure 1.1: Three conductor co-axial power cables cross-sections with round and sectorial inner conductors.

The Fig. 1.1 shows relatively complicated 2-D cross-sections of power-cables. Clearly, the analytic solutions for the current distribution and, therefore, resistance and inductance extraction are not available for such types of cables, so the characterization has to be performed using differential or integral equation techniques. Current versions of PSCAD/EMTDC [Man10] software commonly used for the transient anal-

ysis of power delivery systems cannot handle such cable geometries.

The more complicated version of the full-wave V-EFIE [Che95] is used for a solution of scattering problems on penetrable scatterers with inhomogeneities. The V-EFIE has the benefit of accurately capturing the field behavior in the entire frequency band from DC to multi-GHz without experiencing low-frequency breakdown or internal spurious resonances, although its numerical solution is computationally expensive.

The high computational complexity of the V-EFIE is due to the fact that the volume of the conductors or scatterers is discretized and the resulting matrix equations are dense, as opposed to the surface discretization in the case of Surface Integral Equations (SIE) [PRM98] and solution of sparse matrix equations in the Finite Element Method [Jin02]. For homogeneous objects, however, the computational complexity of electromagnetic modeling can be reduced by using surface integral equation formulations. In such equations, the unknown field quantities reside on the surfaces bounding the homogeneous subregions. Traditional surface integral equation formulations replace the volume distribution of the unknown field within a homogeneous region with coupled electric and magnetic surface current densities [PRM98, KS86]. An alternative is to utilize only a single unknown surface current density that can be done in many different ways [QCS07, Swa99, SC00, VABM08, Gli84, Yeu99, CK92, Mul69, MH78, KM88]. While the traditional SIEs have two unknown functions instead of one, the single-source SIEs have a large number of independent kernels as well as their products rendering their numerical solution difficult.

To overcome these difficulties, we introduce a new integral equation formulation, which has only a single unknown function on the surface and involves only few simple integral operators.

1.2 Thesis Research Scope and Contributions

This thesis presents the novel single-source surface-volume-surface electric field integral equation (SVS-EFIE) for current flow modeling in 2-D and 3-D conductors. It also provides a similar integral equation for solution of full-wave scattering problems for 2-D penetrable cylinders under transverse magnetic polarization. The proposed formulation can handle conductors and scatterers of an arbitrary cross-section using only a single derivative free kernel. The reduction of the volume integral equation to a surface IE is based on the representation of the electric field inside the homogeneous region as a superposition of cylindrical waves emanating from its boundary.

The novel SVS-EFIE is derived for current flow modeling in 2-D transmission lines of an arbitrary cross-section under magneto-quasi-static approximation in Chapter 3 (which is a verbatim copy of [IMS12]). A detailed description of the Method of Moments discretization of the proposed SVS-EFIE for 2-D magneto-quasi-static problems and resultant matrix structure for the example of a co-axial transmission line are presented in Chapter 4 (verbatim copy of [SPI12]).

The proposed formulation is generalized for the solution of full-wave transverse magnetic 2-D scattering problems in Chapter 5 (verbatim copy of [MO13]). This chapter also discusses the difference of the SVS-EFIE and traditional surface EFIEs using electric and magnetic current densities, the Method of Moments discretization of the full-wave SVS-EFIE, and the numerical studies of the optimal ratio between numbers of surface and volume elements.

The SVS-EFIE for current flow modeling and network parameter extraction in 3-D is derived in Chapter 6 (verbatim copy of the journal paper “Surface-Volume-Surface Electric Field Integral Equation for Magneto-Quasi-Static Electromagnetic Analysis of Complex 3-D Interconnects” submitted to IEEE Transactions on Microwave Theory

and Techniques).

Numerical examples demonstrating the benefits of the proposed formulation for network characterisation of complex interconnects and power cables in 2-D and 3-D as well as the solution of a full-wave scattering problem in 2-D under transverse magnetic polarization are presented. In particular, Chapter 7 is dedicated to the benchmark of the numerical implementation of the Method of Moments solution of the proposed SVS-EFIE for parameter extraction of 2-D power cables.

Chapter 2

Volume Electric Field Integral Equations

2.1 Maxwell's Equations

Maxwell's equations for a time-harmonic electromagnetic field in the frequency domain ($e^{i\omega t}$ time-factor) are given by

$$\nabla \times \mathbf{E} = -i\omega\mu\mathbf{H}, \quad (2.1)$$

$$\nabla \times \mathbf{H} = \mathbf{j} + i\omega\epsilon\mathbf{E}, \quad (2.2)$$

$$\nabla \cdot \mathbf{E} = \frac{\rho}{\epsilon_0}, \quad (2.3)$$

$$\nabla \cdot \mathbf{H} = 0, \quad (2.4)$$

where \mathbf{E} is the electric field, \mathbf{H} is the magnetic field, \mathbf{j} is the volume current density, ρ is the total volume charge density, ω is the cyclic frequency, ϵ is the dielectric permittivity, ϵ_0 is the permittivity of free space, and $i = \sqrt{-1}$.

Due to its solenoidal nature, the magnetic field \mathbf{H} can be expressed via magnetic vector potential \mathbf{A}

$$\mu\mathbf{H} = \nabla \times \mathbf{A}. \quad (2.5)$$

Then the Faraday's law (2.1) becomes

$$\nabla \times (\mathbf{E} + i\omega\mathbf{A}) = 0. \quad (2.6)$$

The use of the vector identity [MF53]

$$\nabla \times \nabla\Phi \equiv 0 \quad (2.7)$$

allows for the curl-free vector field $\mathbf{E} + i\omega\mathbf{A}$ in (2.6) being expressed as the gradient of the electric scalar potential Φ . Thus, (2.6) acquires the following form:

$$\mathbf{E} + i\omega\mathbf{A} = -\nabla\Phi. \quad (2.8)$$

2.2 Magneto-Quasi-Static Approximation

Magneto-quasi-static approximation for Maxwell's equations (2.1)–(2.4) is often used for current flow modeling in good conductors that have sufficiently high conductivity σ , so that the displacement current $\omega\epsilon\mathbf{E}$ is negligible [KTW94] at every frequency of the analysis. Mathematically, magneto-quasi-static approximation can be expressed by

$$\sigma >> \omega\epsilon. \quad (2.9)$$

For such conductors, we write the Ampère's circuital law (2.2) in terms of the magnetic vector potential \mathbf{A} , as follows

$$\nabla \times \nabla \times \mathbf{A} = \mu \mathbf{j}, \quad (2.10)$$

where the volumetric current density \mathbf{j} is governed by Ohm's law

$$\mathbf{j} = \sigma \mathbf{E}. \quad (2.11)$$

Using the following vector identity [MF53]

$$\nabla \times \nabla \times \mathbf{F} \equiv \nabla(\nabla \cdot \mathbf{F}) - \nabla^2 \mathbf{F} \quad (2.12)$$

and the definition of the divergence of the magnetic vector potential according to Coulomb gauge

$$\nabla \cdot \mathbf{A} = 0, \quad (2.13)$$

the equation (2.10) is transformed into the vector form of Poisson's equation

$$\nabla^2 \mathbf{A} = -\mu \mathbf{j}. \quad (2.14)$$

2.3 Volume Electric Field Integral Equations

2.3.1 Volume Electric Field Integral Equation for Magneto-Quasi_Statics

The vector form of the Poisson's equation for the magnetic vector potential \mathbf{A} (2.14) under magneto-quasi-static approximation can be represented as a set of three

scalar equations

$$\begin{cases} \nabla^2 A_x = -\mu j_x \\ \nabla^2 A_y = -\mu j_y \\ \nabla^2 A_z = -\mu j_z \end{cases}. \quad (2.15)$$

The solution of (2.15) with a delta-function in the right-hand side is called a Green's function $G(\mathbf{r}, \mathbf{r}')$

$$\nabla^2 G(\mathbf{r}, \mathbf{r}') = -\delta(\mathbf{r} - \mathbf{r}'). \quad (2.16)$$

Thus, using the principle of superposition, we relate the magnetic vector potential \mathbf{A} to the resistive current \mathbf{j} , as follows [KTW94]

$$\mathbf{A}(\mathbf{r}) = \mu \iiint_V dv' \mathbf{j}(\mathbf{r}') G_0^{qs}(\mathbf{r}, \mathbf{r}'), \quad (2.17)$$

where V is the volume of the conductors, $G_0^{qs}(\mathbf{r}, \mathbf{r}')$ is the Green's function of free-space under magneto-quasi-static assumption, μ is the permeability, \mathbf{r} and \mathbf{r}' are the position vector of the observation and source points, respectively.

Consequently, the Volume Electric Field Integral Equations (V-EFIE) [Che95] with respect to the unknown current density \mathbf{j} can be formulated using (2.8), (2.11), and (2.17)

$$\frac{\mathbf{j}(\mathbf{r})}{\sigma} + i\omega\mu \iiint_V dv' \mathbf{j}(\mathbf{r}') G_0^{qs}(\mathbf{r}, \mathbf{r}') = -\nabla\Phi(r). \quad (2.18)$$

The Green's function of free-space is given by [Col92]

$$G_0^{qs}(\mathbf{r}, \mathbf{r}') = \frac{1}{4\pi} \frac{1}{|\mathbf{r} - \mathbf{r}'|}. \quad (2.19)$$

For the case of a 2-D conductor of an arbitrary cross-section S and invariant bulk conductivity σ along the coordinate z , the V-EFIE (2.18) has the following form

$$\frac{j_z(\boldsymbol{\rho})}{\sigma} + i\omega\mu \iint_S ds' j_z(\boldsymbol{\rho}') G_0^{qs,2D}(\boldsymbol{\rho}, \boldsymbol{\rho}') = -\frac{d\Phi}{dz}, \quad (2.20)$$

where $\boldsymbol{\rho}$ and $\boldsymbol{\rho}'$ are the position vector of the observation and source points in cylindrical coordinates, respectively. The Green's function of free-space in 2-D is expressed as [Col92]

$$G_0^{qs,2D}(\boldsymbol{\rho}, \boldsymbol{\rho}') = -\frac{1}{2\pi} \ln(|\boldsymbol{\rho} - \boldsymbol{\rho}'|). \quad (2.21)$$

2.3.2 Volume Electric Field Integral Equation for Scattering under Transverse Magnetic Polarization

We will assume that the medium contains no free charges ($\rho = 0$) and currents ($\mathbf{j} = 0$). Therefore, Maxwell's equations (2.1)–(2.4) can be rewritten, as follows

$$\nabla \times \mathbf{E} = -i\omega\mu\mathbf{H}, \quad (2.22)$$

$$\nabla \times \mathbf{H} = i\omega\epsilon\mathbf{E}, \quad (2.23)$$

$$\nabla \cdot \mathbf{E} = 0, \quad (2.24)$$

$$\nabla \cdot \mathbf{H} = 0. \quad (2.25)$$

Consider a 2-D transverse magnetic scattering problem [Ric65] for a dielectric cylinder directed along z -coordinate and having an arbitrary cross-section S . The cylinder has the dielectric permittivity $\epsilon(x, y)$ and is located in free-space. The total

electric field \mathbf{E} in the computational domain can be decomposed into the incident electric field \mathbf{E}^i and the scattered field \mathbf{E}^s

$$\mathbf{E} = \mathbf{E}^i + \mathbf{E}^s. \quad (2.26)$$

For transverse-magnetic polarization, the incident electric field is directed along z -axis and is independent of z -coordinate

$$\mathbf{E}^i(x, y) = \hat{\mathbf{z}} E_z^i(x, y). \quad (2.27)$$

As the result, Faraday's law (2.22) and Ampère's law (2.23) obtain the following forms, respectively:

$$\nabla \times \mathbf{E} = -i\omega\mu\mathbf{H} = \begin{vmatrix} \hat{\mathbf{x}} & \hat{\mathbf{y}} & \hat{\mathbf{z}} \\ \frac{\partial}{\partial x} & \frac{\partial}{\partial y} & 0 \\ 0 & 0 & E_z \end{vmatrix} = \hat{\mathbf{x}} \frac{\partial}{\partial y} E_z(x, y) - \hat{\mathbf{y}} \frac{\partial}{\partial x} E_z(x, y), \quad (2.28)$$

$$\nabla \times \mathbf{H} = i\omega\epsilon\mathbf{E} = \begin{vmatrix} \hat{\mathbf{x}} & \hat{\mathbf{y}} & \hat{\mathbf{z}} \\ \frac{\partial}{\partial x} & \frac{\partial}{\partial y} & 0 \\ H_x & H_y & 0 \end{vmatrix} = \hat{\mathbf{z}} \left(\frac{\partial}{\partial x} H_y(x, y) - \frac{\partial}{\partial y} H_x(x, y) \right). \quad (2.29)$$

From (2.28) and (2.29), we further derive the partial differential equation with respect to the electric field intensity

$$\nabla^2 E_z(x, y) + \omega^2 \epsilon(x, y) \mu E_z(x, y) = 0. \quad (2.30)$$

Denoting the wavenumber of free space as $k_0 = \omega\sqrt{\mu_0\epsilon_0}$, and rearranging the terms in (2.30), we obtain

$$\nabla^2 E_z(x, y) + k_0^2 E_z(x, y) = i\omega\mu J_z^p(x, y), \quad (2.31)$$

where $J_z^p(x, y)$ is the polarization current density defined as

$$J_z^p(x, y) = i\omega(\epsilon(x, y) - \epsilon_0)E_z(x, y). \quad (2.32)$$

Since the incident field E_z^i satisfies

$$\nabla^2 E_z^i(x, y) + k_0^2 E_z^i(x, y) = 0, \quad (2.33)$$

the following equation for the scattered field E_z^s can be derived by subtracting (2.33) from (2.31)

$$\nabla^2 E_z^s(x, y) + k_0^2 E_z^s(x, y) = i\omega\mu J_z^p(x, y), \quad (2.34)$$

So, the scattered field can be represented as a contribution of equivalent polarization current density radiating in free space [Ric65]

$$E_z^s(x, y) = k_0^2 \iint_S dx' dy' (\epsilon(x, y) - \epsilon_0) G_0(x, y|x', y') E_z(x', y'), \quad (2.35)$$

where $G_0(x, y|x', y')$ is the Green's function of free space given by [Ric65, Col92]

$$G_0(x, y|x', y') = -\frac{i}{4} H_0^{(2)} \left(k_0 \sqrt{(x - x')^2 + (y - y')^2} \right). \quad (2.36)$$

In (2.36), $H_0^{(2)}$ is the second-kind Hankel function of zeroth order [AS64].

Combining (2.35) and (2.26), we obtain the V-EFIE for scattering under transverse magnetic polarization

$$E_z^s(x, y) - k_0^2 \iint_S dx' dy' (\epsilon(x, y) - \epsilon_0) G_0(x, y | x', y') E_z(x', y') = E_z^i(x, y). \quad (2.37)$$

Chapter 3

Novel Surface Integral Equation Formulation for Accurate Broadband RL Extraction in Transmission Lines of Arbitrary Cross-Section

©2012 IEEE. Reprinted, with permission, from *Anton Menshov and Vladimir Okhmatovski, Novel Surface Integral Equation Formulation for Accurate Broadband RL Extraction in Transmission Lines of Arbitrary Cross-Section, IEEE International Microwave Symposium Digest (MTT), June 2012.*

The volume integral equation used in the method of moments based resistance and inductance extractors is reduced to a novel surface integral equation featuring a global surface impedance boundary condition as well as a product of volume and surface integral operators. The reduction is achieved by employing the equivalence principle representation of the electric field in the conductor cross-section via equivalent surface current density on the conductors' boundary. As no approximation is utilized in the reduction of the volume integral equation to the surface one, the method of moment solution of the latter does not compromise the accuracy of volumetric current approximation.

3.1 Introduction

Field accurate broadband prediction of the volumetric current density in multiconductor transmission lines is important for network characterization of both high-speed interconnects and power transmission lines. Such characterization is of the particular challenge for computationally efficient boundary element discretization of the electric field integral equation (EFIE). Two approaches have been commonly used for modeling interconnects with the surface EFIE. The first approach is based on approximate local impedance boundary conditions (LIBC) [1]– [2]. The second approach employs the generalized impedance boundary condition (GIBC) [3]. The advantages of the LIBC’s are sparsity of the discretized surface impedance operator and lack of derivatives in the resultant EFIE. The latter property becomes especially significant in the construction of extractors utilizing the Green’s function of the multilayered media. The GIBC approach is exact. This advantage, however, comes at the expense of both E- and H-field kernels being present in the integral equation.

We propose a new surface EFIE (S-EFIE), which is an alternative to S-EFIE in [3]. We start from the volume EFIE (V-EFIE) with respect to the volumetric current density. We then express the E-field inside the conductor in terms of the equivalent electric current density on its surface. Substitution of the latter into the V-EFIE followed by the restriction of the observation point to the conductor surface leads to a S-EFIE with respect to the surface current density. Thus, derived S-EFIE features a product of volumetric and surface EFIE operators and a global impedance boundary operator. It is shown that the proposed S-EFIE is as accurate as the V-EFIE at all frequencies but computationally is much less expensive.

3.2 Novel Surface Integral Equation Formulation

Consider a 2D wire directed along z -coordinate and having arbitrary cross-section with area S . Under quasi-static approximation and assumption that current density has only z -component we can write the V-EFIE

$$\frac{j_z(\boldsymbol{\rho})}{\sigma} + i\omega\mu_0 \iint_S G_0(\boldsymbol{\rho}, \boldsymbol{\rho}') j_z(\boldsymbol{\rho}') ds' = -V_{p.u.l.}, \quad \boldsymbol{\rho} \in S, \quad (3.1)$$

where j_z is the unknown volumetric current density, $G_0(\boldsymbol{\rho}, \boldsymbol{\rho}') = -\frac{1}{2\pi} \ln(|\boldsymbol{\rho} - \boldsymbol{\rho}'|)$ is the Green's function of free space under quasi-static assumption, $\boldsymbol{\rho}$ and $\boldsymbol{\rho}'$ are the observation and source points, respectively, μ_0 is the permeability of free space, σ is the conductivity of the wire, ω is the cyclic frequency, $i = \sqrt{-1}$, and $V_{p.u.l.}$ is the per-unit-length (p.u.l.) voltage drop along the wire. Consider next the Ohm's law $E_z(\boldsymbol{\rho}) = \frac{j_z(\boldsymbol{\rho})}{\sigma}$ and the equivalence principle relationship between the E-field in the conductor cross-section and the equivalent surface current density $J_z(\boldsymbol{\rho}')$

$$E_z(\boldsymbol{\rho}) = \frac{j_z(\boldsymbol{\rho})}{\sigma} = -i\omega\mu_0 \int_{\partial S} G_\sigma(\boldsymbol{\rho}, \boldsymbol{\rho}') J_z(\boldsymbol{\rho}') d\boldsymbol{\rho}', \quad \boldsymbol{\rho} \in S, \quad (3.2)$$

where $G_\sigma(\boldsymbol{\rho}, \boldsymbol{\rho}') = -\frac{i}{4} H_0^{(2)}(k_\sigma |\boldsymbol{\rho} - \boldsymbol{\rho}'|)$ is the Green's function of the conductor media with wavenumber $k_\sigma = \sqrt{\frac{\omega\mu_0\sigma}{2}}(1 - i)$. Substitution of the (3.2) into (3.1) followed by the restriction of the observation domain to the conductor surface yields the desired S-EFIE with respect to the unknown surface current density

$$\begin{aligned} & -i\omega\mu_0 \int_{\partial S} G_\sigma(\boldsymbol{\rho}, \boldsymbol{\rho}') J_z(\boldsymbol{\rho}') d\boldsymbol{\rho}' - \sigma(\omega\mu_0)^2 \times \\ & \int_{\partial S} \left[\iint_S G_0(\boldsymbol{\rho}, \boldsymbol{\rho}') G_\sigma(\boldsymbol{\rho}, \boldsymbol{\rho}'') ds' \right] J_z(\boldsymbol{\rho}'') d\boldsymbol{\rho}'' = -V_{p.u.l.}, \quad \boldsymbol{\rho} \in \partial S. \end{aligned} \quad (3.3)$$

Denoting the integral operator products entering in (3.3) as

$$T_{\sigma}^{\partial S, \partial S} \circ J_z = -i\omega\mu_0 \int_{\partial S} G_{\sigma}(\boldsymbol{\rho}, \boldsymbol{\rho}') J_z(\boldsymbol{\rho}') d\boldsymbol{\rho}', \quad \boldsymbol{\rho} \in \partial S, \quad (3.4)$$

$$T_{\sigma}^{S, \partial S} \circ J_z = -i\omega\mu_0 \int_{\partial S} G_{\sigma}(\boldsymbol{\rho}, \boldsymbol{\rho}') J_z(\boldsymbol{\rho}') d\boldsymbol{\rho}', \quad \boldsymbol{\rho} \in S, \quad (3.5)$$

$$T_0^{\partial S, S} \circ j_z = -i\omega\mu_0 \iint_S G_0(\boldsymbol{\rho}, \boldsymbol{\rho}') j_z(\boldsymbol{\rho}') ds', \quad \boldsymbol{\rho} \in \partial S, \quad (3.6)$$

we term the new IE (3.3) as Surface-Volume-Surface-EFIE (SVS-EFIE) and write it in the operator form as

$$T_{\sigma}^{\partial S, \partial S} \circ J_z + \sigma T_0^{\partial S, S} \circ T_{\sigma}^{S, \partial S} \circ J_z = -V_{p.u.l.} \quad (3.7)$$

3.3 Method of Moments Discretization

Introducing M surface pulse basis functions P_m on the elements of the surface mesh ∂S_m and N pulse basis functions p_n on the elements S_n of the volume mesh (Fig. 3.2), we approximate surface and volume current densities as

$$J_z(\boldsymbol{\rho}') \cong \sum_{m=1}^M I_m P_m(\boldsymbol{\rho}'), \quad P_m(\boldsymbol{\rho}') = \begin{cases} 1, & \boldsymbol{\rho}' \in \partial S_m \\ 0, & \boldsymbol{\rho}' \notin \partial S_m \end{cases}, \quad (3.8)$$

$$j_z(\boldsymbol{\rho}') \cong \sum_{n=1}^N i_n p_n(\boldsymbol{\rho}'), \quad p_n(\boldsymbol{\rho}') = \begin{cases} 1, & \boldsymbol{\rho}' \in \partial S_n \\ 0, & \boldsymbol{\rho}' \notin \partial S_n \end{cases}. \quad (3.9)$$

Substitution of the current approximations (3.8)–(3.9) into the surface integral equation (3.3) followed by the collocation testing at the centroids of the respective

observation elements reduces the SVS-EFIE (3.3) to the following set of M linear algebraic equations with respect to M unknowns $\mathbf{I} = [I_1, \dots, I_M]$

$$(\mathbf{Z}_\sigma^{\partial S, \partial S} + \sigma \mathbf{Z}_0^{\partial S, S} \cdot \mathbf{Z}_\sigma^{S, \partial S}) \cdot \mathbf{I} = \mathbf{V}. \quad (3.10)$$

In (3.10) ($M \times M$) matrix $\mathbf{Z}_\sigma^{\partial S, \partial S}$ signifies the global impedance boundary condition defined as

$$Z_{\sigma, mm'}^{\partial S, \partial S} = \langle P_{m'}, T_\sigma^{\partial S, \partial S} \circ P_m \rangle = -i\omega\mu_0 L_{m'} \int_0^1 G_\sigma(\boldsymbol{\rho}_m^{(1/2)}, \boldsymbol{\rho}_{m'}(l')) dl', \quad (3.11)$$

where $m, m' = 1, \dots, M$, $\boldsymbol{\rho}_{m'}(l) = \boldsymbol{\nu}_{m'}^{(1)} + l(\boldsymbol{\nu}_{m'}^{(2)} - \boldsymbol{\nu}_{m'}^{(1)})$ is m' 'th surface element parametric definition with $\boldsymbol{\nu}_{m'}^{(2)}$ and $\boldsymbol{\nu}_{m'}^{(1)}$ being its end points, $L_{m'}$ being its length, and $l \in [0, 1]$.

The $Z_{0, mn'}^{\partial S, S}$ 'th element of ($M \times N$) matrix $\mathbf{Z}_0^{\partial S, S}$ corresponds to the electric field at the centroid of m th surface element produced by n 'th volume element

$$Z_{0, mn'}^{\partial S, S} = \langle P_m, T_0^{\partial S, S} \circ p_{n'} \rangle = -i\omega\mu_0 2A_{n'} \int_0^1 \int_0^{1-\eta'} G_0(\boldsymbol{\rho}_m^{(1/2)}, \boldsymbol{\rho}_{n'}(\xi', \eta')) d\xi' d\eta', \quad (3.12)$$

where $m = 1, \dots, M$, $n' = 1, \dots, N$, $\boldsymbol{\rho}_{n'}(\xi, \eta) = \boldsymbol{\nu}_{n'}^{(1)}\xi + \boldsymbol{\nu}_{n'}^{(2)}\eta + \boldsymbol{\nu}_{n'}^{(3)}(1 - \xi - \eta)$ is parametric definition of position-vector on n 'th volumetric element in barycentric coordinates ξ and η [4] with $\boldsymbol{\nu}_{n'}^{(1)}, \boldsymbol{\nu}_{n'}^{(2)}, \boldsymbol{\nu}_{n'}^{(3)}$ being the vertices of the n 'th triangular volumetric element, and $A_{n'}$ being its area.

The $Z_{\sigma, n'm'}^{S, \partial S}$ 'th element of ($N \times M$) matrix $\mathbf{Z}_\sigma^{S, \partial S}$ corresponds to the electric field at the centroid of n th volume element produced by m th element of the surface current density

$$Z_{\sigma, n'm'}^{S, \partial S} = \langle p_{n'}, T_\sigma^{S, \partial S} \circ P_{m'} \rangle = -i\omega\mu_0 L_{m'} \int_0^1 G_\sigma(\boldsymbol{\rho}_{n'}^{(1/3, 1/3)}, \boldsymbol{\rho}_{m'}(l')) dl', \quad (3.13)$$

where $n' = 1, \dots, N$, $m' = 1, \dots, M$, and parametric definitions of position-vectors on surface and volume elements in (3.13) are the same as in (3.11) and (3.12).

It is important to note that as the frequency of analysis increases, so does the sparsity of matrices $\mathbf{Z}_\sigma^{\partial S, \partial S}$, $\mathbf{Z}_\sigma^{S, \partial S}$, and $\mathbf{Z}_0^{\partial S, S}$ in (3.10). The reason for sparsification of $\mathbf{Z}_\sigma^{\partial S, \partial S}$ and $\mathbf{Z}_\sigma^{S, \partial S}$ is the exponential attenuation of the Green's function $G_\sigma(\boldsymbol{\rho}, \boldsymbol{\rho}')$ due to the conductivity of the media. Matrix $\mathbf{Z}_0^{\partial S, S}$ can be sparsified as frequency grows despite its correspondence to the free space kernel $G_0(\boldsymbol{\rho}, \boldsymbol{\rho}')$. This is because the cross-sectional current becomes negligible beyond few skin-depths off the surface. Hence, the columns of $\mathbf{Z}_0^{\partial S, S}$ corresponding to the mesh triangle in the off-surface areas can be preemptively zeroed out based on prescribed tolerance.

3.4 Numerical Results

In the first numerical experiment we consider a single conductor transmission line made of aluminium ($\sigma = 3.57 \cdot 10^7 \text{ S/m}$) that has a circular cross-section with the radius $\rho_0 = 0.025 \text{ m}$. The cross-section is approximated with the regular 20-sided polygon (icosagon). The surface current density J_z is first obtained via MoM solution (3.10) of the proposed surface IE (3.3) under uniform discretization of the conductor surface with $M = 200$ linear segments and its volume — with $N = 3,620$ triangular elements. The solution J_z is then substituted into (3.2) for evaluation of the volumetric current density j_z . In Fig. 3.1 the latter is compared against the analytic solution [5] for ideal circular wire. The relative error of proposed method with respect to the MoM solution of the volumetric IE (3.1) does not exceed 1% and with respect to the analytic solution — 2.5% in the frequency range from 1 Hz to 1 kHz. For convenience of computations the number of basis functions M and N in MoM discretization (3.10) remains the same at all frequencies.

Next, to demonstrate the proper handling by the proposed methodology of geometries with sharp cross-sectional corners, the same circular wire was approximated with the regular 6-sided polygon (hexagon). The MoM discretization (3.10) of the proposed surface IE (3.3) was performed with $M = 60$ line segments and $N = 3,697$ triangles. The same triangular mesh was then utilized in the traditional volumetric MoM solution of the IE (3.1). Fig. 3.2 depicts the cross-sectional distribution of the volumetric current density obtained using the proposed method and its relative error with respect to the traditional volumetric MoM solution of the IE (3.1). It is seen that both edge crowding of the current and skin effect are well resolved.

The dependence of the extracted per-unit-length resistance R and inductance L values on frequency for the circular conductor approximated with 20– and 6-sided polygons is depicted in Fig. 3.3. The R and L values extracted using the proposed novel surface integral equation formulation (3.3) are shown by solid line for the case of 20-sided cross-section boundary and dashed line for the case of the 6-sided one. The circle and cross markers show the values R and L extracted using the traditional volumetric MoM solution of the IE (3.1).

Handling of the proximity effect by the proposed method is depicted in Fig. 3.4. Here the volumetric current density extracted at 60 Hz via MoM solution (3.10) of the SVS-EFIE (3.3) is shown in the cross-section of two circular conductors each approximated with a 6-sided polygon and having radius of $\rho_0 = 0.025\text{ m}$. Centers of the conductors are separated by the distance of 0.06 m . The right conductor is driven by the p.u.l. voltage drop $V_{p.u.l.}^{(1)} = 1\text{ V/m}$, while the left conductor is terminated to the ground $V_{p.u.l.}^{(2)} = 0\text{ V/m}$. In the two-conductor transmission line example the MoM solution (3.10) utilizes $M = 120$ linear segment and $N = 3,094$ triangular elements. The traditional volumetric MoM solution of V-EFIE (3.1) is performed using the same triangular mesh in the cross-section as the one used in the MoM for the SVS-EFIE (3.3).

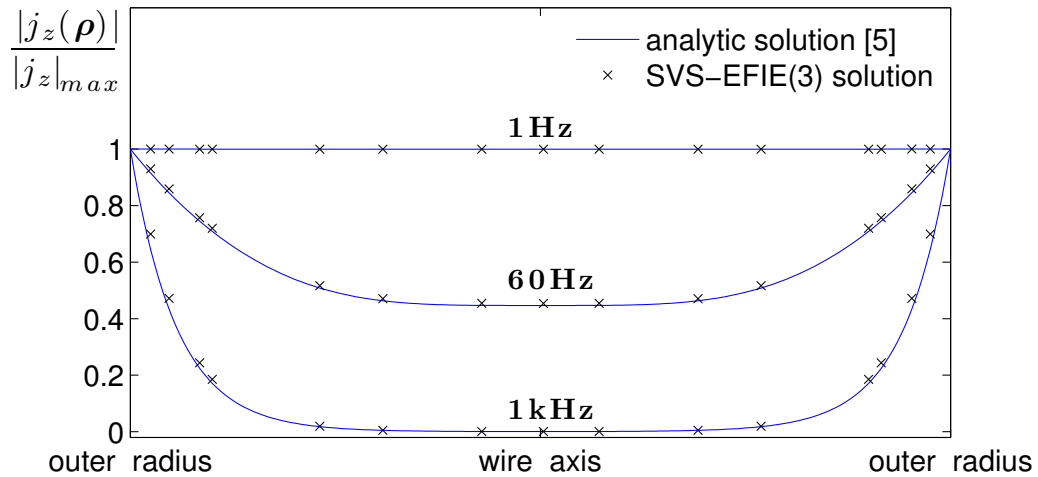


Figure 3.1: Normalized distribution of the volumetric current density j_z across aluminum circular conductor of radius $\rho_0 = 0.025\text{ m}$. © 2012 IEEE.

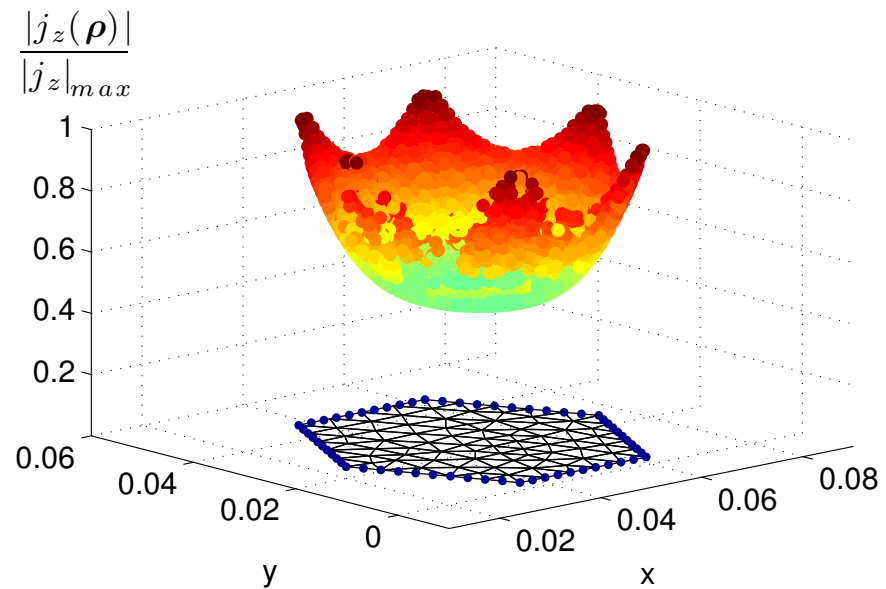


Figure 3.2: Surface (dot markers) and volume meshes utilized in MoM discretization (3.8)–(3.13). Cross-sectional distribution of the volumetric current density obtained via MoM solution (3.10) for the SVS-EFIE (3.3) at 60 Hz. The relative error with respect to the volumetric MoM solution of the V-EFIE (3.1) does not exceed 2.7%. © 2012 IEEE.

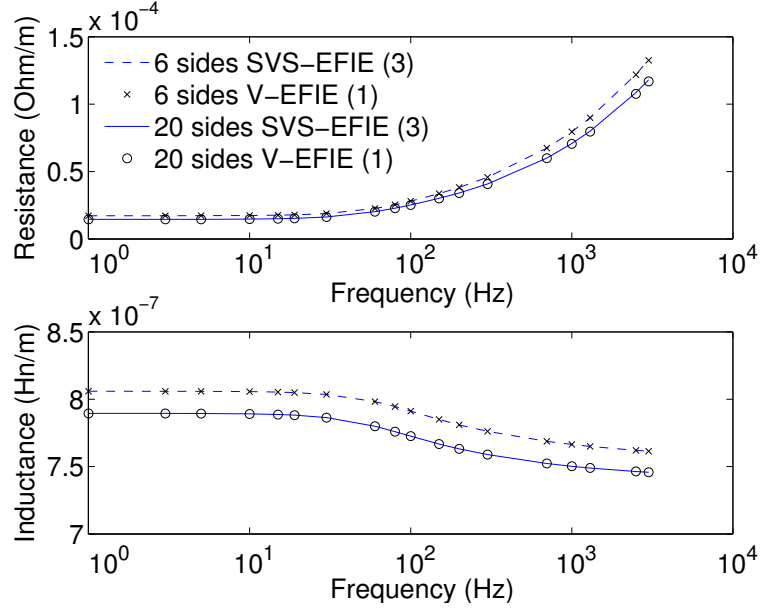


Figure 3.3: Resistance and inductance of circular conductor extracted with MoM solution (3.10) of the proposed SVS-EFIE (3.3) and volumetric MoM solution of the V-EFIE (3.1) for 6-sided and 20-sided polygonal approximation of the circular cross-section. © 2012 IEEE.

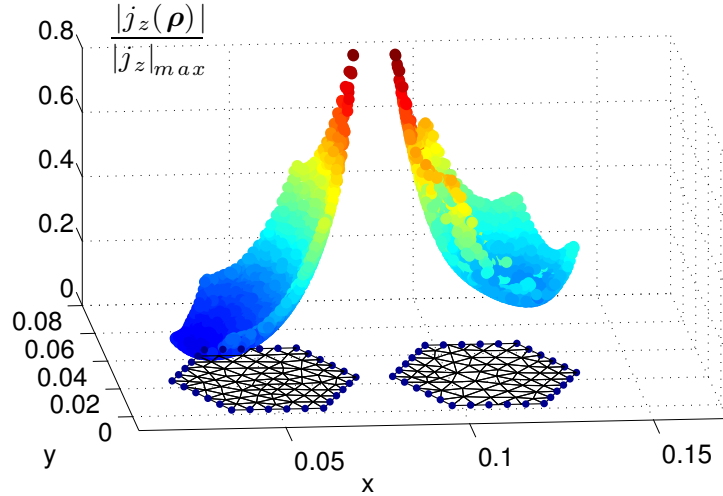


Figure 3.4: Cross-sectional distribution of the volumetric current density in two conductors obtained via MoM solution (3.10) for the SVS-EFIE (3.3) at 60 Hz. The relative error with respect to the volumetric MoM solution of the V-EFIE (3.1) does not exceed 1.8%. © 2012 IEEE.

3.5 Conclusion

This work proposes a novel surface integral equation for broadband RL extraction in multiconductor transmission lines of arbitrary cross-section. The latter features the global surface impedance operator as well as the product of surface-to-volume and volume-to-surface EFIE operators. The method substantially reduces the computational complexity without compromising the accuracy of the traditional volumetric solution.

Bibliography

- [1] E. Tancer, “Extraction of parameters for high speed digital interconnects,” *Ph.D. Dissertation*, Elect. Comput. Eng. Dept., The Univ. Texas at Austin, Austin, TX, 1995.
- [2] E. M. Deely, “Surface impedance near edges and corners in three-dimensional media,” *IEEE Trans. Magn.*, Vol. 26, No. 2, pp. 712–714, Mar. 1990.
- [3] Z. G. Qian, W. C. Chew, and R. Suaya, “Generalized impedance boundary condition for conductor modeling in surface integral equation,” *IEEE Trans. Microw. Theory Techn.*, Vol. 55, No. 11, pp. 2354–2364, Nov. 2007.
- [4] S. Rao, D. Wilton, and A. Glisson, “Electromagnetic scattering by surfaces of arbitrary shape,” *IEEE Trans. Antennas Propag.*, Vol. 30, No. 3, pp. 409–418, May 1982.
- [5] S. Ramo, J. R. Whinnery, T. Van Duzer, *Fields and Waves in Communication Electronics, 2nd Ed.*, New York, Wiley, 1984.

Chapter 4

Method of Moment Solution of Surface-Volume-Surface Electric Field Integral Equation for Two-Dimensional Transmission Lines of Complex Cross-Sections

©2012 IEEE. Reprinted, with permission, from *Anton Menshov and Vladimir Okhmatovski, Method of Moment Solution of Surface-Volume-Surface Electric Field Integral Equation for Two-Dimensional Transmission Lines of Complex Cross-Sections, 2012 IEEE 16th Workshop on Signal and Power Integrity (SPI), May 2012*

The novel Surface–Volume–Surface Electric Field Integral Equation (SVS-EFIE) has been recently proposed for accurate extraction of per-unit-length (p.u.l.) inductance and resistance (RL) matrices in multi-conductor transmission lines (MTL). The SVS-EFIE yields the same accuracy of RL extraction as the traditional volumetric EFIE (V-EFIE) solution while introducing the unknown currents on the conductor surface instead of its volume. This work presents detailed discussion of Method of Moments (MoM) discretization of the SVS-EFIE and resultant matrices. The example of a coaxial transmission line is utilized in derivations to demonstrate method's applicability to MTL's with multi-connected cross-sections.

4.1 Introduction

The quasi-static characterization of interconnects provides a computationally efficient alternative to the full-wave methods either at the low end in the base-band spectrum of the digital signals or for short interconnects in the entire band from DC to multi-GHz frequencies (e.g. ball grid arrays, bond wires, etc.).

Traditional approach to the network parameter extraction in quasi-static regime is through volumetric solution of the EFIE [1]. While the V-EFIE solution comes with the benefit of accurately capturing current behavior due to skin- and proximity-effect, it is computationally expensive. The high computational complexity comes as a result of volumetric discretization of conductors dictated by the skin-depth at a given frequency. Several Surface EFIE (S-EFIE) formulations have been proposed in the past which introduce either a global (GIBC) [2] or local (LIBC) impedance boundary conditions [3] to eliminate the need for volumetric discretization. While the S-EFIE scheme with GIBC maintain rigorously equivalence to the V-EFIE and provide comparable accuracy, they feature both electric and magnetic field Green's function kernels making them difficult to implement in the presence of layered substrates. The S-EFIE schemes with LIBC, on the other hand, offer efficiency and simplicity in implementation but usually lack generality to handle arbitrary MTL cross-sections.

We have recently showed [4] that an alternative surface integral equation formulation to the above two approaches can be derived. The SVS-EFIE comes with the benefit of having the derivative-free electric field kernels only and the same number of unknowns in MoM discretization as that in the S-EFIE. In this paper we elaborate on the details of MoM discretization of the SVS-EFIE for RL extraction in conductors by considering example transmission lines with co-axial cross-sections.

4.2 Surface-Volume-Surface EFIE and MoM Discretization

4.2.1 Integral Equation

In [4] we showed that the classical V-EFIE of magneto-quasistatics [1]

$$\frac{j(\boldsymbol{\rho})}{\sigma} + i\omega\mu_0 \iint_S G_0(\boldsymbol{\rho}, \boldsymbol{\rho}') j(\boldsymbol{\rho}') ds' = -V_{p.u.l.}, \boldsymbol{\rho} \in S, \quad (4.1)$$

with respect to the unknown volume current density j in MTL cross-section S , can be cast in a form of the SVS-EFIE with respect to the unknown surface density of current J on the surface ∂S

$$\begin{aligned} & -i\omega\mu_0 \int_{\partial S} G_\sigma(\boldsymbol{\rho}, \boldsymbol{\rho}') J(\boldsymbol{\rho}') d\boldsymbol{\rho}' - \sigma(\omega\mu_0)^2 \times \\ & \iint_S G_0(\boldsymbol{\rho}, \boldsymbol{\rho}') \int_{\partial S} G_\sigma(\boldsymbol{\rho}', \boldsymbol{\rho}'') J(\boldsymbol{\rho}'') d\boldsymbol{\rho}'' ds' = -V_{p.u.l.}, \boldsymbol{\rho} \in \partial S. \end{aligned} \quad (4.2)$$

In (4.1) – (4.2) $G_0(\boldsymbol{\rho}, \boldsymbol{\rho}') = -\frac{1}{2\pi} \ln(|\boldsymbol{\rho} - \boldsymbol{\rho}'|)$ is the Green's function of free space under the quasi-static assumption, $G_\sigma(\boldsymbol{\rho}, \boldsymbol{\rho}') = -\frac{i}{4} H_0^{(2)}(k_\sigma |\boldsymbol{\rho} - \boldsymbol{\rho}'|)$ is the Green's function of the conductor media with wavenumber $k_\sigma = \sqrt{\omega\mu_0\sigma/2}(1-i)$, $\boldsymbol{\rho}$, $\boldsymbol{\rho}'$, $\boldsymbol{\rho}''$ are position-vectors of the observation and source points, μ_0 is the permeability of free space, σ is the conductivity of the wire, ω is the cyclic frequency, $i = \sqrt{-1}$, and $V_{p.u.l.}$ is the per-unit-length (p.u.l.) voltage drop along the wire.

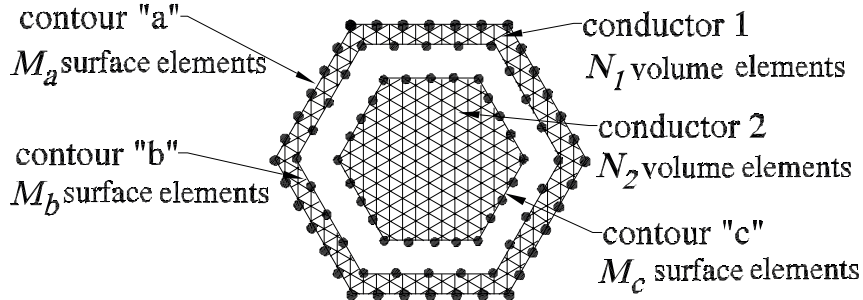


Figure 4.1: Volume and surface meshes utilized in MoM discretization of the SVS-EFIE (4.2). © 2012 IEEE.

4.2.2 Surface and volume meshes

The SVS-EFIE (4.2) involves the product of integral operators. First operator maps the unknown surface current density J from the surface ∂S to the volume current density in the conductor cross-section S . The second integral operator maps the volume current density j from S to the scattered electric field on the conductor surface ∂S . Hence, MoM discretization of (4.2) requires both volumetric and surface meshes. The depiction of the surface and volume meshes for the example of a coaxial transmission line is given in Fig. 4.1. Here, the outer shell is labeled as ‘conductor 1’ and the inner conductor is labeled as ‘conductor 2’. The circular boundaries of the conductors are approximated with hexagons. The surface mesh is depicted with black dot markers. It is important to note that the surface mesh is independent from the volume triangle mesh discretizing the cross-section S .

To formalize the structure of the matrix resulting from MoM discretization of (4.2), we assume that the outer surface of the coaxial line shell ∂S_a is discretized with M_a line elements, its inner surface ∂S_b is discretized with M_b line elements, and the surface of central conductor ∂S_c is discretized with M_c line elements (Fig. 4.1). Parametric

definition of the radius-vector on m th element of the surface ∂S_α is given by

$$\rho_m^\alpha(l) = \mathbf{v}_m^{\alpha,1} + l(\mathbf{v}_m^{\alpha,2} - \mathbf{v}_m^{\alpha,1}), \quad l \in [0, 1], \quad (4.3)$$

where $\alpha = a, b, c$ is the index identifying conductor sub-surfaces ∂S_α such that $\partial S = \partial S_a + \partial S_b + \partial S_c$, $\mathbf{v}_m^{\alpha,2}$ and $\mathbf{v}_m^{\alpha,1}$ are the end and start points of the m th element on ∂S_α , L_m^α is its length, and $m = 1, \dots, M_\alpha$. The cross-section of the outer conductor S_1 is discretized with N_1 volumetric elements (2D simplexes), and the inner conductor's cross-section S_2 is discretized with N_2 volumetric elements. The radius-vector on m th triangular element of the cross-section S_β can be defined parametrically in barycentric coordinates as follows:

$$\rho_m^\beta(\xi, \eta) = \mathbf{v}_m^{\beta,1}\xi + \mathbf{v}_m^{\beta,2}\eta + \mathbf{v}_m^{\beta,3}(1 - \xi - \eta), \quad \xi, \eta \in [0, 1], \quad (4.4)$$

where $\xi + \eta \leq 1$, $\beta = 1, 2$ is the index identifying conductor sub-volumes S_β such that $S = S_1 + S_2$, $\mathbf{v}_m^{\beta,1}$, $\mathbf{v}_m^{\beta,2}$, $\mathbf{v}_m^{\beta,3}$ are the three vertices of the m th triangle on S_β , A_m^β is the area of the m th triangle, and $m = 1, \dots, N_\beta$. It's important to note that the number of surface elements M is independent of frequency and typically is relatively low in case of 2D MTLs. The density of the volumetric mesh, however, grows with frequency in order to maintain accurate approximation of the volumetric current according to skin-effect. Thus, as frequency grows, N typically becomes much larger than M .

4.2.3 MoM discretization of SVS-EFIE's surface-to-volume operator

We discretize the unknown surface current densities J^a and J^b on the outer conductor surfaces ∂S_a and ∂S_b and surface current density J^c on the surface of the inner

conductor ∂S_c with piece-wise basis functions (pulse basis) as follows:

$$J^\alpha(\boldsymbol{\rho}'') \cong \sum_{m=1}^{M_\alpha} I_m^\alpha P_m^\alpha(\boldsymbol{\rho}''), \quad P_m^\alpha(\boldsymbol{\rho}'') = \begin{cases} 1, & \boldsymbol{\rho}'' \in \partial S_{\alpha,m} \\ 0, & \boldsymbol{\rho}'', \notin \partial S_{\alpha,m} \end{cases}, \quad (4.5)$$

where $\alpha = a, b, c$ is the character identifying conductor surfaces, and $\partial S_{\alpha,m}$ is m th surface mesh element on α th conductor surface ∂S_α . Substitution of the discretized surface current J from (4.5) into the equivalence principle integral operator relation $j = \mathcal{T}_\sigma^{S,\partial S}\{J\}$ to the volumetric current density j , followed by testing of the volumetric current density at the centroids of the volumetric mesh discretizing the range $\boldsymbol{\rho}' \in S$ of operator $\mathcal{T}_\sigma^{S,\partial S}\{\dots\} = -i\omega\mu_0\sigma \int_{\partial S} G_\sigma(\boldsymbol{\rho}', \boldsymbol{\rho}'')\{\dots\} d\boldsymbol{\rho}''$, establishes the matrix relationship

$$\begin{bmatrix} \mathbf{i}^{(1)} \\ \mathbf{i}^{(2)} \end{bmatrix} = \begin{bmatrix} \mathbf{Z}_\sigma^{S_1, \partial S_a} & \mathbf{Z}_\sigma^{S_1, \partial S_b} & 0 \\ 0 & 0 & \mathbf{Z}_\sigma^{S_2, \partial S_c} \end{bmatrix} \cdot \begin{bmatrix} \mathbf{I}^a \\ \mathbf{I}^b \\ \mathbf{I}^c \end{bmatrix} \quad (4.6)$$

between vector of M unknown coefficients of the surface current expansion $\mathbf{I} = [I_1^a, \dots, I_{M_a}^a; I_1^b, \dots, I_{M_b}^b; I_1^c, \dots, I_{M_c}^c]^T$ and N samples $\mathbf{i} = [i_1^{(1)}, \dots, i_{N_1}^{(1)}; i_1^{(2)}, \dots, i_{N_2}^{(2)}]^T$ of the volume current density j at the N_1 centroids of the volumetric mesh discretizing cross-section of the outer ‘conductor 1’ and N_2 centroids of the volumetric elements discretizing the inner ‘conductor 2’. The matrix elements in (4.6) are formally defined as inner products

$$Z_{\sigma, n'm''}^{S_\beta, \partial S_\alpha} = \langle t_{n'}^\beta, \mathcal{T}_\sigma^{S_\beta, \partial S_\alpha}\{P_{m''}^\alpha\} \rangle = -i\omega\mu_0\sigma L_{m''}^\alpha \int_0^1 G_\sigma(\boldsymbol{\rho}_{n'}^\beta(1/3, 1/3), \boldsymbol{\rho}_{m''}^\alpha(l'')) dl'', \quad (4.7)$$

where $t_{n'}^\beta(\boldsymbol{\rho}) = \delta(\boldsymbol{\rho} - \boldsymbol{\rho}_{n'}^\beta(1/3, 1/3))$ is testing delta-function at the centroid of n' th volume elements in S_β , α is the index of conductor surface ∂S_α , β is the index identifying cross-section surface S_β , $n' = 1, \dots, N_\beta$ are the indexes of surface elements on ∂S_β , and $m'' = 1, \dots, M_\alpha$ are the indexes of volume elements in S_β . The parametric definitions of position-vectors on the surface and volume elements in (4.7) are given in (4.3) and (4.4), respectively.

4.2.4 MoM discretization of SVS-EFIE's volume-to-surface operator

In order to discretize the integral operator in (4.2), which maps the volumetric current density j in the cross-section of the transmission line S to the magnetic vector potential A on conductor's surface ∂S , we discretize the volumetric current density j with pulse basis functions defined on the elements of the volumetric mesh $S_{\beta,m}$, $m = 1, \dots, N_\beta$ as follows:

$$j^\beta(\boldsymbol{\rho}') \cong \sum_{n=1}^{N_\beta} i_n^\beta p_n^\beta(\boldsymbol{\rho}'), \quad p_n^\beta(\boldsymbol{\rho}') = \begin{cases} 1, & \boldsymbol{\rho}' \in S_{\beta,n} \\ 0, & \boldsymbol{\rho}' \notin S_{\beta,n} \end{cases}, \quad (4.8)$$

where $\beta = 1, 2$ is the index identifying the sub-volume S_β in the MTL's cross-section. Next, we substitute the discretized volume current density j from (4.8) into its integral relation to the magnetic vector potential $A = \mathcal{T}_0^{\partial S, S}\{j\}$, where operator $\mathcal{T}_0^{\partial S, S}$ is defined as $\mathcal{T}_0^{\partial S, S}\{\dots\} = \mu_0 \int_S G_0(\boldsymbol{\rho}, \boldsymbol{\rho}') \{\dots\} ds'$, $\boldsymbol{\rho} \in \partial S$. Testing of the magnetic vector potential A at the centroids of the surface mesh elements yields the matrix equation

formalizing the discretization of the continuous operator $\mathcal{T}_0^{\partial S, S}$

$$\begin{bmatrix} \mathbf{A}^a \\ \mathbf{A}^b \\ \mathbf{A}^c \end{bmatrix} = \begin{bmatrix} \mathbf{Z}_0^{\partial S_a, S_1} & \mathbf{Z}_0^{\partial S_a, S_2} \\ \mathbf{Z}_0^{\partial S_b, S_1} & \mathbf{Z}_0^{\partial S_b, S_2} \\ \mathbf{Z}_0^{\partial S_c, S_1} & \mathbf{Z}_0^{\partial S_c, S_2} \end{bmatrix} \cdot \begin{bmatrix} \mathbf{i}^{(1)} \\ \mathbf{i}^{(2)} \end{bmatrix}. \quad (4.9)$$

In (4.9), $\mathbf{A} = [A_1^a, \dots, A_{M_a}^a; A_1^b, \dots, A_{M_b}^b; A_1^c, \dots, A_{M_c}^c]^T$ is a vector of M samples of the magnetic vector potential A at the centroids of the surface mesh elements discretizing surfaces of the conductors. Matrix elements in (4.9) are defined as the following inner products

$$Z_{0,mn'}^{\partial S_\alpha, S_\beta} = \langle T_m^\alpha, \mathcal{T}_0^{\partial S_\alpha, S_\beta} \{p_{n'}^\alpha\} \rangle = 2\mu_0 A_{n'}^\beta \int_0^1 \int_0^{1-\eta'} G_0(\boldsymbol{\rho}_m^\alpha(1/2), \boldsymbol{\rho}_{n'}^\beta(\xi', \eta') d\xi' d\eta', \quad (4.10)$$

where $T_m^\alpha(\boldsymbol{\rho}) = \delta(\boldsymbol{\rho} - \boldsymbol{\rho}_m^\alpha(1/2))$ is testing delta-function at the centroid of m th surface element in ∂S_α , α is the index of conductor surface ∂S_α , β is the index identifying cross-section surface S_β , $n' = 1, \dots, N_\beta$ are the indexes of volume elements on S_β , and $m = 1, \dots, M_\alpha$ are the indexes of surface elements in ∂S_α . The parametric definitions of position-vectors on surface and volume elements are given in (4.3) and (4.4), respectively.

4.2.5 MoM discretization of SVS-EFIE's surface-to-surface operator

The first term in the left-hand side of (4.2) expresses the electric field E via the surface current density J which can be written in operator form as $E = \mathcal{T}_\sigma^{\partial S, \partial S}\{J\}$. Unlike the operator $\mathcal{T}_\sigma^{S, \partial S}$ we have considered previously, the operator $\mathcal{T}_\sigma^{\partial S, \partial S}\{\dots\} =$

$-i\omega\mu_0 \int_{\partial S} G_\sigma(\boldsymbol{\rho}, \boldsymbol{\rho}') \{ \dots \} d\boldsymbol{\rho}'$ has both its domain and range at the conductor surface ∂S . This operator has the physical meaning of the global surface impedance boundary condition as it relates the tangential magnetic field (surface current density) and electric field on the conductor surface. Discretizing the domain and range of $\mathcal{T}_\sigma^{\partial S, \partial S}$ in the same way as the domain and range of the operators $\mathcal{T}_\sigma^{S, \partial S}$ and $\mathcal{T}_0^{\partial S, S}$, respectively, we obtain equivalent discretized global impedance boundary condition in the following matrix form

$$\begin{bmatrix} \mathbf{E}^a \\ \mathbf{E}^b \\ \mathbf{E}^c \end{bmatrix} = \begin{bmatrix} \mathbf{Z}_\sigma^{\partial S_a, \partial S_a} & \mathbf{Z}_\sigma^{\partial S_a, \partial S_b} & 0 \\ \mathbf{Z}_\sigma^{\partial S_b, \partial S_a} & \mathbf{Z}_\sigma^{\partial S_b, \partial S_b} & 0 \\ 0 & 0 & \mathbf{Z}_\sigma^{\partial S_c, \partial S_c} \end{bmatrix} \cdot \begin{bmatrix} \mathbf{I}^a \\ \mathbf{I}^b \\ \mathbf{I}^c \end{bmatrix}, \quad (4.11)$$

where $\mathbf{E} = [E_1^a, \dots, E_{M_a}^a; E_1^b, \dots, E_{M_b}^b; E_1^c, \dots, E_{M_c}^c]^T$ is a vector of M samples of the electric field E at the centroids of the surface mesh elements discretizing surfaces of the conductors. The matrix elements in (4.11) are defined as

$$Z_{\sigma, mm'}^{\partial S_\alpha, \partial S_{\alpha'}} = \langle T_m^\alpha, \mathcal{T}_\sigma^{\partial S, \partial S} \{ P_{m'}^{\alpha'} \} \rangle = -i\omega\mu_0 L_{m'}^{\alpha'} \int_0^1 G_\sigma(\boldsymbol{\rho}_m^\alpha(1/2), \boldsymbol{\rho}_{m'}^{\alpha'}(l')) dl', \quad (4.12)$$

where $\alpha, \alpha' = a, b, c$ are conductor surface indexes, $m = 1, \dots, M_\alpha$, and $m' = 1, \dots, M_{\alpha'}$.

4.2.6 Matrix form of MoM discretized SVS-EFIE

In (4.6), (4.9), (4.11) we obtained matrix forms $\mathbf{Z}_\sigma^{S, \partial S}$, $\mathbf{Z}_0^{\partial S, S}$, $\mathbf{Z}_\sigma^{\partial S, \partial S}$ of MoM discretized integral operators $\mathcal{T}_\sigma^{S, \partial S}$, $\mathcal{T}_0^{\partial S, S}$, $\mathcal{T}_\sigma^{\partial S, \partial S}$, respectively, which form the SVS-EFIE (4.2). This reduces the integral equation (4.2) to the following set of M linear

$$\begin{aligned}
 & \left(\mathbf{Z}_\sigma^{\partial S, \partial S} + \sigma \mathbf{Z}_0^{\partial S, S} \cdot \mathbf{Z}_\sigma^{S, \partial S} \right) \cdot \mathbf{I} = \mathbf{V} \\
 & \left(\begin{array}{c|cc|cc|cc}
 & M_a & M_b & & & & \\
 \hline
 M_a & Z_\sigma^{\partial S_a, \partial S_a} & Z_\sigma^{\partial S_a, \partial S_b} & 0 & & & \\
 \hline
 M_b & Z_\sigma^{\partial S_b, \partial S_a} & Z_\sigma^{\partial S_b, \partial S_b} & & & & \\
 \hline
 & 0 & Z_\sigma^{\partial S_c, \partial S_b} & & & & \\
 \hline
 \end{array} \right) + \left(\begin{array}{c|cc|cc|cc}
 & N_I & & & & & \\
 \hline
 M_a & Z_0^{\partial S_a, S_I} & Z_0^{\partial S_a, S_z} & & & & \\
 \hline
 M_b & Z_0^{\partial S_b, S_I} & Z_0^{\partial S_b, S_z} & & & & \\
 \hline
 & Z_0^{\partial S_c, S_I} & Z_0^{\partial S_c, S_z} & & & & \\
 \hline
 \end{array} \right) \cdot \left(\begin{array}{c|cc|cc|cc}
 & M_a & M_b & & & & \\
 \hline
 M_a & Z_\sigma^{S_I, \partial S_a} & Z_\sigma^{S_I, \partial S_b} & 0 & & & \\
 \hline
 M_b & & & & & & \\
 \hline
 & 0 & Z_\sigma^{\partial S_c, \partial S_c} & & & & \\
 \hline
 \end{array} \right) \cdot \left(\begin{array}{c|cc|cc|cc}
 & N_I & & & & & \\
 \hline
 M_a & I^a & & & & & \\
 \hline
 M_b & I^b & & & & & \\
 \hline
 & I^c & & & & & \\
 \hline
 \end{array} \right) = \mathbf{V}
 \end{aligned}$$

Figure 4.2: Matrix form (4.13) of the SVS-EFIE (4.2) discretized with the Method of Moments utilizing volume and surface meshes depicted in Fig. 4.1. © 2012 IEEE.

algebraic equations with M unknowns

$$(\mathbf{Z}_\sigma^{\partial S, \partial S} + \sigma \mathbf{Z}_0^{\partial S, S} \cdot \mathbf{Z}_\sigma^{S, \partial S}) \cdot \mathbf{I} = \mathbf{V}, \quad (4.13)$$

which can be solved numerically to determine unknown coefficients \mathbf{I} . The matrix equation (4.13) as well as the structure of the matrices entering into it are shown graphically in Fig. 4.2.

Note that due to the exponential attenuation of the Green's function $G_\sigma(\boldsymbol{\rho}, \boldsymbol{\rho}')$ in the conductor media, matrices $\mathbf{Z}_\sigma^{\partial S, \partial S}$ and $\mathbf{Z}_\sigma^{S, \partial S}$ become sparse as the frequency of analysis increases. Because the rows of matrix $\mathbf{Z}_\sigma^{S, \partial S}$ corresponding to the volume elements situated several skin-depths away from the surface are exponentially small, one can also zero out corresponding columns in $\mathbf{Z}_0^{\partial S, S}$ as these matrices enter in (4.13) as a product $\mathbf{Z}_0^{\partial S, S} \cdot \mathbf{Z}_\sigma^{S, \partial S}$. The above described sparsity patterns of the matrices forming MoM discretized SVS-EFIE allow to maintain the CPU time and memory complexity of the proposed method comparable to the S-EFIE schemes with LIBCs (e.g. [3]) but without sacrificing the accuracy of the solution.

4.3 Numerical Results

In the first numerical experiment we consider a single coaxial cable transmission line (Fig. 4.4) of circular cross-section with the outer radius $\rho_1 = 0.0019\text{ m}$ for outer shell made of steel ($\sigma_1 = 1.45 \cdot 10^6\text{ S/m}$), inner conductor made of copper ($\sigma_2 = 5.96 \cdot 10^7\text{ S/m}$) with the radius $\rho_2 = 0.0014\text{ m}$, and insulator with the outer radius $\rho_3 = 0.0018\text{ m}$. To demonstrate the proper handling by the proposed methodology of the geometries with sharp cross-sectional corners, this cable was approximated with 3 regular hexagons. The MoM discretization (4.13) of the proposed surface IE (4.2) was performed with $M = 180$ line segments (60 for each surface) and $N = 4,666$ triangles. The same triangular mesh was then utilized in the traditional volumetric MoM solution of the IE (4.1). Fig. 4.3 depicts the cross-sectional distribution of the volumetric current density obtained using the proposed method. It is seen that both edge crowding of the current and skin effect are well resolved.

Now, to demonstrate the dependence of the extracted per-unit-length resistance R and inductance L on frequency, the cross-section is approximated with the 6-sided (as on Fig. 4.3) and 20-sided polygons. The MoM discretization (4.13) of the proposed surface IE (4.2) on 20-sides polygon was performed with $M = 300$ line segments (100 for each surface) and $N = 5,374$ triangles. The result is depicted in Fig. 4.4, where solid line shows the case of 20-sided approximation and dashed line indicates the case of 6-sided one. The circle and cross markers show the R and L values extracted using the traditional volumetric MoM solution of the IE (4.1). The relative error with respect to the volumetric MoM solution does not exceed 1.5%.

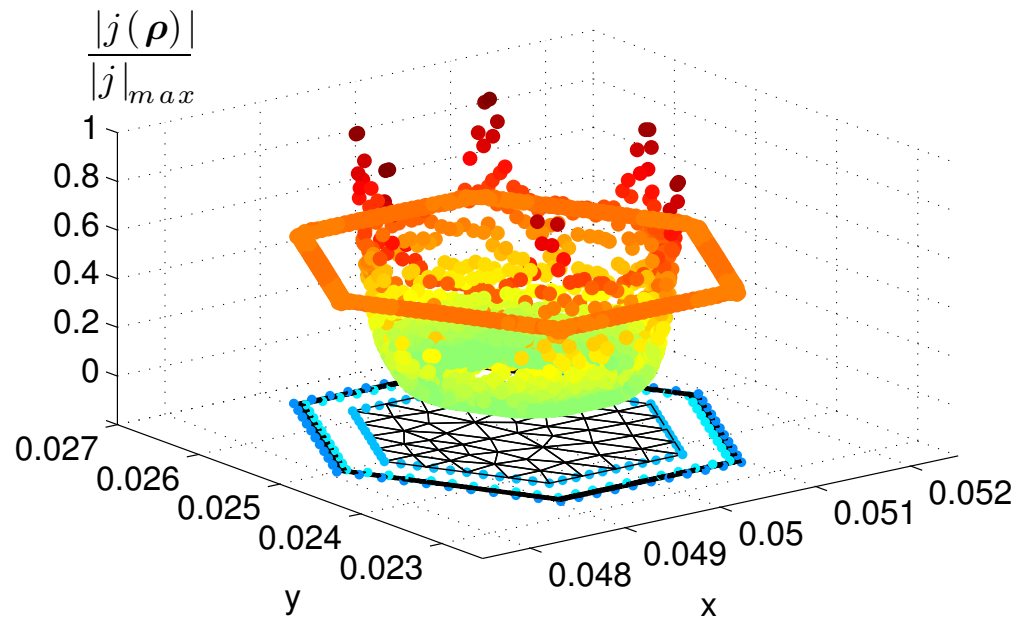


Figure 4.3: Surface (blue dot markers) and volume meshes utilized in MoM discretization (4.5)–(4.13). Volumetric current density obtained via MoM solution (4.13) for SVS-EFIE (4.2) at 400 kHz. The relative error of the V-EFIE (4.1) and the SVS-EFIE MoM solutions does not exceed 1.5%. © 2012 IEEE.

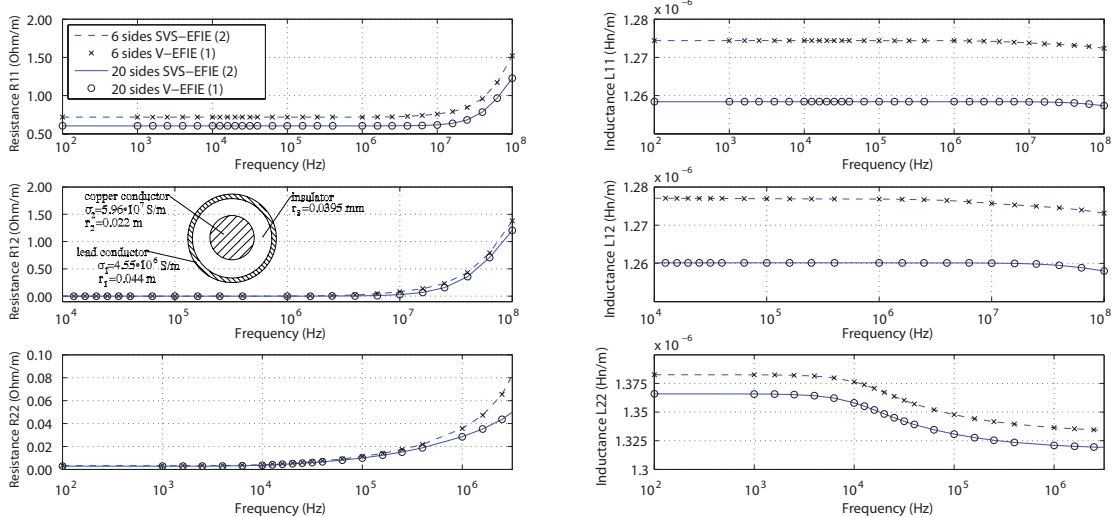


Figure 4.4: Resistance and inductance of circular co-axial conductor extracted with MoM solution (4.13) of the proposed SVS-EFIE (4.2) and volumetric MoM solution of the V-EFIE (4.1) for 6-sided and 20-sided polygonal approximation. © 2012 IEEE.

4.4 Conclusions

The paper provides detailed derivation of pertinent matrices in the Method of Moment discretization of Surface-Volume-Surface Electric Field Integral Equation. As the latter features the products of surface-to-volume, volume-to-surface and surface-to-surface integral operators, the Method of Moments requires both volumetric discretization of conductor cross-section and surface discretization of its boundaries. The example of a coaxial transmission is considered to demonstrate applicability of the SVS-EFIE solution to the conductors with multi-connected cross-sections.

Bibliography

- [1] M. Kamon, M. J. Tsuk, and J. White, “FASTHENRY: A Multipole Accelerated 3-D Inductance Extraction Program,” *IEEE Trans. Microw. Theory Techn.*, Vol. 42, No. 9, pp. 1750–1758, 1994.
- [2] Z. G. Qian, W. C. Chew, and R. Suaya, “Generalized impedance boundary condition for conductor modeling in surface integral equation,” *IEEE Trans. Microw. Theory Techn.*, Vol. 55, No. 11, pp. 2354–2364, Nov. 2007.
- [3] M. Al-Qedra and V. Okhmatovski, “Full-periphery surface impedance for skin-effect approximation in EFIE,” *IEEE Microwave Wireless Lett. Comp.*, Vol. 19, No. 1, pp. 9–11, Jan. 2009.
- [4] A. Menshov and V. Okhmatovski, “Novel surface integral equation formulation for accurate broadband RL extraction in transmission lines of arbitrary cross-section,” *Microwave Symposium Digest (MTT)*, 2012 IEEE MTT-S International, pp. 1-3, 17–22 June 2012.

Chapter 5

New Single-Source Surface Integral Equations for Scattering on Penetrable Cylinders and Current Flow Modelling in Two-Dimensional Conductors

©2013 IEEE. Reprinted, with permission, from *Anton Menshov and Vladimir Okhmatovski, New Single-Source Surface Integral Equations for Scattering on Penetrable Cylinders and Current Flow Modelling in Two-Dimensional Conductors, IEEE Transactions on Microwave Theory and Techniques, January 2013*

The traditional volume electric field integral equation used for solution of full-wave scattering problems on penetrable scatterers of arbitrary cross-section and its magnetostatic counterpart commonly utilized for the resistance and inductance extraction problem are reduced to a novel derivative-free single-source surface integral equation. The reduction of volume to surface integral equation is based on representation of the electric field in the cylinder cross-section in the form of a single-layer ansatz. Substitution of such surface based electric field representation into the volume integral equation reduces it to a surface integral equation with respect to the unknown surface current density. Since the new surface integral equation enforces exactly the field continuity at the material interfaces, the radiation condition as well as underlying Helmholtz equations both inside and outside the penetrable cylinder, it is rigorously equivalent to the solution of Maxwell's equations. The method of moments discretization of the new integral equation is shown to produce an error-controllable field approximation. Due to the presence of a product of surface-to-volume and volume-to-surface integral operators, the discretization of the novel surface-volume-surface integral equation requires both surface and volume meshes.

5.1 Introduction

The Volume Electric Field Integral Equation (V-EFIE) [1] has been widely used in computational electromagnetics for the rigorous solution of the Maxwell's equations in both quasi-static and full-wave regimes. Under quasi-static approximation, the V-EFIE is foundational to the evaluation of the current distribution in the cross-sections of two-dimensional (2D) [2] as well as three-dimensional (3D) conductors [3]. Such solutions have an important practical application in the extraction of per-unit-length and terminal characteristics of the multi-conductor transmission lines (MTL) [4]. In the full-wave regime, the V-EFIE is most commonly used for solution of the scattering problems on penetrable scatterers with inhomogeneous distribution of permittivity and/or conductivity [1]. Such problems are commonly encountered in microwave imaging [5], remote sensing [6], design of radar absorber materials [7], [8], and various other areas.

The use of the V-EFIE may be avoided, however, when the scatterer is homogeneous or partially homogeneous. In these situations it is common to utilize the surface integral equations instead [9], [10]. The main benefit of surface integral equation formulations compared to the V-EFIE is in confinement of the unknown field quantities to the boundaries of material interfaces, the property which greatly reduces the computational complexity associated with their numerical solution. For the purpose of discussion in this paper, however, it is important to note that the traditional surface integral equations [9], [10] have two unknown functions, tangential electric and magnetic fields, on the boundary of material domains with different physical parameters. These surface IEs also feature first and/or second order derivatives acting on their kernels. In the quest to further reduce the computational complexity, alternative single-source surface integral equation (SSIE) formulations have been also

introduced [11–16] that utilize only a single unknown current density at the material boundaries. These formulations though come at a price of having a large number of independent kernels as well as their products rendering the numerical solutions difficult. Due to this large number of operator products, the SSIEs may produce higher computational complexity compared with the standard Muller or PMCHWT (formulation proposed by Poggio, Miller, Chang, Harrington, Wu and Tsai) equations despite the latter having two unknown surface currents.

To further simplify evaluation of electromagnetic fields in the presence of penetrable objects, in this work we propose an alternative single-source surface integral equation. The new formulation features a single unknown current density similar to other SSIEs [11–16] but has only a single product of integral operators. These operators also have an additional advantage of being derivative free. The absence of the derivative comes as an important property if the kernels are available only through a numerical evaluation procedure as, for example, in the case of multilayered media [1]. Such derivatives act as amplifiers of the numerical error, and their presence greatly increases the accuracy requirements on the evaluation of already computationally demanding Sommerfeld integrals [1, 22].

In the derivation of the new surface integral equation, we start from the traditional V-EFIE. Assuming the material properties of the scatterer homogeneous, we can represent the electric field at any point inside the scatter as a superposition of the elementary cylindrical waves emanating from the scatterer's boundary. Such electric field representation is in the form of the surface integral of the product of a surface current density multiplied with the Green's function also known as single-layer ansatz [17], which is different from that of the traditional field representation via the equivalence principle [18]. In the latter both tangential electric and magnetic fields participate in the formation of the electric field. In the single-layer ansatz representation of the field, however, the surface current density has no apparent relationship to either electric and magnetic field on the surface. It has the meaning of merely being a weighting function for the elementary waves emanating from the surface and each satisfying the Helmholtz equation inside the scatterer. This single-source representation of the field upon substitution of the V-EFIE followed by the restriction of its observation domain to the scatter's surface reduces the V-EFIE to a single-source surface integral equation. Due to the nature of field translations in the resultant integral equation, we further term it as the Surface-Volume-Surface Electric Field Integral Equation (SVS-EFIE). The approach described above has proven to be applicable for both problems of magneto-quasistatics [19], [20] as well as to the full-wave problems of scattering on penetrable objects. The latter applications are originally described in the present paper and constitute a major extension to our prior work published in [19], [20].

5.2 Novel Single-Source Surface-Volume-Surface Integral Equation Formulation

5.2.1 Magnetostatics Formulation

The electric field $\mathbf{E} = \hat{\mathbf{z}}E_z$ inside a 2-D conductor of arbitrary cross-section S having invariant bulk conductivity σ along the coordinate z and linear variation of electrostatic potential ϕ along the same coordinate is governed by the following V-EFIE of magneto-quasistatics [2], [3]

$$E_z(\boldsymbol{\rho}) + i\omega\mu_0\sigma \iint_S G_0^{qs}(\boldsymbol{\rho}, \boldsymbol{\rho}') E_z(\boldsymbol{\rho}') ds' = -\frac{d\phi}{dz}, \boldsymbol{\rho} \in S, \quad (5.1)$$

where ω is the cyclic frequency, $i = \sqrt{-1}$, $\boldsymbol{\rho}$ and $\boldsymbol{\rho}'$ are the observation and source points in the conductor's cross-section, respectively, $G_0^{qs}(\boldsymbol{\rho}, \boldsymbol{\rho}') = -\frac{1}{2\pi} \ln(|\boldsymbol{\rho} - \boldsymbol{\rho}'|)$ is the 2D Green's function of the vacuum exterior to the conductor $-\frac{i}{4}H_0^{(2)}(k_0|\boldsymbol{\rho} - \boldsymbol{\rho}'|)$ under quasi-static assumption $k_0|\boldsymbol{\rho} - \boldsymbol{\rho}'| \ll 1$, μ_0 , ε_0 , and $k_0 = \omega\sqrt{\mu_0\varepsilon_0}$ are the permeability, permittivity, and wavenumber of vacuum, respectively. The constant derivative of linearly varying scalar potential with respect to the coordinate z in the right-hand side of V-EFIE (5.1) is commonly termed as per-unit-length (p.u.l.) voltage drop [4] along the wire $V_{p.u.l.} = -\frac{d\phi}{dz}$.

Assuming the bulk conductivity σ homogeneous throughout the conductor cross-section and taking into consideration the fact that the electric field E_z inside the conductor satisfies the homogeneous Helmholtz equation

$$\nabla^2 E_z(\boldsymbol{\rho}) + k_\sigma^2 E_z(\boldsymbol{\rho}) = 0, \boldsymbol{\rho} \in S, \quad (5.2)$$

we express the E -field in the conductor cross-section as a superposition of cylindrical waves emanating from its boundary

$$E_z(\boldsymbol{\rho}) = -i\omega\mu_0 \int_{\partial S} G_\sigma(\boldsymbol{\rho}, \boldsymbol{\rho}') J_z(\boldsymbol{\rho}') d\boldsymbol{\rho}', \boldsymbol{\rho} \in S. \quad (5.3)$$

In (5.3), $J_z(\boldsymbol{\rho}')$ is an auxiliary surface current density that plays a role of a weighting function for the elementary cylindrical waves $G_\sigma(\boldsymbol{\rho}, \boldsymbol{\rho}') = -\frac{i}{4} H_0^{(2)}(k_\sigma |\boldsymbol{\rho} - \boldsymbol{\rho}'|)$ emanating from the surface S , $H_0^{(2)}$ is the second kind Hankel function of zero-th order [21]. The latter satisfies the Helmholtz equation

$$\nabla^2 G_\sigma(\boldsymbol{\rho}, \boldsymbol{\rho}') + k_\sigma^2 G_\sigma(\boldsymbol{\rho}, \boldsymbol{\rho}') = 0 \quad (5.4)$$

at the points in the cross-section S excluding the boundary ∂S containing the source points $\boldsymbol{\rho}'$. In (5.2)–(5.4), $k_\sigma = -i\sqrt{i\omega\mu_0\sigma}$ is the wavenumber of the conductor material. It's important to note that the integral field representation (5.3), called single layer ansatz [17], is different from that of the standard equivalence principle

$$E_z(\boldsymbol{\rho}) = i\omega\mu_\sigma \int_{\partial S} G_\sigma(\boldsymbol{\rho}, \boldsymbol{\rho}') J_z^e(\boldsymbol{\rho}') d\boldsymbol{\rho}' + \int_{\partial S} \frac{\partial G_\sigma(\boldsymbol{\rho}, \boldsymbol{\rho}')}{\partial n} J_t^m(\boldsymbol{\rho}') d\boldsymbol{\rho}', \boldsymbol{\rho} \in S. \quad (5.5)$$

The field representation (5.5) utilizes both equivalent electric current density J_z^e and magnetic current density J_t^m for the field representation inside the conductor. In subsequent discussion of the numerical results the auxiliary surface current density J_z in (5.3) is depicted against the electric and magnetic current densities $J_z^{e,m}$ for TM_z wave scattering from a single dielectric cylinder, showing that there is no apparent relationship between the auxiliary surface current density J_z and tangential electric and magnetic field components $J_z^{e,m}$. It can be shown also that auxiliary surface current density J_z cannot be represented as a superposition of the equivalent electric current density J_z^e and magnetic current density J_t^m either.

Substitution of the (5.3) into (5.1) followed by the restriction of the observation domain to the conductor surface produces a single-source integral equation with respect to the unknown auxiliary surface current density J_z as follows:

$$-i\omega\mu_0 \int_{\partial S} G_\sigma(\boldsymbol{\rho}, \boldsymbol{\rho}') J_z(\boldsymbol{\rho}') d\boldsymbol{\rho}' - \sigma(\omega\mu_0)^2 \times \\ \int_{\partial S} \left[\iint_S G_0^{qs}(\boldsymbol{\rho}, \boldsymbol{\rho}') G_\sigma(\boldsymbol{\rho}, \boldsymbol{\rho}'') ds' \right] J_z(\boldsymbol{\rho}'') d\boldsymbol{\rho}'' = -V_{p.u.l.}, \quad \boldsymbol{\rho} \in \partial S. \quad (5.6)$$

Using the following notation for the integral operators entering in (5.6)

$$\mathcal{T}_\sigma^{\partial S, \partial S} \circ J_z = -i\omega\mu_0 \int_{\partial S} G_\sigma(\boldsymbol{\rho}, \boldsymbol{\rho}') J_z(\boldsymbol{\rho}') d\boldsymbol{\rho}', \quad \boldsymbol{\rho} \in \partial S, \quad (5.7)$$

$$\mathcal{T}_\sigma^{S, \partial S} \circ J_z = -i\omega\mu_0 \int_{\partial S} G_\sigma(\boldsymbol{\rho}, \boldsymbol{\rho}') J_z(\boldsymbol{\rho}') d\boldsymbol{\rho}', \quad \boldsymbol{\rho} \in S, \quad (5.8)$$

$$\mathcal{T}_0^{\partial S, S} \circ E_z = -i\omega\mu_0 \iint_S G_0^{qs}(\boldsymbol{\rho}, \boldsymbol{\rho}') E_z(\boldsymbol{\rho}') ds', \quad \boldsymbol{\rho} \in \partial S, \quad (5.9)$$

we can re-write IE (5.6) in the concise operator form as

$$\mathcal{T}_\sigma^{\partial S, \partial S} \circ J_z + \sigma \mathcal{T}_0^{\partial S, S} \circ \mathcal{T}_\sigma^{S, \partial S} \circ J_z = -V_{p.u.l.} \quad (5.10)$$

The derived integral equation is termed the Surface-Volume-Surface EFIE (SVS-EFIE) [19], [20] due to the nature of the field translation operations from the surface of conductor to its volume and subsequent translation of the field back to the surface as expressed by the product of integral operators $\mathcal{T}_0^{\partial S, S} \circ \mathcal{T}_\sigma^{S, \partial S}$. The SVS-EFIE is rigorous since it forces the field to satisfy the Helmholtz equations both inside and outside the conductor as well as satisfies the continuity of tangential field components at the conductor boundary, which is inherent to the V-EFIE (5.1). The SVS-EFIE also comes with the benefit of being free of derivatives acting on the kernels. This property becomes important when conductor is situated in multilayered media for which the Green's function is only available through the numerical evaluation [1], [22] and the derivatives act as numerical noise amplifiers. The new integral equation (5.10) also contains only a single unknown surface function J_z as opposed to the traditional surface integral equations based on the equivalence principle field representation (5.5) requiring two unknown functions J_z^e and J_t^m . These benefits, however, come at the price of having the conductor's volume as the intermediate range and domain in the product of the operators which requires both volume and surface discretization in the MoM solution, as shown in Section 5.3.

5.2.2 Full-Wave Formulation

Similar new single-source integral equation can be derived from the V-EFIE for full-wave scattering problems. Consider a 2D TM-scattering problem for a dielectric

cylinder directed along z -coordinate and having arbitrary cross-section with area S .

The V-EFIE in the electrodynamic case is written as [1], [23]

$$E_z(\boldsymbol{\rho}) - k_0^2(\epsilon - 1) \iint_S G_0(\boldsymbol{\rho}, \boldsymbol{\rho}') E_z(\boldsymbol{\rho}') ds' = E_z^{inc}(\boldsymbol{\rho}), \boldsymbol{\rho} \in S, \quad (5.11)$$

where E_z is the unknown distribution of the field inside the cylinder,

$$G_0(\boldsymbol{\rho}, \boldsymbol{\rho}') = -\frac{i}{4} H_0^{(2)}(k_0 |\boldsymbol{\rho} - \boldsymbol{\rho}'|)$$

is the Green's function of free space, $\epsilon = \varepsilon + \sigma/(i\omega\varepsilon_0) = \varepsilon(1 - i\tan\delta)$ is the complex relative permittivity of the dielectric cylinder, and E_z^{inc} is the incident field impinging on the cylinder.

Similar to the magnetostatic case, we represent the distribution of the field inside the cylinder E_z satisfying the Helmholtz equation $\nabla^2 E_z + k_\epsilon^2 E_z = 0$ as a superposition of cylindrical waves emanating from the cylinder's surface and having the strength defined with the function $J_z(\boldsymbol{\rho}')$ playing the role of an auxiliary surface current density

$$E_z(\boldsymbol{\rho}) = -i\omega\mu_0 \int_{\partial S} G_\epsilon(\boldsymbol{\rho}, \boldsymbol{\rho}') J_z(\boldsymbol{\rho}') d\boldsymbol{\rho}', \boldsymbol{\rho} \in S. \quad (5.12)$$

In (5.12), $G_\epsilon(\boldsymbol{\rho}, \boldsymbol{\rho}') = -\frac{i}{4} H_0^{(2)}(k_\epsilon |\boldsymbol{\rho} - \boldsymbol{\rho}'|)$ is the Green's function of the dielectric media with the wavenumber $k_\epsilon = \omega\sqrt{\mu_0\varepsilon_0\epsilon}$ satisfying the Helmholtz equation $\nabla^2 G_\epsilon + k_\epsilon^2 G_\epsilon = 0$ everywhere in S excluding the boundary ∂S . Once again, we emphasize here that the weighted superposition of cylindrical waves (5.12) is different from the equivalence principle field representation in terms of the tangential field components on the boundary of the cylinder.

Substitution of (5.12) into (5.11) followed by the restriction of the observation

domain to the conductor surface yields the desired SVS-EFIE with respect to the unknown current density

$$\begin{aligned} & -i\omega\mu_0 \int_{\partial S} G_\epsilon(\boldsymbol{\rho}, \boldsymbol{\rho}') J_z(\boldsymbol{\rho}') d\boldsymbol{\rho}' + i\omega\mu_0 k_0^2 (\epsilon - 1) \times \\ & \quad \int_{\partial S} \left[\iint_S G_0(\boldsymbol{\rho}, \boldsymbol{\rho}') G_\epsilon(\boldsymbol{\rho}, \boldsymbol{\rho}'') ds' \right] J_z(\boldsymbol{\rho}'') d\boldsymbol{\rho}'' = E_z^{inc}(\boldsymbol{\rho}), \quad \boldsymbol{\rho} \in \partial S. \end{aligned} \quad (5.13)$$

In the operator form the above SVS-EFIE is expressed as follows:

$$T_\epsilon^{\partial S, \partial S} \circ J_z + T_0^{\partial S, S} \circ T_\epsilon^{S, \partial S} \circ J_z = E_z^{inc}, \quad (5.14)$$

where the integral operators are defined as

$$T_\epsilon^{\partial S, \partial S} \circ J_z = -i\omega\mu_0 \int_{\partial S} G_\epsilon(\boldsymbol{\rho}, \boldsymbol{\rho}') J_z(\boldsymbol{\rho}') d\boldsymbol{\rho}', \quad \boldsymbol{\rho} \in \partial S, \quad (5.15)$$

$$T_\epsilon^{S, \partial S} \circ J_z = -i\omega\mu_0 \int_{\partial S} G_\epsilon(\boldsymbol{\rho}, \boldsymbol{\rho}') J_z(\boldsymbol{\rho}') d\boldsymbol{\rho}', \quad \boldsymbol{\rho} \in S, \quad (5.16)$$

$$T_0^{\partial S, S} \circ E_z = k_0^2 (\epsilon - 1) \iint_S G_0(\boldsymbol{\rho}, \boldsymbol{\rho}') E_z(\boldsymbol{\rho}') ds', \quad \boldsymbol{\rho} \in \partial S. \quad (5.17)$$

5.3 Method of Moments Discretization

The MoM discretization of the SVS-EFIE (5.6) for magneto-quasistatics was discussed in details in [20] for the case of a coaxial cable model featuring a multi-connected domain formed by the outer shell and a single-connected domain formed by the cable's inner conductor. In this paper we present a similar detailed description of the MoM discretization for the case of the full-wave SVS-EFIE (5.13), (5.14) applied to the problem of TM_z wave scattering on a pair of dielectric cylinders of an arbitrary cross-section depicted in Fig. 5.1.

The range of the integral operator $\mathbf{T}_\epsilon^{S,\partial S}$ in (5.16) mapping the auxiliary surface current density \mathbf{J}_z to the volumetric polarization current $j_z = k_0^2(\epsilon - 1)\mathbf{E}_z$ is on the cross-section of the scatterers S_A and S_B . The same is true for the domain of the operator $\mathbf{T}_0^{\partial S,S}$ in (5.17), which maps the polarization current j_z to the scattered electric field \mathbf{E}_z^{scat} . These cross-sections are therefore discretized with a volumetric mesh consisting of $N_A + N_B$ triangular elements. The surfaces of the scatters ∂S_A and ∂S_B forming the ranges and domains of the remaining operators in the SVS-EFIE (5.13), (5.14) are discretized with M_A and M_B linear elements, respectively. Depiction of the combined volumetric and surface meshes is shown in Fig. 5.1.

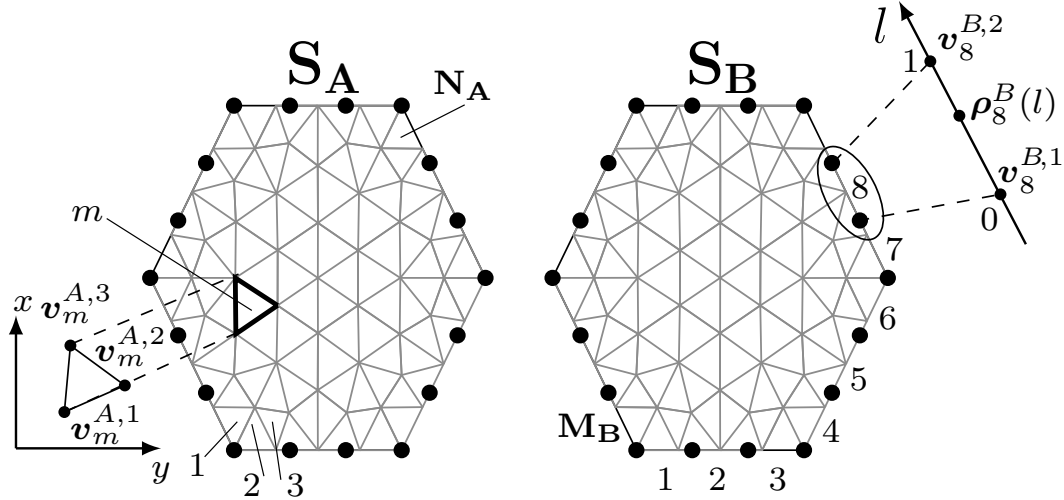


Figure 5.1: Volume and surface meshes utilized in the MoM discretization of the SVS-EFIE (5.13). © 2013 IEEE.

It is important to mention here that while in our previous work [19], [20] the size of the volume and surface meshes were reported to be independent, our further studies have shown that choosing these meshes independently is suboptimal. To obtain the minimum error, the sizes of the surface and volume meshes must be related to both the frequency and each other. Quantitative description of the error dependence on the mesh sizes is presented in Section 5.4.

The radius-vector on m th straight element of the mesh discretizing surfaces ∂S_α is defined parametrically as

$$\rho_m^\alpha(l) = \mathbf{v}_m^{\alpha,1} + l(\mathbf{v}_m^{\alpha,2} - \mathbf{v}_m^{\alpha,1}), \quad l \in [0, 1], \quad \alpha = A, B, \quad (5.18)$$

where $\mathbf{v}_m^{\alpha,2}$ and $\mathbf{v}_m^{\alpha,1}$ are the vertices of m th element on ∂S_α , L_m^α is its length $|\mathbf{v}_m^{\alpha,2} - \mathbf{v}_m^{\alpha,1}|$, and $m = 1, \dots, M_\alpha$.

Similarly, the position-vector on m th triangular element of the cross-section S_β is

defined parametrically in the barycentric coordinates [18] as

$$\boldsymbol{\rho}_m^\beta(\xi, \eta) = \mathbf{v}_m^{\beta,1}\xi + \mathbf{v}_m^{\beta,2}\eta + \mathbf{v}_m^{\beta,3}(1 - \xi - \eta), \quad \xi, \eta \in [0, 1], \quad (5.19)$$

where $\xi + \eta \leq 1$, $\beta = A, B$ is the scatterer's label, $\mathbf{v}_m^{\beta,1}, \mathbf{v}_m^{\beta,2}, \mathbf{v}_m^{\beta,3}$ are the m th element vertices, and $m = 1, \dots, N_\beta$.

5.3.1 MoM discretization of SVS-EFIE's surface-to-volume

operator $T_\epsilon^{S, \partial S}$

Discretization of the unknown surface current densities J_z^A and J_z^B on the scatterer's sub-surfaces ∂S_A and ∂S_B is performed using the piece-wise basis functions [24]

$$J^\alpha(\boldsymbol{\rho}'') \cong \sum_{m=1}^{M_\alpha} I_m^\alpha P_m^\alpha(\boldsymbol{\rho}''), \quad P_m^\alpha(\boldsymbol{\rho}'') = \begin{cases} 1, & \boldsymbol{\rho}'' \in \partial S_{\alpha,m} \\ 0, & \boldsymbol{\rho}'', \notin \partial S_{\alpha,m} \end{cases}, \quad (5.20)$$

$\alpha = A, B$ being the sub-surface label, and $\partial S_{\alpha,m}$ denoting the m th surface mesh element on ∂S_α . In (5.20) and throughout this Section, the subscript z denoting the component of the currents and fields is omitted for brevity. As testing functions we use delta-functions positioned at the centroid of the volumetric mesh triangles

$$t_{n'}^\beta(\boldsymbol{\rho}) = \delta(\boldsymbol{\rho} - \boldsymbol{\rho}_{n'}^\beta(1/3, 1/3)). \quad (5.21)$$

In (5.21), $\boldsymbol{\rho}_{n'}^\beta(1/3, 1/3)$ is the radius-vector to the centroid of the n' th volume element in S_β cross-section.

Substitution of (5.20) into the operator relation $j = T_\epsilon^{S, \partial S} \circ J$ in (5.16) followed by the point-sampling of polarization current j in its range with test functions (5.21)

casts (5.16) into the following matrix form

$$\begin{bmatrix} \mathbf{i}^A \\ \mathbf{i}^B \end{bmatrix} = \begin{bmatrix} \mathbf{Z}_\epsilon^{S_A, \partial S_A} & 0 \\ 0 & \mathbf{Z}_\epsilon^{S_B, \partial S_B} \end{bmatrix} \cdot \begin{bmatrix} \mathbf{I}^A \\ \mathbf{I}^B \end{bmatrix}. \quad (5.22)$$

In (5.22), $\mathbf{I} = [I_1^A, \dots, I_{M_A}^A; I_1^B, \dots, I_{M_B}^B]^T$ is the vector of unknown current expansion coefficients in (5.20), and vector $\mathbf{i} = [i_1^A, \dots, i_{N_A}^A; i_1^B, \dots, i_{N_B}^B]^T$ contains the N values of polarization current j at the $N_A + N_B$ centroids of the triangle mesh elements discretizing cross-section of the scatterers S_A and S_B . The matrix elements in (5.22) are the inner products [24]

$$Z_{\epsilon, n' m''}^{S_\beta, \partial S_\alpha} = \langle t_{n'}^\beta, \mathbf{T}_\epsilon^{S_\beta, \partial S_\alpha} \circ P_{m''}^\alpha \rangle = -i\omega\mu_0 L_{m''}^\alpha \int_0^1 G_\epsilon(\boldsymbol{\rho}_{n'}^\beta(1/3, 1/3), \boldsymbol{\rho}_{m''}^\alpha(l'')) dl'', \quad (5.23)$$

where $n' = 1, \dots, N_\alpha$ are the indexes of the surface elements on ∂S_α , and $m'' = 1, \dots, M_\beta$ are the indexes of the volume elements in S_β . Parametric definitions of position-vectors on the surface and volume elements in (5.23) are given in (5.18) and (5.19), respectively.

The evaluation of line integrals in (5.23) can be done to desired precision using standard Gauss-Legendre Q -point quadrature rules [25] with weights w_q and abscissas l_q , $q = 1, \dots, Q$, applied to the integrand after its singular part $-\frac{1}{2\pi} \ln |\boldsymbol{\rho} - \boldsymbol{\rho}'|$ has been extracted

$$Z_{\epsilon, n' m''}^{S_\beta, \partial S_\alpha} = i\omega\mu_0 L_{m''}^\alpha \int_0^1 \frac{\ln |\boldsymbol{\rho}_{n'}^\beta(1/3, 1/3) - \boldsymbol{\rho}_{m''}^\alpha(l'')|}{2\pi} dl'' - i\omega\mu_0 L_{m''}^\alpha \sum_{q=1}^Q w_q \times \\ \left[G_\epsilon(\boldsymbol{\rho}_{n'}^\beta(1/3, 1/3), \boldsymbol{\rho}_{m''}^\alpha(l_q)) + \frac{\ln |\boldsymbol{\rho}_{n'}^\beta(1/3, 1/3) - \boldsymbol{\rho}_{m''}^\alpha(l_q)|}{2\pi} \right]. \quad (5.24)$$

The integral of logarithmic function over a linear element can be evaluated analytically for an arbitrary observation point location using the technique in [26].

5.3.2 MoM discretization of SVS-EFIE's volume-to-surface

operator $T_0^{\partial S, S}$

Discretization of the domain of the volume-to-surface integral operator $T_0^{\partial S, S}$ in (5.17), which maps the volumetric polarization current density $j = k_0^2(\epsilon - 1)E$ inside the scatterer volume S to the scattered electric field $E^{scat} = -i\omega\mu_0 \int_S G_0 j ds'$ on scatterer's surface ∂S , is performed using pulse basis functions [10], [24] defined on the volumetric mesh

$$j^\beta(\boldsymbol{\rho}') \cong \sum_{n=1}^{N_\beta} i_n^\beta p_n^\beta(\boldsymbol{\rho}'), \quad p_n^\beta(\boldsymbol{\rho}') = \begin{cases} 1, & \boldsymbol{\rho}' \in S_{\beta,n} \\ 0, & \boldsymbol{\rho}' \notin S_{\beta,n} \end{cases}, \quad (5.25)$$

where $S_{\beta,n}$, $n = 1, \dots, N_\beta$ are the volumetric mesh elements and $\beta = A, B$ is the index identifying the sub-volume S_β of the scatterer's cross-section. The range of the $T_0^{\partial S, S}$ operator is tested with delta-functions [10], [24]

$$T_m^\alpha(\boldsymbol{\rho}) = \delta(\boldsymbol{\rho} - \boldsymbol{\rho}_m^\alpha(1/2)), \quad (5.26)$$

positioned at the centroids of m th elements in the surface discretization of the scatterer's boundary ∂S_α . Here, α is the index of a sub-scatterer ∂S_α , and $m = 1, \dots, M_\alpha$ are the indexes of the surface elements in ∂S_α .

Substitution of the volume polarization current j expansion (5.25) into its integral relation to the scattered field $E^{scat} = T_0^{\partial S, S} \circ j$ in (5.17) produces the following matrix

relationship

$$\begin{bmatrix} \mathbf{E}^{scat,A} \\ \mathbf{E}^{scat,B} \end{bmatrix} = \begin{bmatrix} \mathbf{Z}_0^{\partial S_A, S_A} & \mathbf{Z}_0^{\partial S_A, S_B} \\ \mathbf{Z}_0^{\partial S_B, S_A} & \mathbf{Z}_0^{\partial S_B, S_B} \end{bmatrix} \cdot \begin{bmatrix} \mathbf{i}^A \\ \mathbf{i}^B \end{bmatrix}, \quad (5.27)$$

where $\mathbf{E}^{scat} = [E_1^{scat,A}, \dots, E_{M_A}^{scat,A}; E_1^{scat,B}, \dots, E_{M_B}^{scat,B}]^T$ is a vector of M samples of the scattered electric field E^{scat} produced at the centroids of the surface mesh elements by the polarization current j , and the matrix elements in (5.27) are defined as the inner products

$$Z_{0,mn'}^{\partial S_\alpha, S_\beta} = \langle T_m^\alpha, T_0^{\partial S_\alpha, S_\beta} \circ p_{n'}^\alpha \rangle = -i\omega\mu_0 2A_{n'}^\beta \int_0^1 \int_0^{1-\eta'} G_0(\boldsymbol{\rho}_m^\alpha(1/2), \boldsymbol{\rho}_{n'}^\beta(\xi', \eta')) d\xi' d\eta'. \quad (5.28)$$

In order to match discretized range of the $T_\epsilon^{S, \partial S}$ (5.16), which is sampled with the test delta-functions (5.21) to the discretized domain of the $T_0^{\partial S, S}$ (5.17) expanded over piece-wise basis functions (5.25), the integral over triangular area is approximated with the one-point quadrature rule as follows:

$$Z_{0,mn'}^{\partial S_\alpha, S_\beta} \cong -i\omega\mu_0 A_{n'}^\beta G_0[\boldsymbol{\rho}_m^\alpha(1/2), \boldsymbol{\rho}_{n'}^\beta(1/3, 1/3)]. \quad (5.29)$$

We note that the adopted discretization procedure chosen here for the domain of operator $T_0^{S,\partial S}$ can be viewed as taking delta-functions as the basis functions (5.25) instead of taking the piece wise basis functions and selecting the single-point integration quadrature over the volume elements. Alternative choices for the basis and testing functions are also possible [10], [24]. In the general case, however, when the domain of $T_0^{\partial S,S}$ is expanded over a different basis than the range of the operator $T_\epsilon^{S,\partial S}$, the product of operators $T_0^{\partial S,S} \circ T_\epsilon^{S,\partial S}$ requires the appropriate Gramian matrix [27] affecting the conversion of spaces spanning the domain of $T_0^{\partial S,S}$ and the range of $T_\epsilon^{S,\partial S}$.

5.3.3 MoM discretization of SVS-EFIE's surface-to-surface operator $T_\epsilon^{\partial S,\partial S}$

The representation of the electric field inside the scatter as a superposition of cylindrical waves (5.12) has the form of a global surface impedance operator $T_\epsilon^{\partial S,\partial S}$ relating the auxiliary surface current density \mathbf{J} to the electric field \mathbf{E} as formalized by (5.15). Both domain and range of $T_\epsilon^{\partial S,\partial S}$ are at the scatterer's surface ∂S . Discretizing the domain of $T_\epsilon^{\partial S,\partial S}$ over piece-wise basis functions as in (5.20) and testing the total electric field in its range with the delta-functions (5.26), we cast the surface impedance operator into a matrix form

$$\begin{bmatrix} \mathbf{E}^A \\ \mathbf{E}^B \end{bmatrix} = \begin{bmatrix} \mathbf{Z}_\epsilon^{\partial S_A, \partial S_A} & 0 \\ 0 & \mathbf{Z}_\epsilon^{\partial S_B, \partial S_B} \end{bmatrix} \cdot \begin{bmatrix} \mathbf{I}^A \\ \mathbf{I}^B \end{bmatrix}. \quad (5.30)$$

In (5.30), vector $\mathbf{E} = [E_1^A, \dots, E_{M_A}^A; E_1^B, \dots, E_{M_B}^B]^T$ contains M samples of the electric field E at the centroids of the surface mesh elements on the scatterer's surface ∂S ,

and the inner products defining the matrix elements in (5.30) are

$$Z_{\epsilon,mm'}^{\partial S_\alpha, \partial S_{\alpha'}} = \langle T_m^\alpha, \mathbf{T}_\epsilon^{\partial S, \partial S} \circ P_{m'}^{\alpha'} \rangle = -i\omega\mu_0 L_{m'}^{\alpha'} \int_0^1 G_\epsilon(\boldsymbol{\rho}_m^\alpha(1/2), \boldsymbol{\rho}_{m'}^{\alpha'}(l')) dl', \quad (5.31)$$

where $\alpha, \alpha' = A, B$ are indexes of scatterer's sub-surfaces,

$m=1, \dots, M_\alpha$, and $m'=1, \dots, M_{\alpha'}$. The singular integrals in (5.31) are handled via singularity extraction similar to (5.24)

$$\begin{aligned} Z_{\epsilon,mm'}^{\partial S_\alpha, \partial S_{\alpha'}} &= i\omega\mu_0 L_{m'}^{\alpha'} \int_0^1 \frac{\ln |\boldsymbol{\rho}_m^\alpha(1/2) - \boldsymbol{\rho}_{m'}^{\alpha'}(l')|}{2\pi} dl' - i\omega\mu_0 L_{m'}^{\alpha'} \sum_{q=1}^Q w_q \times \\ &\left[G_\epsilon(\boldsymbol{\rho}_m^\alpha(1/2), \boldsymbol{\rho}_{m'}^{\alpha'}(l'_q)) + \frac{\ln |\boldsymbol{\rho}_m^\alpha(1/2) - \boldsymbol{\rho}_{m'}^{\alpha'}(l'_q)|}{2\pi} \right]. \end{aligned} \quad (5.32)$$

Alternatively, the singular integrals can be handled using specially developed quadrature rules [28].

5.3.4 Matrix form of MoM discretized SVS-EFIE:

The MoM discretization of the integral operators $\mathbf{T}_\epsilon^{S,\partial S}$, $\mathbf{T}_0^{\partial S,S}$, $\mathbf{T}_\epsilon^{\partial S,\partial S}$ in the SVS-EFIE (5.13) produces corresponding matrix relations (5.22), (5.27), (5.30). As a result, the SVS-EFIE is reduced to the following set of linear algebraic equations with respect to the $(M \times 1)$ vector of unknown coefficients \mathbf{I} in the expansion of the auxiliary surface current density (5.20)

$$(\mathbf{Z}_\epsilon^{\partial S,\partial S} + \mathbf{Z}_0^{\partial S,S} \cdot \mathbf{Z}_\epsilon^{S,\partial S}) \cdot \mathbf{I} = \mathbf{V}. \quad (5.33)$$

$$\begin{aligned}
& \left(\begin{array}{c} \mathbf{Z}_\epsilon^{\partial S, \partial S} \\ \hline M \end{array} \right) + \left(\begin{array}{c} \mathbf{Z}_0^{\partial S, S} \\ \hline N \end{array} \right) \cdot \left(\begin{array}{c} \mathbf{Z}_\epsilon^{S, \partial S} \\ \hline M \end{array} \right) \cdot \mathbf{I} \\
& M \left\{ \begin{array}{c} M_A \left\{ \begin{array}{c|c} \mathbf{Z}_\epsilon^{\partial S_A, \partial S_A} & \mathbf{0} \\ \hline \mathbf{0} & \mathbf{Z}_\epsilon^{\partial S_B, \partial S_B} \end{array} \right\} \\ \hline M_B \left\{ \begin{array}{c|c} \mathbf{0} & \mathbf{Z}_\epsilon^{\partial S_A, \partial S_B} \\ \hline \mathbf{Z}_\epsilon^{\partial S_B, \partial S_A} & \mathbf{0} \end{array} \right\} \end{array} \right\} + \left(\begin{array}{c} \mathbf{Z}_0^{\partial S_A, S_A} \quad \mathbf{Z}_0^{\partial S_A, S_B} \\ \hline \mathbf{Z}_0^{\partial S_B, S_A} \quad \mathbf{Z}_0^{\partial S_B, S_B} \end{array} \right) \cdot \left\{ \begin{array}{c} M_A \left\{ \begin{array}{c|c} \mathbf{Z}_\epsilon^{S_A, \partial S_A} & \mathbf{0} \\ \hline \mathbf{0} & \mathbf{Z}_\epsilon^{S_B, \partial S_B} \end{array} \right\} \\ \hline M_B \left\{ \begin{array}{c|c} \mathbf{0} & \mathbf{Z}_\epsilon^{S_A, \partial S_B} \\ \hline \mathbf{Z}_\epsilon^{S_B, \partial S_A} & \mathbf{0} \end{array} \right\} \end{array} \right\} N_A \cdot \left\{ \begin{array}{c} \mathbf{I}^A \\ \hline \mathbf{I}^B \end{array} \right\} M
\end{aligned}$$

Figure 5.2: Matrix form (5.33) of the SVS-EFIE (5.13) discretized with the MoM utilizing depicted volume and surface meshes. © 2013 IEEE.

The above matrix equation (5.33) can be solved either directly via LU decomposition [25] or iteratively using GMRES [29] or CG [30] algorithms. In case of the iterative solution, the matrix-vector products (MVP) pertinent to (5.33) can be accelerated via the Fast Multipole Method [31] or the FFT-based methods [32], [33]. The comparison of the computational complexity of different algorithms is given in Table 5.1. Computational time and memory requirements are described as a function of the number of unknowns M on the surface of the scatterer with the assumption that the cross-section is discretized with M^2 elements.

It is important to note that upon acceleration of the matrix-vector multiplies using FFT-based methods [32], [33], the proposed SVS-EFIE solution exhibits the same $O(M^2)$ computational complexity as the solution of the traditional surface IEs [9], [10]. In the traditional surface IE solutions the $O(M^2)$ complexity arises due to the usage of 2D FFT operations with the majority of 2D FFT grid samples populated with zeros due to the localization of the unknown currents on the scatterer's surface [6]. In the proposed method the $O(M^2)$ complexity arises naturally due to surface-to-volume and volume-to-surface field translations. The proposed SVS-EFIE features the same computational complexity as the traditional surface IEs if the field inside the scatterer is calculated. Moreover, the field inside obtained via SVS-EFIE is less expensive to compute, because it requires only M matrix vector products, since the matrix $\mathbf{Z}_\epsilon^{S,\partial S}$ associated with the surface-to-volume operator $\mathbf{T}_\epsilon^{S,\partial S}$ is already calculated and does not involve computationally expensive operations.

Table 5.1: Computational Complexity Comparison for Direct and Iterative Solution of the V-EFIE (5.11), SVS-EFIE (5.13), and PMCHWT [10] Equations. © 2013 IEEE.

	V-EFIE	SVS-EFIE	PMCHWT
Matrix Fill	$\mathbf{Z}^{S,S}$	$\mathbf{Z}^{S,\partial S}, \mathbf{Z}^{\partial S,S}$	$\mathbf{Z}^{\partial S,\partial S}$
LU [25]	$O(M^4)$	$O(M^3) + O(M^4)$	$O(M^2)$
Iterative (e.g. GMRES)		$O(M^3)$	
MVP	$\mathbf{Z}^{S,S} \cdot \mathbf{I}^S$	$\mathbf{Z}^{S,\partial S} \cdot \mathbf{I}^{\partial S}, \mathbf{Z}^{\partial S,S} \cdot \mathbf{I}^S$	$\mathbf{Z}^{\partial S,\partial S} \cdot \mathbf{I}^{\partial S}$
Direct [25]	$O(M^4)$	$O(M^3)$	$O(M^2)$
FMM aided [6]	$O(M^2)$	$O(M^2) + O(M^2)$	$O(M \log M)$
FFT aided [6]			$O(M^2)$
LU-solve	$O(M^6)$	$O(M^3)$	$O(M^3)$
Calculating the E-field inside S			
LU, Iterative	Available directly	$O(M^3)$	$O(M^3)$
FMM, FFT aided		$O(M^2)$	$O(M^2)$
Required Memory without Calculation of the E-field inside of S			
LU, Iterative	$O(M^4)$	$O(M^3)$	$O(M^2)$
FMM aided [6]	$O(M^2)$	$O(M^2)$	$O(M \log M)$
FFT aided [6]			$O(M^2)$
Required Memory with Calculation of the E-field inside of S			
LU, Iterative	$O(M^4)$	$O(M^3)$	$O(M^3)$
FMM, FFT aided	$O(M^2)$	$O(M^2)$	$O(M^2)$

5.4 Numerical Studies

Numerical studies for the magneto-quasistatic solution using the proposed SVS-EFIE were considered in detail in our prior publications [19], [20]. In [19], the MoM solution of the SVS-EFIE was compared against the analytic solution for the current flow in a homogeneous conductor of a circular cross-section at low, intermediate, and high frequencies. The other numerical examples include the MoM solutions for the single and multiple transmission line configurations with arbitrary cross-sections. This includes the coaxial cable transmission line, which features a cross-section with the topological multi-connectedness [20].

In this work we present numerical studies related to the electrodynamic formulation of the proposed SVS-EFIE. In the first numerical experiment we consider TM_z plane wave scattering from a single dielectric cylinder with the relative permittivity $\varepsilon = 11$ as shown in Fig. 5.3. The cylinder has a circular cross-section of the radius $\rho_0 = 25$ mm. The plane wave of the frequency $f = 2$ GHz and of electric field magnitude 1.0 V/m impinges on the cylinder at 45° angle. The surface current density \mathbf{J}_z is first obtained via the MoM solution (5.33) of the proposed SVS-EFIE (5.13) under the uniform discretization of the conductor surface with $M = 100$ linear segments and its volume with $N = 7,450$ triangular elements. In order to evaluate the electric field $E_z^{(1)}$ inside the cylinder cross-section, the auxiliary current \mathbf{J}_z is substituted into (5.12).

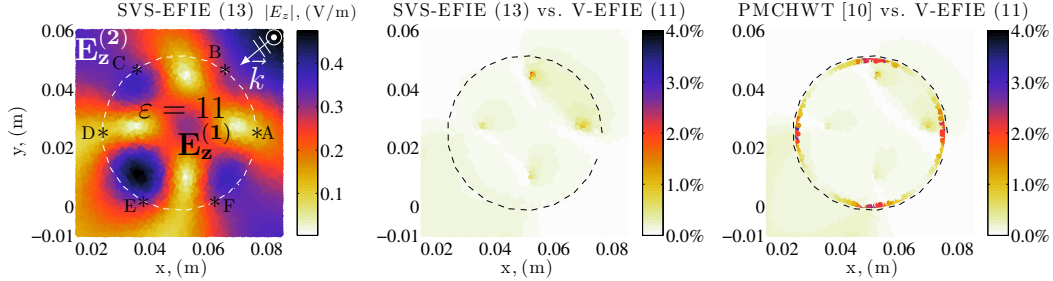


Figure 5.3: Distribution of the electric field inside $E_z^{(1)}$ and outside $E_z^{(2)}$ the dielectric cylinder obtained via MoM solution (5.33). The relative error of the latter (center plot) and the MoM solution of the PMCHWT surface IE solution (right plot) with respect to the volumetric MoM solution of the V-EFIE (5.11). Points A – F correspond to the points in the Fig. 5.4. © 2013 IEEE.

In Fig. 5.3, the E-field evaluated via the proposed SVS-EFIE (5.13) and the E-field from the classic PMCHWT solution [10] are compared against the traditional volumetric MoM solution of the V-EFIE (5.11). The field outside the dielectric body $E_z^{(2)}$ is calculated in two steps. First, the field in the volume of the scatterer is calculated using the single-layer ansatz relation (5.12). Second, the volumetric distribution of the field inside the scatterer is substituted into the volume equivalence principle to calculate the field outside. The relative error of the proposed V-EFIE solution with respect to the MoM solution of the volumetric IE (5.11) does not exceed 3.2% and has the mean of 0.136% and the standard deviation of 0.116%. In case of the PMCHWT solution, the relative error is bound by 3.3%, has the mean of 0.139% and the standard deviation of 0.198%.

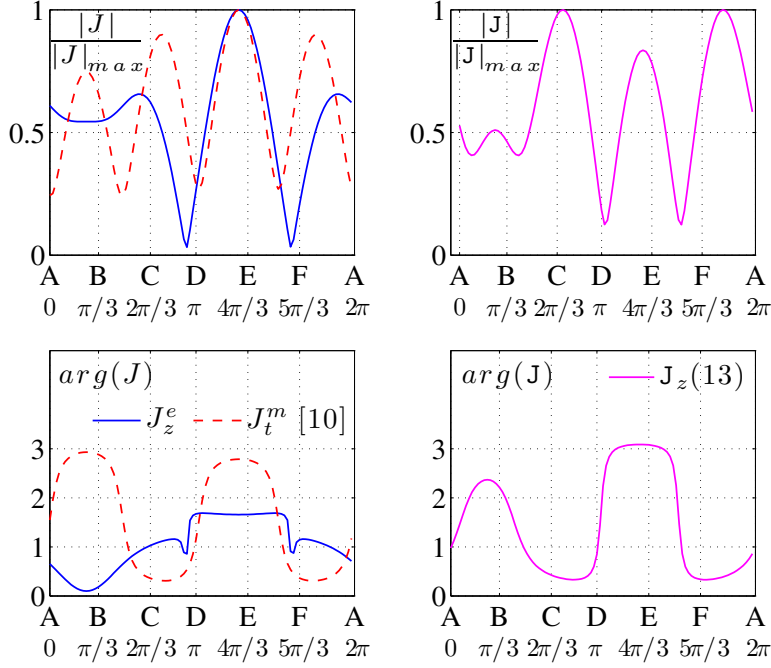


Figure 5.4: Equivalent electric and magnetic surface current densities (J_z^e , J_t^m on the left) obtained with the MoM solution of PMCHWT surface IE and the auxiliary surface current density (J_z on the right) obtained with the MoM solution of the proposed SVS-EFIE (5.13) for TM_z wave scattering from a single dielectric cylinder. Points A – F correspond to the points in the Fig. 5.3. © 2013 IEEE.

The equivalent electric current density J_z^e and magnetic current density J_t^m are also found with the MoM solution of the PMCHWT surface IE [10] on the same surface mesh. In Fig. 5.4, the current densities for both methods are shown along the surface of the cylinder's cross-section. From visual comparison in Fig. 5.4 of the equivalent electric and magnetic current densities J_z^e , J_t^m against the auxiliary surface current density J_z from the SVS-EFIE, it is clear that the latter has no apparent relationship to either J_z^e or J_t^m . The auxiliary current J_z is not a superposition of J_z^e and J_t^m . This becomes obvious from J_z behavior for the geometries featuring prominent geometric singularities in the cross-section, for which J_z remains a continuous function along the surface including the corner points where J_z^e , for example, becomes discontinuous.

The execution time and memory consumption for this experiment are shown in Table 5.2. The results were obtained for a Mathcad worksheet on a single Intel Core 2 Duo processor running at 2.4 GHz. All matrix-vector products were computed directly without using FMM or FFT based accelerators [6]. The solution for the field inside the dielectric cylinder was calculated for three meshes via the MoM solution of the V-EFIE (5.11), PMCHWT [10] and proposed SVS-EFIE (5.13). The execution time and memory consumtion for the case of the MoM solution of the V-EFIE for the 7,460-element mesh is projected from the data for the 1,890-element mesh according to the computational complexity of the operations. The behavior of the execution time and memory consumption data reflects the computational complexity analysis results from the previous section. The novel SVS-EFIE is faster than the V-EFIE at all steps and allows to compute the field inside the scatterer at the lower price than in case of the MoM solution of the PMCHWT surface IE.

Table 5.2: Computational Time and Memory for the Solution of the V-EFIE, SVS-EFIE, and PMCHWT Equations in Mathcad. © 2013 IEEE.

	V-EFIE (5.11)	PMCHWT [10]	SVS-EFIE (5.13)
M = 10 linear elements, N = 278 triangular elements			
Total Time	229.5 s	2.4 s	1.0 s
Fill Time	228.9 s	0.5 s	0.9 s
Solve Time	0.7 s	≈ 0.1 s	≈ 0.1 s
Field in S	—	1.9 s	≈ 0.1 s
Memory	13 Mb	≈ 1 Mb	≈ 1 Mb
M = 20, N = 1,890			
Total Time	≈ 4 hrs	26.3 s	8.8 s
Fill Time	≈ 4 hrs	1.6 s	8.7 s
Solve Time	28.7 s	≈ 0.1 s	≈ 0.1 s
Field in S	—	24.7 s	≈ 0.1 s
Memory	147 Mb	4 Mb	12 Mb
M = 100, N = 7,450			
Total Time	<i>2.5 days (projected)</i>	245.9 s	80.8 s
Fill Time	<i>2.5 days</i>	8.2 s	80.5 s
Solve Time	<i>7.5 m</i>	0.1 s	0.1 s
Field in S	—	237.7 s	0.2 s
Memory	<i>2 Gb</i>	40 Mb	82 Mb

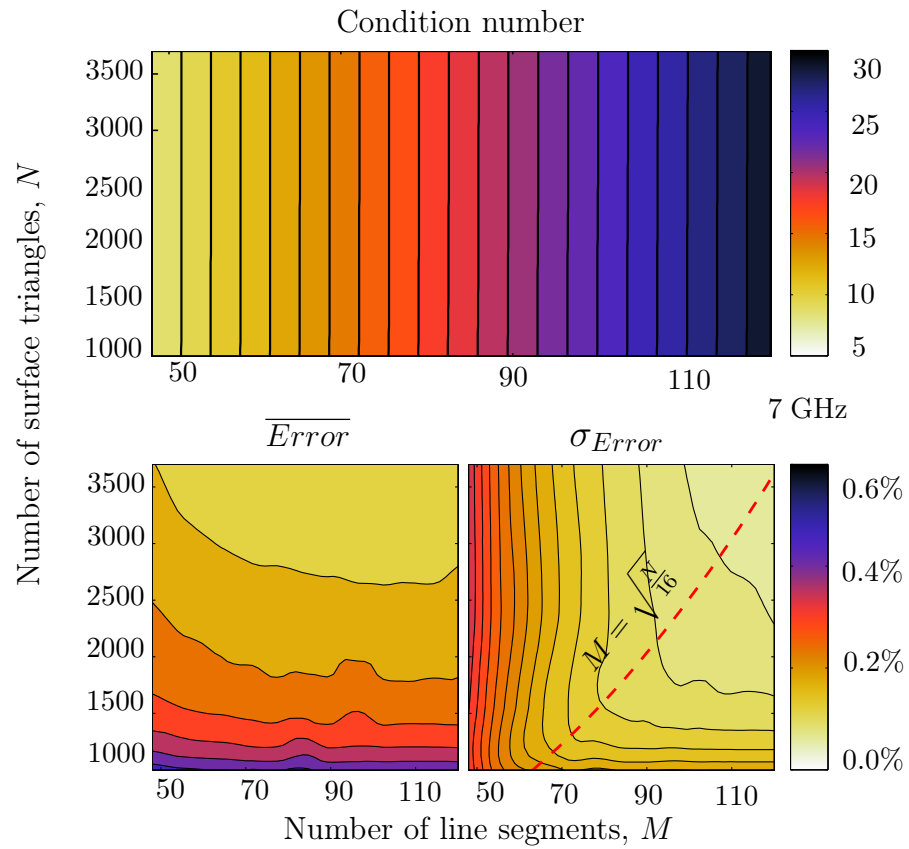


Figure 5.5: Condition number of the matrix (5.33), mean and standard deviation of the relative error of the cross-sectional distribution of the E-field inside the dielectric cylinder obtained via MoM solution (5.33) with respect to the volumetric MoM solution of the V-EFIE (5.11) as a function of surface and volume mesh refinement. Optimal volume/surface elements ratio $M = \sqrt{N/16}$. © 2013 IEEE.

Next, to demonstrate the error behavior of the proposed SVS-EFIE (5.13) solution upon the h -refinement [18] of the MoM's surface and volume meshes, the cross-section of the hexagonal dielectric cylinder is discretized with the meshes featuring from 48 to 120 line segments and from 1000 to 3,719 surface triangles. The mean and standard deviation of the relative error with respect to the volumetric MoM solution of the V-EFIE (5.11), as well as the condition number with respect to the L2-norm, are depicted in Fig. 5.4. The condition number of the resultant matrix for the frequency $f = 7 \text{ GHz}$ is small and weakly depends on the number of surface triangles in the mesh. The behavior of the condition number for the low frequency $f = 100 \text{ MHz}$ is similar, with variation of the condition number from 130 to 330 for the same set of the surface and volume meshes. It is also seen that the mean value of the relative error is not dependent of the number of surface elements and remains at the same level for a fixed number of volume elements. The optimum number of surface elements M , however, is proportional to the square root of the number of volume elements N as seen from the plot of the standard deviation in Fig. 5.4. For the particular case of the TM_z scattering from the dielectric cylinder with the relative permittivity $\varepsilon = 2$ and the incident plane wave of frequency $f = 7 \text{ GHz}$ the optimum values of M lie near the curve $M = \sqrt{N/16}$. The same Fig. 5.4 demonstrates the error-controllable properties of the MoM discretized SVS-EFIE. The latter numerically corroborates the rigorous nature of the proposed SVS-EFIE.

The relative error, condition number and the number of CG-iterations [30] comparison between the MoM solutions of the proposed SVS-EFIE (5.13) and PMCHWT surface IE is depicted in Fig. 5.4 for the relative dielectric permittivity of the cylinder varying from 2 to 14. The MoM solution (5.33) for all values of permittivity utilizes $M = 120$ linear elements and $N = 3,719$ triangular elements. The MoM solution of PMCHWT surface IE [10] is found using the same surface mesh (albeit it operates with the twice number of unknowns from J_z^e and J_t^m). The systematic accuracy advantage of the proposed SVS-EFIE (5.13) against the PMCHWT formulation is apparent for all values of ε in both the mean value and standard deviation of the relative error, as well as the smaller condition number and required number of CG-iterations to find the solution for the system of linear equations.

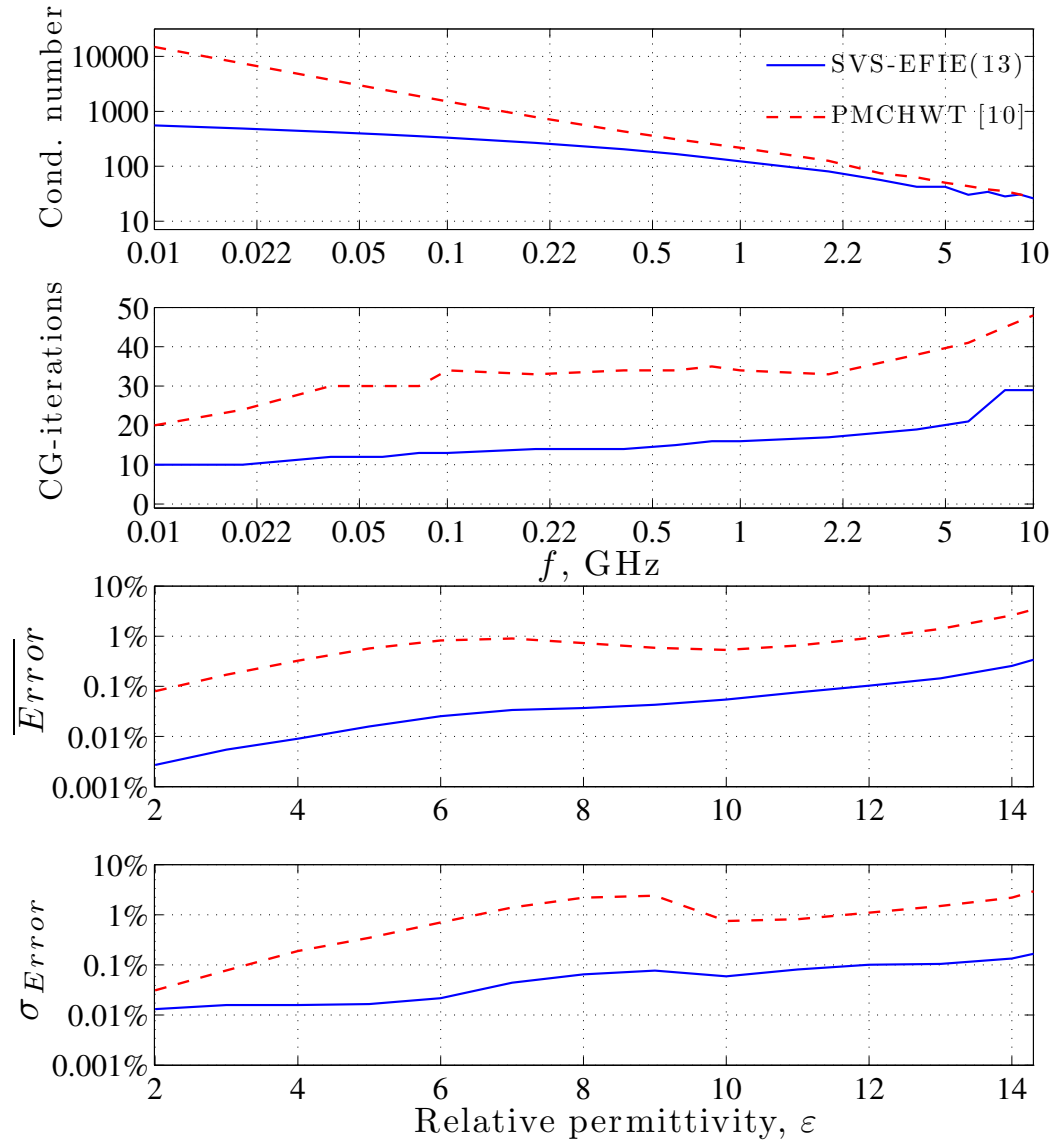


Figure 5.6: The condition number of the matrix (5.33) and impedance matrix for PMCHWT [10] surface IE, required number of CG-iterations, mean value and standard deviation of the relative error of the MoM solutions (5.33) and PMCHWT surface IE for 6-sided polygonal approximation of the circular cross-section with radius $\rho_0 = 25$ mm due to plane-wave incidence at 2 GHz. © 2013 IEEE.

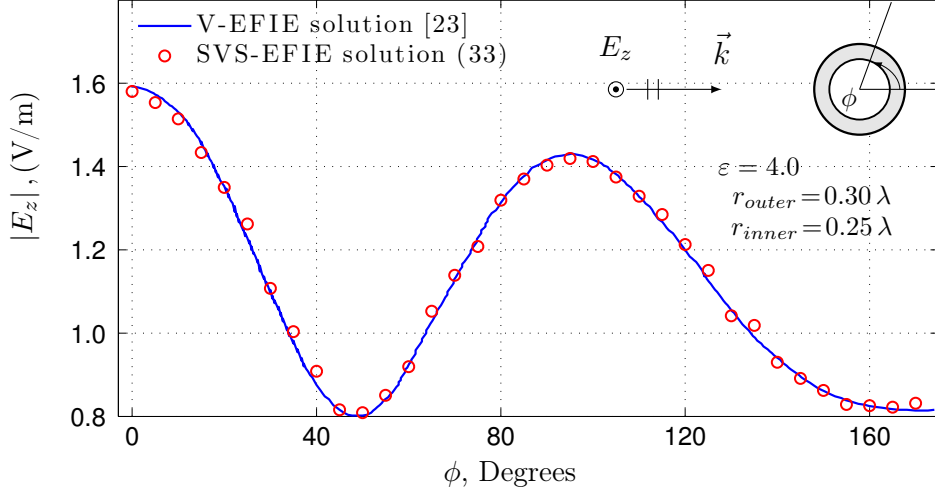


Figure 5.7: Electric field distribution in circular dielectric cylindrical shell with plane-wave incident. The MoM solution (5.33) and numerical results from [23]. © 2013 IEEE.

Last study compares the MoM solution of the proposed SVS-EFIE (5.13) against the traditional volumetric MoM solution of the V-EFIE (5.11) for TM_z wave scattering from a dielectric shell presented in [23]. Fig. 5.7 shows the electric field distribution inside the dielectric shell due to the incident plane wave of 1.0 V/m magnitude. In this example, the MoM solution (5.33) of the SVS-EFIE (5.13) utilizes $M = 80$ linear elements and $N = 520$ triangular elements. A good agreement of the field values is observed with this independent reference solution [23] despite its significantly different MoM discretization of the V-EFIE from the one in the present work.

5.5 Conclusion

The paper presents a novel rigorous single-source derivative-free surface integral equation for the problems of determining distribution of volumetric current flow in multi-conductor transmission lines and full-wave scattering on homogeneous permeable cylinders. The new surface integral equation is derived from the classical Volume Electric Field Integral Equation via the single-layer ansatz representation of the volume current density. The new surface integral equation is free of internal resonances. It is shown to produce a notably higher accuracy than the standard PMCHWT integral equation while featuring only a single surface unknown function. This advantage comes at the cost of the field translations performed from surface to volume domains and back unlike the less computationally expensive surface-to-surface field translations in PMCHWT formulation. The new integral equation does not feature derivatives acting on its kernels, as such may be particularly suitable for the analysis in multilayered media.

Bibliography

- [1] W. C. Chew, *Waves and Field in Inhomogeneous Media*, IEEE Press, 1995.
- [2] Jason Morsey, “Integral Equation Methodologies for the Signal Integrity Analysis of PCB and Interconnect Structures in Layered Media from DC to Multi-GHz Frequencies,” *Ph.D. Thesis, Univ. of Illinois at U.-C., 2004*.
- [3] M. Kamon, M. J. Tsuk, and J. White, “FASTHENRY: A Multipole Accelerated 3-D Inductance Extraction Program,” *IEEE Trans. Microw. Theory Techn.*, Vol. 42, No. 9, pp. 1750–1758, 1994.
- [4] B. Young, *Digital Signal Integrity*, New York: McGraw-Hill, 2001.
- [5] P. Mojabi and J. LoVetri, “Comparison of TE and TM inversions in the framework of the Gauss-Newton Method,” *IEEE Trans. Antennas Propag.*, Vol. 58, No. 4, pp. 1336–1348, 2010.
- [6] W. C. Chew, J. - M. Jin, E. Michielssen, and J. Song, (ed.), *Fast and Efficient Algorithms in Computational Electromagnetics*, Norwood: Artech House, 2001.
- [7] Serdar Cadirci, “RF Stealth and Counter-RF Stealth Technologies,” *M.Sc. Thesis, Naval Postgraduate School, 2009*.

- [8] Kubilay Sertel, “Multilevel Fast Multipole Method for Modeling Permeable Structures Using Conformal Finite Elements,” *Ph.D. Thesis, University of Michigan, 2003.*
- [9] A. Kishk and L. Shafai, “Different formulations for numerical solutions of single or multibodies of revolution with mixed boundary conditions,” *IEEE Trans. Antennas Propag.*, Vol. 34, No. 5, pp. 666–673, May 1986.
- [10] A. Peterson, S. Ray, and R. Mittra, *Computational Methods for Electromagnetics*, IEEE Press, 1998.
- [11] Z. G. Qian, W. C. Chew, and R. Suaya, “Generalized impedance boundary condition for conductor modeling in surface integral equation,” *IEEE Trans. Microw. Theory Techn.*, Vol. 55, No. 11, pp. 2354–2364, Nov. 2007.
- [12] David Swatek, “Investigation of Single Source Surface Integral Equation for Electromagnetic Wave Scattering by Dielectric Bodies,” *Ph.D. Thesis, Univ. of Manitoba, 1999.*
- [13] D. R. Swatek, I. R. Ceric, “A recursive single source integral equation analysis for wave scattering by heterogeneous dielectric bodies,” *IEEE Trans. Antennas Propag.*, Vol. 48, No. 8, pp. 1175–1185, Aug. 2000.
- [14] F. Valdes, F. P. Andriulli, H. Bagci, and E. Michielssen, “On the discretization of single source integral equations for analyzing scattering from homogeneous penetrable objects,” *IEEE Antennas and Propag. Soc. Int. Symp.*, pp. 1–4, July 2008.

- [15] A. Glisson, “An integral equation for electromagnetic scattering from homogeneous dielectric bodies,” *IEEE Trans. Antennas Propag.*, Vol. 32, No. 2, pp. 173–175, Feb. 1984.
- [16] M. S. Yeung, “Single integral equation for electromagnetic scattering by three-dimensional homogeneous dielectric objects,” *IEEE Trans. Antennas Propag.*, Vol. 47, No. 10, pp. 1615–1622, Oct. 1999.
- [17] D. Colton and R. Kress, (ed.), *Integral Equation Methods in Scattering Theory*, Malabar, Florida: Krieger Publishing Company, 1992.
- [18] J.-M. Jin, *The Finite Element Method in Electromagnetics*, 2nd Ed., New York: Wiley, 2002.
- [19] A. Menshov and V. Okhmatovski, “Novel surface integral equation formulation for accurate broadband RL extraction in transmission lines of arbitrary cross-section,” Microwave Symposium Digest (MTT), 2012 IEEE MTT-S International, pp. 1-3, 17–22 June 2012.
- [20] A. Menshov and V. Okhmatovski, “Method of moment solution of Surface-Volume-Surface Electric Field Integral Equation for two-dimensional transmission lines of complex cross-sections,” Signal and Power Integrity (SPI), 2012 IEEE 16th Workshop on, pp. 31–34, 13–16 May 2012.
- [21] M. Abramovitz and I. Stegun, (ed.) *Handbook of Mathematical Functions*, Dover, 1964.
- [22] Feng Ling, “Fast Electromagnetic Modeling of Multilayer Microstrip Antennas and Circuits,” *Ph.D. Thesis, Univ. of Illinois at U.-C., 2000*.

- [23] J. Richmond, “Scattering by a dielectric cylinder of arbitrary cross section shape,” *IEEE Trans. Antennas Propag.*, Vol. 13, No. 3, pp. 334–341, 1965.
- [24] R. Harrington, *Field Computation by Moment Methods*, IEEE Press, 1993.
- [25] W. H. Press, et. al. *Numerical Recipes: The Art of Scientific Computing*, Cambridge University Press, 2007.
- [26] D. Wilton, A. Glisson, D. Schaubert, O. Al-Bundak, C. Butler, “Potential integrals for uniform and linear source distributions on polygonal and polyhedral domains,” *IEEE Trans. Antennas Propag.*, Vol. 32, No. 3, pp. 276–281, Mar. 1984.
- [27] F. R. Gantmacher, *Matrix Theory* New York: Chelsea Publishing Company, 1959.
- [28] J. H. Ma, V. Rokhlin, and S. Wandzura, “Generalized Gaussian quadrature rules for systems of arbitrary functions,” *SIAM J. Numer. Anal.*, Vol. 33, No. 3, pp. 971–996, June 1996.
- [29] V. Fraysse, L. Giraud, and S. Gratton, “A set of GMRES routines for real and complex arithmetics,” *CERFACS Tech. Rep. TR/PA/97/49*, www.cerfacs.fr
- [30] C. H. Smith, A. F. Peterson, and R. Mitra, “The biconjugate gradient method for electromagnetic scattering,” *IEEE Trans. Antennas Propag.*, Vol. 38, No. 6, pp. 938–940, June 1990.
- [31] L. Greengard and V. Rokhlin, “The fast algorithm for particle simulations,” *J. Comp. Phys.*, Vol. 73, No. 2, pp. 325–348, Dec. 1987.

- [32] E. Bleszynski, M. Bleszynski, and T. Jaroszewicz, “AIM: Adaptive integral method for solving large-scale electromagnetic scattering and radiation problems,” *Radio Science*, Vol. 31, No. 5, pp. 1255–1251, Sept.–Oct. 1996.
- [33] M. F. Catedra, R. F. Torres, J. Basterrechea, E. Cago, *The CG-FFT Method: Application of Signal Processing Techniques to Electromagnetics*, Artech House, 1995.

Chapter 6

Surface-Volume-Surface Electric Field Integral Equation for Magneto-Quasi-Static Electromagnetic Analysis of Complex 3-D Interconnects

©2014 IEEE. Reprinted, with permission, from *Surface-Volume-Surface Electric Field Integral Equation for Magneto-Quasi-Static Electromagnetic Analysis of Complex 3-D Interconnects, IEEE Transactions on Microwave Theory and Techniques, Submitted*

A novel single-source surface-volume-surface integral equation is proposed for accurate broadband resistance and inductance extraction in 3-D interconnects. The new equation originates in the volume integral equation traditionally used for magneto-quasi-static modeling of current flow in 3-D wires. The latter is reduced to a surface integral equation by representing the electric field inside each conductor segment as a superposition of cylindrical waves emanating from the conductor's boundary. As no approximation is utilized and all underlying boundary conditions and pertinent equations are satisfied in the reduction, the new integral equation is rigorously equivalent to the solution of the traditional volume electric field integral equation. The rigorous nature of the proposed single-source surface integral equation is corroborated numerically. In this paper a detailed description of the Method of Moments discretization for the proposed surface integral equation is also presented. Numerical solution of the proposed surface integral equation for a twelve-conductor bond-wire package is used to demonstrate the accuracy of the method and its computational benefits compared to the traditional solution based on the volume integral equation.

6.1 Introduction

Transmission lines of complex topological shapes are found in various industrial applications ranging from buried power cables spanning several kilometres [1, 2] to electronic interconnects of sub-micron dimensions [3]. Electromagnetic-based modelling of current flow, which accounts for both the proximity and skin effects [3], is important for obtaining accurate broadband terminal characteristics of interconnects, such as Z-parameters [4]. The latter are used to generate equivalent lump circuit models [5] that allow the interconnect model to be cascaded with source and termination components connected at its ports. Subsequent time-domain analysis of the entire channel including the sources, the circuit of the interconnect, and the termination loads in a SPICE-like [6] circuit simulator produces the desired waveforms describing dynamic behavior of the channel and quality of the signal transmission [3, 7].

When physical dimensions of an interconnect are within a tenth of the wavelength in the surrounding medium, the modelling of current flow in the conductors can be accurately performed under a quasi-static approximation of Maxwell equations [8]. This approximation makes the electromagnetic analysis significantly simpler and faster due to the non-oscillatory nature of the quasi-static interactions [9]. While both differential [10] and integral equation [11] based formulations are available for calculation of the electromagnetic fields produced by the interconnects, the formulations based on integral equations often lead to discretized problems of a substantially smaller size [9]. The reduced problem size in integral equation formulations is attributed to the discretization of the conductors only, whereas methods based on the direct solution of the differential equations discretize the entire space including the volume surrounding conductors [10]. Furthermore, the integral equations allow for formulations in which the unknown field quantities reside on the conductors' surface rather

than in their volume. Boundary element discretization of such surface integral equations results in the possibly minimum number of degrees of freedom associated with the numerical solution of Maxwell equations. The classical surface integral equations of electromagnetics involve two unknown functions on the conductor surface, namely the tangential electric and tangential magnetic fields [11–13]. In the class of single-source surface integral (SSIE) equations, one of the unknown functions is eliminated analytically [14–18]. Such elimination, however, comes at the expense of a large number of integral operator product terms introduced into the resultant SSIE, so that it renders the numerical solution inefficient.

In this work, we construct a new SSIE for quasi-static characterization of 3-D interconnects that is substantially different from its predecessors. Instead of starting from the classical surface integral equation and performing a subsequent reduction to an SSIE, we take the volume integral equation (VIE) [19] as the initial formulation. Under the assumption of the conductor segment lengths being substantially larger than their respective cross-sectional dimensions [20], current is assumed to flow strictly along the wire direction and to be independent along each wire segment. Taking this into consideration, we represent the volumetric current density within each wire segment cross-section as a superposition of cylindrical waves emanating from the conductor surface. The magnitude of these cylindrical waves is defined by an auxiliary function, which is determined on the conductor surface and plays the role of the unknown in the integral equation. Substitution of such a cylindrical wave representation for the volumetric current density into the VIE produces an integral equation with the unknown function defined on the conductor surface instead of the conductor volume. Hence, observation point locations in the VIE can be restricted to the conductor surface as well. The resulting integral equation is in the form of

the SSIE with a single unknown function that acts as the weighting function for the cylindrical waves emanating from the conductor surface. Since the additional integral operator is introduced to represent the volumetric current, the resultant SSIE features a product of two integral operators. One operator translates the field from the conductor surface to its volume, while the second operator translates the field from the conductor volume to the surface. We initially constructed the analogous SSIE for magnetostatic [21] and full-wave scattering problems [22] in 2-D. Here we present generalization of the new SSIE formulation for the magnetostatic analysis of 3-D interconnects under the aforementioned assumptions. A detailed description of the Method of Moments (MoM) discretization of the 3-D SSIE is also presented.

Numerical analysis demonstrates the rigorous nature of the new 3-D SSIE formulation. The solution of the SSIE is compared against the traditional VIE solution. It is demonstrated that the error of current extraction can be controlled through the discretization density. Furthermore, the new SSIE formulation was shown to allow for substantially faster extraction of the broadband network parameters in multiport interconnects than the VIE-based formulation without sacrificing the accuracy.

6.2 Single-Source SVS-EFIE for Current Flow Modeling in 3-D

Consider an interconnect consisting of N_s piece-wise straight segments. We denote the index identifying the segment number as $\alpha = 1, \dots, N_s$. The axis of each segment is parallel to the unit vector $\hat{\ell}_\alpha$, and the length of each segment is given by L_α . The contour bounding the cross-section of the α -th segment, the cross-section area itself, and the segment inner volume are indicated as ∂S_α , S_α , and V_α , respectively. An example of a single-conductor interconnect consisting of $N_s = 2$ segments is depicted in Fig. 6.1a.

The electric field $\mathbf{E}(\mathbf{r})$ inside the conductor is governed by the following V-EFIE [19] under a magneto-quasi-static approximation

$$\mathbf{E}(\mathbf{r}) + i\omega\mu_0\sigma \iiint_V dv' G_0(\mathbf{r}, \mathbf{r}') \mathbf{E}(\mathbf{r}') = -\nabla\Phi(\mathbf{r}), \quad \mathbf{r} \in V, \quad (6.1)$$

$$G_0(\mathbf{r}, \mathbf{r}') = \frac{1}{4\pi} \frac{1}{|\mathbf{r} - \mathbf{r}'|}, \quad (6.2)$$

where $G_0(\mathbf{r}, \mathbf{r}')$ is the 3-D quasi-static Green's function of free space, σ is the wire conductivity, ω is the cyclic frequency, $\Phi(\mathbf{r})$ is the scalar potential, \mathbf{r} and \mathbf{r}' are the observation and source points, respectively.

If conductivity of the wire σ is homogeneous, the electric field inside the volume of the α -th segment satisfies the homogeneous Helmholtz equation

$$\nabla^2 \mathbf{E}_\alpha(\mathbf{r}) + k_\sigma^2 \mathbf{E}_\alpha(\mathbf{r}) = 0, \quad \mathbf{r} \in V_\alpha \quad (6.3)$$

and is assumed to be constant along the length of the wire:

$$\mathbf{E}_\alpha(\mathbf{r}) = E_\alpha(\boldsymbol{\rho}) \hat{\ell}_\alpha, \quad \mathbf{r} = \boldsymbol{\rho} + \ell \hat{\ell}_\alpha, \ell \in [0, L_\alpha], \boldsymbol{\rho} \in S_\alpha, \quad (6.4)$$

where \mathbf{r} and $\boldsymbol{\rho}$ are the position vectors of the observation point inside the volume V_α and its projection on the cross-section S_α of the conductor segment, respectively. The position vectors $\mathbf{r}(\ell = 0)$ and $\mathbf{r}(\ell = L_\alpha)$ are located at the α -th conductor segment end points. The wavenumber k_σ and skin-depth are defined as follows:

$$k_\sigma(f, \sigma) = \sqrt{-i\omega\mu_0\sigma}, \quad \delta(f, \sigma) = \frac{1}{\Re(k_\sigma(f, \sigma))}, \quad (6.5)$$

where $\Re(\dots)$ denotes the real part.

Since the electric field is directed along the axis of the conductor segment and is independent along its length, it can be expressed at any point inside the segment as a superposition of the cylindrical waves emanating from its boundary $\partial S_{\alpha'}$

$$\mathbf{E}_{\alpha'}(\mathbf{r}) = i\omega\mu_0 \hat{\ell}_{\alpha'} \oint_{\partial S_{\alpha'}} dc' G_\sigma(\boldsymbol{\rho}, \boldsymbol{\rho}') J_{\alpha'}(\boldsymbol{\rho}'), \quad \boldsymbol{\rho} \in S_{\alpha'}, \mathbf{r} \in V_{\alpha'}, \quad (6.6)$$

$$G_\sigma(\boldsymbol{\rho}, \boldsymbol{\rho}') = -\frac{i}{4} H_0^{(2)}(k_\sigma |\boldsymbol{\rho} - \boldsymbol{\rho}'|), \quad k_\sigma = \sqrt{-i\omega\mu_0\sigma}, \quad (6.7)$$

where $G_\sigma(\boldsymbol{\rho}, \boldsymbol{\rho}')$ is the 2-D Green's function of the conductor media with the wavenumber k_σ , $H_0^{(2)}$ is the second-kind Hankel function of zeroth order [23], and $\mathbf{J}_{\alpha'}(\boldsymbol{\rho}') = J_{\alpha'}(\boldsymbol{\rho}') \hat{\ell}_{\alpha'}$ is the auxiliary surface current density acting as the weighting function for the cylindrical waves emanating from the conductor boundary $\partial S_{\alpha'}$. It is important to emphasize that the integral field representation (6.6) is different from the standard equivalence principle, as shown in [22]. The proposed formulation uses only one

unknown $J_{\alpha'}(\boldsymbol{\rho}')$, called a single layer ansatz [24]. Substitution of (6.6) into (6.1) followed by restriction of the observation domain to the contour ∂S_α forming the conductor cross-section S_α results in the SVS-EFIE with respect to the unknown auxiliary surface current density $J_{\alpha'}(\boldsymbol{\rho}')$ (6.8). The resulting equation is scalarized by taking the dot-product with the directing vector $\hat{\ell}_\alpha$ corresponding to the conductor segment present at the observation location \mathbf{r}

$$\begin{aligned} i\omega\mu_0 \oint_{\partial S_\alpha} dc' G_\sigma(\boldsymbol{\rho}, \boldsymbol{\rho}') J_\alpha(\boldsymbol{\rho}') \\ -\sigma(\omega\mu_0)^2 \hat{\ell}_\alpha \cdot \sum_{\alpha'=1}^{N_s} \hat{\ell}_{\alpha'} \left[\iint_{S_{\alpha'}} ds' \int_{L_{\alpha'}} d\ell' G_0(\mathbf{r}, \mathbf{r}') \oint_{\partial S_{\alpha'}} dc'' G_\sigma(\boldsymbol{\rho}', \boldsymbol{\rho}'') J_{\alpha'}(\boldsymbol{\rho}'') \right] = -\nabla\Phi(\mathbf{r}) \cdot \hat{\ell}_\alpha, \\ \mathbf{r} = \boldsymbol{\rho} + \ell \hat{\ell}_\alpha, \mathbf{r}' = \boldsymbol{\rho}' + \ell' \hat{\ell}_{\alpha'}, \ell \in [0, L_\alpha], \ell' \in [0, L_{\alpha'}], \boldsymbol{\rho} \in \partial S_\alpha. \end{aligned} \quad (6.8)$$

In (6.8), $\alpha, \alpha' = 1, \dots, N_s$ are the indexes of the conductor segment at the observation and source points, respectively. For the conductors with a cross-section significantly smaller compared to their length, the scalar potential $\Phi(\mathbf{r})$ under magneto-quasi-static approximation is constant within the cross-section of the conductor S_α and varies linearly along the axis of the segments $\hat{\ell}_\alpha$ [20]. Thus, the right-hand side of (6.8) can be written as a difference of the potentials at the junction nodes of the α -th segment that has the meaning of the branch voltage V_α across the α th segment

$$\nabla\Phi(\mathbf{r}) \cdot \hat{\ell}_\alpha = \frac{\partial\Phi(\mathbf{r})}{\partial\ell_\alpha} = \frac{\Phi(\mathbf{r}|_{\ell=L_\alpha}) - \Phi(\mathbf{r}|_{\ell=0})}{L_\alpha} = -V_\alpha. \quad (6.9)$$

It is convenient to express the SVS-EFIE (6.8) by using the following notation for

the integral operators

$$\mathcal{T}_\sigma^{\partial S_\alpha, \partial S_\alpha} \circ J_\alpha = i\omega\mu_0 \oint_{\partial S_\alpha} dc' G_\sigma(\boldsymbol{\rho}, \boldsymbol{\rho}') J_\alpha(\boldsymbol{\rho}'), \quad \boldsymbol{\rho} \in \partial S_\alpha, \quad (6.10)$$

$$\mathcal{T}_\sigma^{V_{\alpha'}, \partial S_{\alpha'}} \circ J_{\alpha'} = i\omega\mu_0 \oint_{\partial S_{\alpha'}} dc'' G_\sigma(\boldsymbol{\rho}', \boldsymbol{\rho}'') J_{\alpha'}(\boldsymbol{\rho}''), \quad \boldsymbol{\rho}' \in S_{\alpha'}, \quad (6.11)$$

$$\mathcal{T}_0^{\partial S_\alpha, V_{\alpha'}} \circ j_{\alpha'} = \mu_0 \iint_{S_{\alpha'}} ds' \int_{L_{\alpha'}} d\ell' G_0(\mathbf{r}, \mathbf{r}') j_{\alpha'}(\mathbf{r}'), \quad \mathbf{r} \in \partial S_\alpha \quad (6.12)$$

in a compact form

$$\mathcal{T}_\sigma^{\partial S_\alpha, \partial S_\alpha} \circ J_\alpha + i\omega \hat{\boldsymbol{\ell}}_\alpha \cdot \sum_{\alpha'=1}^{N_s} \hat{\boldsymbol{\ell}}_{\alpha'} \left(\mathcal{T}_0^{\partial S_\alpha, V_{\alpha'}} \circ \sigma \mathcal{T}_\sigma^{V_{\alpha'}, \partial S_{\alpha'}} \circ J_{\alpha'} \right) = \mathbf{v}_\alpha, \quad (6.13)$$

where the operator $\mathcal{T}_\sigma^{\partial S_\alpha, \partial S_\alpha}$ has the meaning of the global surface impedance boundary condition relating the auxiliary surface current density J_α and electric field on the conductor boundary ∂S_α . The operator $\mathcal{T}_0^{\partial S_\alpha, V_{\alpha'}}$ in (6.12) maps the volumetric current density inside the α' th conductor segment to the magnetic vector potential produced at the boundary ∂S_α of the α th conductor segment.

6.3 Method of Moments Discretization

As the SVS-EFIE (6.8) incorporates the product of integral operators having ranges and domains (6.13) in conductor contour ∂S_α and its volume V_α , discretization of both the contour and cross-section is required. Without loss of generality, we consider an example of a single-conductor interconnect consisting of $N_s = 2$ piecewise-straight segments of the length L_α , as shown in Fig. 6.1a. The axes of the segments are parallel to the unit vectors $\hat{\ell}_\alpha$. The volume V_α of the α -th segment is discretized with N_α filaments (triangular prisms), and the contour ∂S_α – with M_α line elements. The radius-vector on the m th line element of the surface ∂S_α is given by

$$\rho_m^\alpha(c) = \mathbf{v}_m^{\alpha,1} + c(\mathbf{v}_m^{\alpha,2} - \mathbf{v}_m^{\alpha,1}), \quad c \in [0, 1], \quad (6.14)$$

where $\alpha = 1, 2$ is the index identifying the conductor segment, $\mathbf{v}_m^{\alpha,2}$ and $\mathbf{v}_m^{\alpha,1}$ are the end and start points of the m th line element on ∂S_α , and $m = 1, \dots, M_\alpha$. The contour ∂S_α is located in the middle of the α th conductor segment as depicted in Fig. 6.1.

The radius-vector on the n th triangular prism in the discretization of the volume V_α is defined in barycentric coordinates ξ, η over prism cross-section [10] and linear coordinate ℓ along its length as follows:

$$\begin{aligned} \mathbf{r}_n^\alpha(\xi, \eta, \ell) &= \mathbf{v}_n^{\alpha,1}\xi + \mathbf{v}_n^{\alpha,2}\eta + \mathbf{v}_n^{\alpha,3}(1 - \xi - \eta) + \ell\hat{\ell}_\alpha, \\ \xi, \eta &\in [0, 1], \xi + \eta \leq 1, \quad \ell \in [0, L_\alpha], \end{aligned} \quad (6.15)$$

where $\mathbf{v}_n^{\alpha,1}, \mathbf{v}_n^{\alpha,2}, \mathbf{v}_n^{\alpha,3}$ are the three vertices of the triangle forming the base of the n th prism in V_α , and $n = 1, \dots, N_\alpha$.

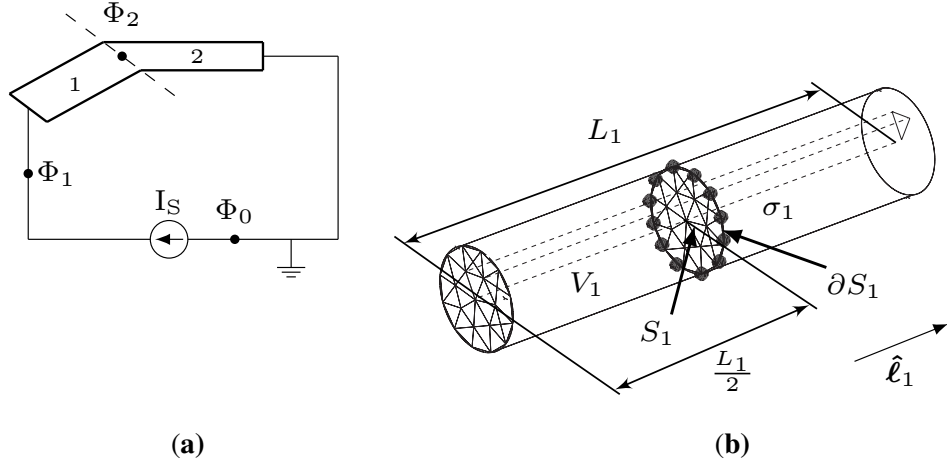


Figure 6.1: (a) Interconnect formed by two piecewise-straight conductor segments. (b) Segment 1 directed along the vector $\hat{\ell}_1$ with depicted volume and contour meshes utilized in the MoM discretization of the SVS-EFIE (6.8). © 2014 IEEE.

Note that the density of the volume mesh grows with frequency in order to capture the behavior of the volumetric current according to the skin-effect. Hence, the total number of contour elements $M = \sum_{\alpha=1}^{N_s} M_\alpha$ is relatively low in comparison to the total number of volume elements $N = \sum_{\alpha=1}^{N_s} N_\alpha$. The optimal number of contour and volume elements can be found numerically by using a procedure similar to the one for the 2-D SVS-EFIE presented in [22], where $M_\alpha \sim \sqrt{N_\alpha}$ was shown.

The unknown auxiliary surface current density $J_\alpha(\boldsymbol{\rho}')$ on the surface of the α th segment ∂S_α and the volumetric current density $j_\alpha(\mathbf{r}')$ in the cross-section of the α th segment S_α are discretized by using piece-wise basis functions [25]

$$J_\alpha(\boldsymbol{\rho}') \cong \sum_{m'=1}^{M_\alpha} I_{m'}^\alpha P_{m'}^\alpha(\boldsymbol{\rho}'), \quad (6.16)$$

$$j_\alpha(\mathbf{r}') \cong \sum_{n'=1}^{N_\alpha} i_{n'}^\alpha p_{n'}^\alpha(\mathbf{r}'), \quad (6.17)$$

where $\alpha = 1, 2$ is the index identifying the conductor segment, $I_{m'}^\alpha$ and $i_{n'}^\alpha$ are the unknown coefficients in the expansion of the surface current density J_α and the volumetric current density j_α in the α th segment, respectively. The pulse basis functions $P_{m'}^\alpha(\boldsymbol{\rho}')$ and $p_{n'}^\alpha(\mathbf{r}')$ are defined as follows:

$$P_{m'}^\alpha(\boldsymbol{\rho}') = \begin{cases} 1, & \boldsymbol{\rho}' \in \partial S_{\alpha,m'} \\ 0, & \boldsymbol{\rho}', \notin \partial S_{\alpha,m'} \end{cases}, \quad (6.18)$$

$$p_{n'}^\alpha(\mathbf{r}') = \begin{cases} 1, & \mathbf{r}' \in V_{\alpha,n'} \\ 0, & \mathbf{r}' \notin V_{\alpha,n'} \end{cases}, \quad (6.19)$$

where $\partial S_{\alpha,m'}$ is the m' th contour mesh element on the α th conductor segment and $V_{\alpha,n'}$ is the n' th volume mesh element in the α th conductor segment. The unknown coefficients $I_{m'}^\alpha$ and $i_{n'}^\alpha$ in the current expansions (6.16), (6.17) can be organized as an $M \times 1$ and an $N \times 1$ vectors, respectively. Thus, for a two-segment example $M = M_1 + M_2$, $N = N_1 + N_2$, and the unknown coefficient vectors are given by

$$\mathbf{I} = [\mathbf{I}^1; \mathbf{I}^2]^T = [I_1^1, \dots, I_{M_1}^1; \quad I_1^2, \dots, I_{M_2}^2]^T, \quad (6.20)$$

$$\mathbf{i} = [\mathbf{i}^1; \mathbf{i}^2]^T = [i_1^1, \dots, i_{N_1}^1; \quad i_1^2, \dots, i_{N_2}^2]^T. \quad (6.21)$$

The ranges of the integral operators ∂S_α and V_α are tested with delta-functions $T(\mathbf{r})$ and $t(\mathbf{r})$ defined as follows:

$$T_m^{\alpha,Q}(\boldsymbol{\rho}) = \sum_{q=1}^Q w_q \delta \left(\boldsymbol{\rho} - \boldsymbol{\rho}_m^\alpha \left(\frac{1}{2} \right) - l_q L_\alpha \hat{\ell}_\alpha \right), \quad (6.22)$$

$$t_n^\alpha(\mathbf{r}) = \delta\left(\mathbf{r} - \mathbf{r}_n^\alpha\left(\frac{1}{3}, \frac{1}{3}, \frac{L_\alpha}{2}\right)\right), \quad (6.23)$$

where w_q and l_q are the weights and abscissas of a standard Gauss-Legendre Q -point quadrature rule [26], L_α and $\hat{\ell}_\alpha$ are the length and directing unit vector of the α th segment, respectively.

Thus, according to (6.22), Q delta-functions $T_m^{\alpha,Q}(\boldsymbol{\rho})$ are positioned at the centroid of the m th element in the α th segment contour mesh and shifted by distance $l_q L_\alpha$ from the α th conductor segment end point, $q = 1, \dots, Q$. The delta-function $t_n^\alpha(\mathbf{r})$ is positioned at the centroid the n th triangular prism of the α th conductor segment. The definitions of the position vectors $\boldsymbol{\rho}_m^\alpha$ and \mathbf{r}_n^α are given in (6.14) and (6.15), respectively.

6.3.1 Method of Moments discretization of the contour-to-volume operator $\mathcal{T}_\sigma^{V_{\alpha'}, \partial S_{\alpha'}}$

Discretization of the contour-to-volume operator (6.6) is done through piece-wise basis functions (6.18), and the range of the operator is tested with delta-functions (6.23). Substitution of the discretized auxiliary surface current density $J_{\alpha'}(\boldsymbol{\rho}'')$ (6.16) into (6.6) followed by testing the volumetric current density at the central axis of the triangular prisms constituting the volumetric mesh establishes the matrix expression

$$\begin{bmatrix} \mathbf{i}^1 \\ \mathbf{i}^2 \end{bmatrix} = \begin{bmatrix} \mathbf{Z}_\sigma^{V_1, \partial S_1} & \mathbf{0} \\ \mathbf{0} & \mathbf{Z}_\sigma^{V_2, \partial S_2} \end{bmatrix} \cdot \begin{bmatrix} \mathbf{I}^1 \\ \mathbf{I}^2 \end{bmatrix} \quad (6.24)$$

relating an $M \times 1$ vector of unknown coefficients in the expansion of the auxiliary surface current density $J_{\alpha'}(\boldsymbol{\rho}'')$ and an $N \times 1$ vector of samples of the volumetric current density $j_{\alpha'}(\mathbf{r}')$ at the central axis of the volumetric elements discretizing the

cross-section of the conductor. The matrix elements in (6.24) are defined as inner products

$$\begin{aligned} Z_{\sigma,n'm''}^{V_{\alpha'}, \partial S_{\alpha'}} &= \langle t_{n'}^{\alpha'}, \sigma \mathcal{T}_{\sigma}^{V_{\alpha'}, \partial S_{\alpha'}} \circ P_{m''}^{\alpha'} \rangle = i\omega\mu_0\sigma C_{m''}^{\alpha'} \\ &\times \int_0^1 dc'' G_{\sigma} \left(\mathbf{r}_{n'}^{\alpha'} \left(\frac{1}{3}, \frac{1}{3}, \frac{L_{\alpha'}}{2} \right), \boldsymbol{\rho}_{m''}^{\alpha'}(c'') \right), \quad (6.25) \end{aligned}$$

where $\boldsymbol{\rho}_{m''}^{\alpha'}$ and $\mathbf{r}_{n'}^{\alpha'}$ are the parametric definitions of the position vectors on the contour and volume elements given in (6.14) and (6.15), respectively, $\alpha' = 1, 2$ is the index of the conductor segment, $n' = 1, \dots, N_{\alpha'}$ is the index of the volume elements in the $V_{\alpha'}$ discretization, $m'' = 1, \dots, M_{\alpha'}$ is the index of the contour elements of the length $C_{m''}^{\alpha'}$ in the discretization of $\partial S_{\alpha'}$.

The evaluation of the line integrals in (6.25) can be done using Gauss-Legendre quadrature rule, after extraction the singular part of the integral kernel $-\frac{1}{2\pi} \ln |\mathbf{r} - \mathbf{r}'|$ [26]. The analytic expression for integrating a logarithmic function over a line element are also given in [27].

6.3.2 Method of Moments discretization of the volume-to-contour operator $\mathcal{T}_0^{\partial S_{\alpha}, V_{\alpha'}}$

Discretization of the volume-to-contour operator (6.12) is also performed using piece-wise basis functions (6.19), and the range of the operator is tested with delta-functions (6.22). Substitution of the discretized volume current density $j_{\alpha'}(\mathbf{r}')$ from (6.17) into (6.12) followed by testing the magnetic vector potential A at the

centroids of the contour mesh ∂S_α produces the following matrix expression

$$\begin{bmatrix} \mathbf{A}^1 \\ \mathbf{A}^2 \end{bmatrix} = \begin{bmatrix} \mathbf{Z}_0^{\partial S_1, V_1} & \mathbf{Z}_0^{\partial S_1, V_2} \\ \mathbf{Z}_0^{\partial S_2, V_1} & \mathbf{Z}_0^{\partial S_2, V_2} \end{bmatrix} \cdot \begin{bmatrix} \mathbf{i}^1 \\ \mathbf{i}^2 \end{bmatrix}, \quad (6.26)$$

which relates an $N \times 1$ vector of samples of the volumetric current density $j_{\alpha'}(\mathbf{r}')$ and an $M \times 1$ vector of samples of the magnetic vector potential. In (6.26), $\mathbf{A} = [\mathbf{A}^1; \mathbf{A}^2] = [A_1^1, \dots, A_{M_1}^1; A_1^2, \dots, A_{M_2}^2]^T$, and the matrix elements are defined as inner products

$$\begin{aligned} Z_{0,mn'}^{\partial S_\alpha, V_{\alpha'}} &= \langle T_m^{\alpha,Q} \hat{\ell}_\alpha, i\omega \hat{\ell}_{\alpha'} \mathcal{T}_0^{\partial S_\alpha, V_{\alpha'}} \circ p_{n'}^{\alpha'} \rangle \\ &= 2i\omega\mu_0 A_{n'}^{\alpha'} \hat{\ell}_\alpha \cdot \hat{\ell}_{\alpha'} \sum_{q=1}^Q \left[w_q \int_{L_{\alpha'}} d\ell' \int_0^1 \int_0^{1-\eta'} d\xi' d\eta' G_0 \left(\boldsymbol{\rho}_m^\alpha \left(\frac{1}{2} \right) \right. \right. \\ &\quad \left. \left. = l_q L_\alpha \hat{\ell}_\alpha, \mathbf{r}_{n'}^{\alpha'} (\xi', \eta', \ell') \right) \right], \quad (6.27) \end{aligned}$$

where $\boldsymbol{\rho}_m^\alpha$ and $\mathbf{r}_{n'}^{\alpha'}$ are the parametric definitions of the position vectors on the contour and volume elements given in (6.14) and (6.15), respectively, $\alpha, \alpha' = 1, 2$ are the indexes of the conductor segment, $A_{n'}^{\alpha'}$ is the base area of the n' th prism, $n' = 1, \dots, N_{\alpha'}$ is the index of the volume elements in $V_{\alpha'}$ discretization, and $m = 1, \dots, M_\alpha$ is the index of the contour elements in the discretization of ∂S_α . In (6.27), w_q and l_q are the weights and abscissas of a standard Gauss-Legendre Q -point quadrature rule [26], L_α and $\hat{\ell}_\alpha$ are the length and directing unit vector of the α th segment.

Analytic expression for integrating $\frac{1}{|\mathbf{r}-\mathbf{r}'|}$ function over a triangular prism for an arbitrary observation point are given in [27]. It is worth to note that in the numerical implementation of the MoM discretization of the SVS-EFIE, the testing along the central axis for the volume-to-contour integral operator $\mathcal{T}_0^{\partial S_\alpha, V_{\alpha'}}$ was done for several points along each segment. Such testing is required for the convergence of the calculated currents to their true values.

6.3.3 Method of Moments discretization of the contour-to-contour operator $\mathcal{T}_\sigma^{\partial S_\alpha, \partial S_\alpha}$

Similarly to the previous two operators, we discretize the contour-to-contour operator (6.10) using piece-wise basis functions (6.18) and test the range of the operator with delta-functions (6.22). This integral operator has both domain and range at the conductor contour ∂S_α forming the cross-section and carries the meaning of the global surface impedance boundary condition relating the auxiliary surface current density and electric field on the surface of the conductor segment. The discretization of the operator leads to the following matrix relationship

$$\begin{bmatrix} \mathbf{E}^1 \\ \mathbf{E}^2 \end{bmatrix} = \begin{bmatrix} \mathbf{Z}_\sigma^{\partial S_1, \partial S_1} & \mathbf{0} \\ \mathbf{0} & \mathbf{Z}_\sigma^{\partial S_2, \partial S_2} \end{bmatrix} \cdot \begin{bmatrix} \mathbf{I}^1 \\ \mathbf{I}^2 \end{bmatrix}, \quad (6.28)$$

where $\mathbf{E} = [\mathbf{E}^1; \mathbf{E}^2] = [E_1^1, \dots, E_{M_1}^1; E_1^2, \dots, E_{M_2}^2]^T$ is an $M \times 1$ vector of samples of the electric field at the centroids of the contour mesh elements. The matrix elements

in (6.28) are defined as

$$\begin{aligned} Z_{\sigma,mm'}^{\partial S_\alpha, \partial S_\alpha} &= \langle T_m^{\alpha,Q}, \mathcal{T}_\sigma^{\partial S, \partial S} \circ P_{m'}^\alpha \rangle = i\omega\mu_0 C_{m'}^\alpha \\ &\times \sum_{q=1}^Q w_q \int_0^1 dc' G_\sigma \left(\rho_m^\alpha \left(\frac{1}{2} \right) + l_q L_\alpha \hat{\ell}_\alpha, \rho_{m'}^\alpha(c') \right), \end{aligned} \quad (6.29)$$

where $\alpha = 1, 2$ is the index of the conductor segment, $m, m' = 1, \dots, M_\alpha$ are the indexes of contour elements of the length $C_{m'}^\alpha$ in ∂S_α discretization. In (6.29), w_q and l_q are the weights and abscissas of a standard Gauss-Legendre Q -point quadrature rule [26], L_α and $\hat{\ell}_\alpha$ are the length and directing unit vector of the α th segment. It is worth noting that in the numerical implementation of the MoM discretization of the SVS-EFIE, the testing along the central axis for the contour-to-contour integral operator $\mathcal{T}_\sigma^{\partial S_\alpha, \partial S_\alpha}$ was done for only one point along each segment ($Q = 1$). The usage of one-point Gauss-Legendre quadrature rule was sufficient enough for the convergence of the calculated currents to their true values.

6.3.4 Matrix form of the MoM discretized SVS-EFIE

Combining together the matrix forms $\mathbf{Z}_\sigma^{V, \partial S}$, $\mathbf{Z}_0^{\partial S, V}$, and $\mathbf{Z}_\sigma^{\partial S, \partial S}$ of the discretized integral operators $\mathcal{T}_\sigma^{V_{\alpha'}, \partial S_{\alpha'}}$, and $\mathcal{T}_0^{\partial S_\alpha, V_{\alpha'}}, \mathcal{T}_\sigma^{\partial S_\alpha, \partial S_{\alpha'}}$, we obtain the matrix form of the MoM discretized SVS-EFIE (6.8)

$$(\mathbf{Z}_\sigma^{\partial S, \partial S} + \sigma \mathbf{Z}_0^{\partial S, V} \cdot \mathbf{Z}_\sigma^{V, \partial S}) \cdot \mathbf{I} = \mathbf{V}, \quad (6.30)$$

where \mathbf{V} is the vector of unknown branch voltages (6.9).

As opposed to the 2-D problem described in [21], the 3-D current flow modeling via SVS-EFIE (6.8) requires continuity of current to be enforced so that the unknown branch voltages \mathbf{V} in the right-hand side of the SVS-EFIE (6.8) as well as the unknown coefficients \mathbf{I} of the auxiliary surface current density expansion (6.16) can be computed.

6.3.5 Nodal Analysis

Continuity of current $\nabla \cdot \mathbf{j} = 0$ can be written in matrix form as [28]

$$\mathbf{A}^V \mathbf{j} = \mathbf{I}_s, \quad (6.31)$$

where \mathbf{j} is an $N \times 1$ vector of volumetric current densities, \mathbf{I}_s is an $\mathbb{N}_s \times 1$ vector of current sources, and \mathbf{A}^V is an $\mathbb{N}_s \times N$ volumetric incidence matrix. The matrix elements in \mathbf{A}^V are defined as follows:

$$A_{b,n}^V = \begin{cases} -1 & \text{if current } j_n \text{ leaves node } b \\ 1 & \text{if current } j_n \text{ enters node } b \\ 0 & \text{otherwise,} \end{cases} \quad (6.32)$$

where $b = 1, \dots, \mathbb{N}_s$ is the index of the conductor segments, and $n = 1, \dots, N$ are the indexes of the volume elements in the discretization of the conductor. For the two-segment interconnect example depicted in Fig. 6.1, the volumetric incidence matrix \mathbf{A}^V is defined as

$$\mathbf{A}^V = \left[\begin{array}{c|c} 1 \times N_1 & 1 \times N_2 \\ \hline -\mathbf{1} & \mathbf{0} \\ \hline \mathbf{1} & -\mathbf{1} \end{array} \right], \quad (6.33)$$

where N_1 and N_2 are the number of filaments discretizing the volumes of the first and second segment, so that $N_1 + N_2 = N$.

The volumetric current density \mathbf{j} is not explicitly present in the SVS-EFIE (6.8), so by using the contour-to-volume operator (6.11), we can obtain \mathbf{j} in terms of the auxiliary surface current density \mathbf{J} at any point inside the conductor. Since the matrix form $\mathbf{Z}_\sigma^{V,\partial S}$ (6.24) of the MoM discretized operator $\mathcal{T}_\sigma^{V,\partial S}$ (6.11) is already calculated at the matrix (6.30) filling stage, the current continuity is enforced as

$$\bar{\mathbf{A}}^V \mathbf{Z}_\sigma^{V,\partial S} \mathbf{J} = \mathbf{I}_s, \quad (6.34)$$

where $\bar{\mathbf{A}}^V$ is the incidence matrix \mathbf{A}^V , where each element $A_{b,n}^V$ is multiplied by the corresponding prism base area A_n .

The vector of the branch voltages \mathbf{V} can be also represented via surface incidence matrix $\mathbf{A}^{\partial S}$, the vector of the unknown potentials at the conductor segment terminals Φ of the size $N_s \times 1$, as follows:

$$\mathbf{A}^{\partial S T} \Phi = \mathbf{V}. \quad (6.35)$$

In (6.35), $\mathbf{A}^{\partial S}$ is an $N_s \times M$ matrix defined as

$$A_{b,m}^{\partial S} = \begin{cases} -1 & \text{if surface current density } J_m \text{ leaves node } b \\ 1 & \text{if surface current density } J_m \text{ enters node } b \\ 0 & \text{otherwise,} \end{cases} \quad (6.36)$$

where $b = 1, \dots, N_s$ is the index of the conductor segments, and $m = 1, \dots, M$ are the indexes of the contour elements in the discretization of the conductor. For the two-segment interconnect example depicted in Fig. 6.1, the volumetric incidence ma-

trix $\mathbf{A}^{\partial S}$ is defines as

$$\mathbf{A}^{\partial S} = \left[\begin{array}{c|c} 1 \times M_1 & 1 \times M_2 \\ \hline -\mathbf{1} & \mathbf{0} \\ \mathbf{1} & -\mathbf{1} \end{array} \right], \quad (6.37)$$

where M_1 and M_2 are the number of linear elements discretizing the contours bounding the cross-section of the first and second segment, so that $M_1 + M_2 = M$.

Combined together, (6.30), (6.34), and (6.35) reduce the integral equation (6.8) to the set of $M + N_s$ linear algebraic equations (SLAE)

$$\begin{bmatrix} \left(\mathbf{Z}_{\sigma}^{\partial S, \partial S} + \sigma \mathbf{Z}_0^{\partial S, V} \cdot \mathbf{Z}_{\sigma}^{V, \partial S} \right) & -\mathbf{A}^{\partial S T} \\ \bar{\mathbf{A}}^V \cdot \mathbf{Z}_{\sigma}^{V, \partial S} & \mathbf{0} \end{bmatrix} \cdot \begin{bmatrix} \mathbf{J} \\ \Phi \end{bmatrix} = \begin{bmatrix} \mathbf{0} \\ \mathbf{I}_s \end{bmatrix}. \quad (6.38)$$

The SLAE (6.38) can be solved numerically either directly via LU-decomposition [26] or iteratively [29], [30] to determine both the unknown auxiliary surface current density \mathbf{J} and the potential values Φ at the end points of the conductor segments. The required Z-parameter matrix can be obtained without additional efforts from the part of the solution for (6.38) corresponding to the calculated potential values Φ and the known values of impressed currents. For the two-segment interconnect example depicted in Fig. 6.1, Z_{11} can be determined as follows:

$$\Phi = \begin{bmatrix} \Phi_1 \\ \Phi_2 \end{bmatrix}, \mathbf{I}_s = \begin{bmatrix} -1 \\ 0 \end{bmatrix}, Z_{11} = \frac{\Phi_1}{-I_{s1}}. \quad (6.39)$$

6.4 Numerical Results

The validation of the numerical implementation of (6.38) is conducted via comparison to the results obtained using FastHenry network parameter extractor [28] and the MoM solution of the traditional V-EFIE (6.1). In the numerical experiments, we consider a twelve-conductor interconnect package depicted in Fig. 6.2. Each of the twelve conductors consists of three piece-wise straight segments made of copper ($\sigma = 5.8 \cdot 10^7 \text{ S/m}$). The cross-section of each segment in the package is a $20 \mu\text{m}$ side square. The package has two planes of symmetry, so only geometric locations of the points corresponding to the first four conductors A–D are given in Fig. 6.2.

At first, the dependence of the resistance R and inductance L values on frequency are obtained via MoM solution (6.38) of the proposed SVS-EFIE (6.8) under the two-samples per skin-depth $\delta(f, \sigma)$ (6.5) discretization of the conductor boundary ∂S and the conductor volume V . The extracted values of resistance R_A and self-inductance L_{AA} for the conductor A, and mutual inductance L_{AB} between conductors A and B — are depicted in Fig. 6.3 for the frequency sweep from 10 MHz to 10 GHz.

Next, to demonstrate the error behavior of the proposed SVS-EFIE (6.8) solution upon the h -refinement, the resistance and inductance of the same interconnect package are obtained via MoM discretization (6.38) of the proposed SVS-EFIE (6.8) featuring from 1.0 to 5.0 samples per skin-depth (6.5). The values of the relative error with respect to the FastHenry reference solution [28] are shown in Fig. 6.4. The behavior of the relative error numerically corroborates the rigorous nature of the proposed SVS-EFIE in 3-D, as the error is being consistently reduced with increasing discretization density.

The volumetric current density \mathbf{j} inside the conductors forming the interconnect is obtained by substitution of the solution \mathbf{J} of (6.38) into the single-layer ansatz operator (6.6). For this numerical experiment, the right-hand side of (6.38) is constructed in such a way, that the conductor A is current-driven, while other eleven conductors in the package are left open-ended. The frequency is fixed at 1 GHz, and the MoM discretization of the SVS-EFIE (6.8) is performed by using two samples per skin-depth (6.5). Fig. 6.2a depicts the distribution of the volumetric current density \mathbf{j} inside the so-called “aggressor-conductor” A, and Fig. 6.2b — inside the “victim-conductor” B. The relative error in the volumetric current density $|\mathbf{j}|$ does not exceed 17% for the conductor A and is shown to be less than 3% in the vicinity of the conductor boundary, where the major part of the current flows at 1 GHz.

The last study compares the computational time and memory consumption required to obtain the Z-parameter matrix using the MoM solution of the traditional V-EFIE (6.1) and the proposed SVS-EFIE (6.8). The resistance and inductance are extracted for the twelve-conductor interconnect package depicted in Fig. 6.2 under the 2 samples per skin-depth (6.5) MoM discretization for 0.5 GHz, 1.0 GHz, and 1.5 GHz frequencies. The MoM solution of the aforementioned integral equations is implemented in C++, and the SLAE’s arising from the MoM discretization of (6.1) and (6.8) are solved directly via LU-decomposition [26]. The results obtained on a single-core Intel Core i7 processor running at 2.7 GHz are shown in Table 6.1. The behavior of the execution time and memory consumption data confirm that the proposed SVS-EFIE (6.38) is faster than the traditional V-EFIE (6.1) at both the matrix fill-time and the solution of the SLAE.

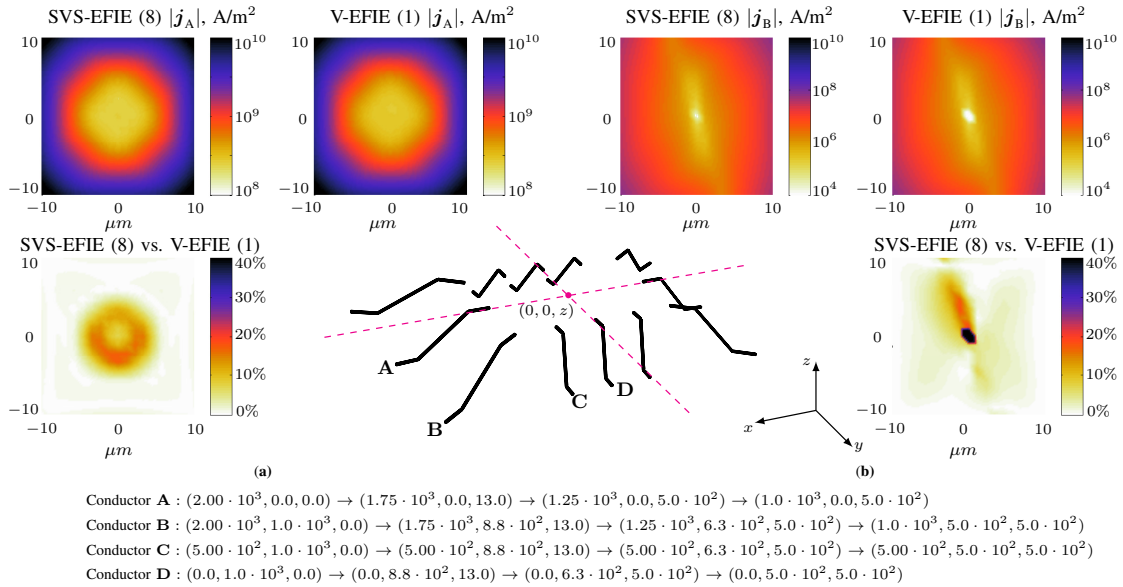


Figure 6.2: Distribution of the volumetric current density j inside the conductors constituting the depicted twelve-conductor package. Conductor A is driven by 1A current source at 1 GHz frequency, other conductors are left floating. The package has two planes of symmetry shown with dashed lines. Geometric locations of the terminal points at the axes of the conductor segments are given for four conductors A – D in μm .

- (a) Volumetric current density j inside the cross-section of the “aggressor-conductor” A obtained via the MoM solution (6.38) of the proposed SVS-EFIE (6.8) and traditional V-EFIE (6.1), and their relative error.
- (b) Volumetric current density j inside the cross-section of the “victim-conductor” B obtained via the MoM solution (6.38) of the proposed SVS-EFIE (6.8) and traditional V-EFIE (6.1), and their relative error. © 2014 IEEE.

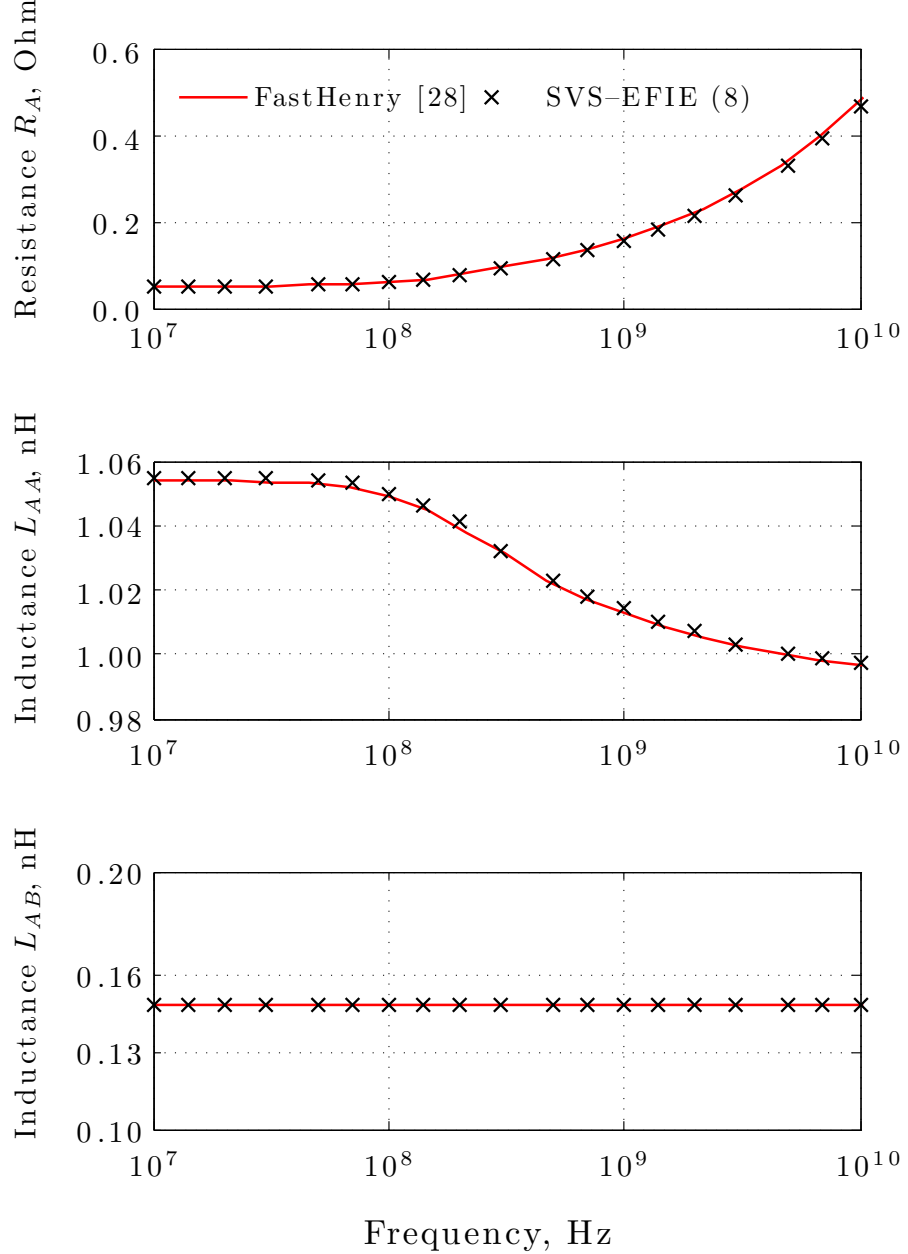


Figure 6.3: Resistance R_A , self-inductance L_{AA} , and mutual inductance L_{AB} of conductors A and B in the twelve-conductor package depicted in Fig. 6.2. The results are first obtained under the two samples per skin-depth MoM discretization of the SVS-EFIE (6.8) and compared against the FastHenry reference solution [28]. The relative error does not exceed 4% for resistance and 0.2% for inductance at frequencies from 10 MHz to 10 GHz. © 2014 IEEE.

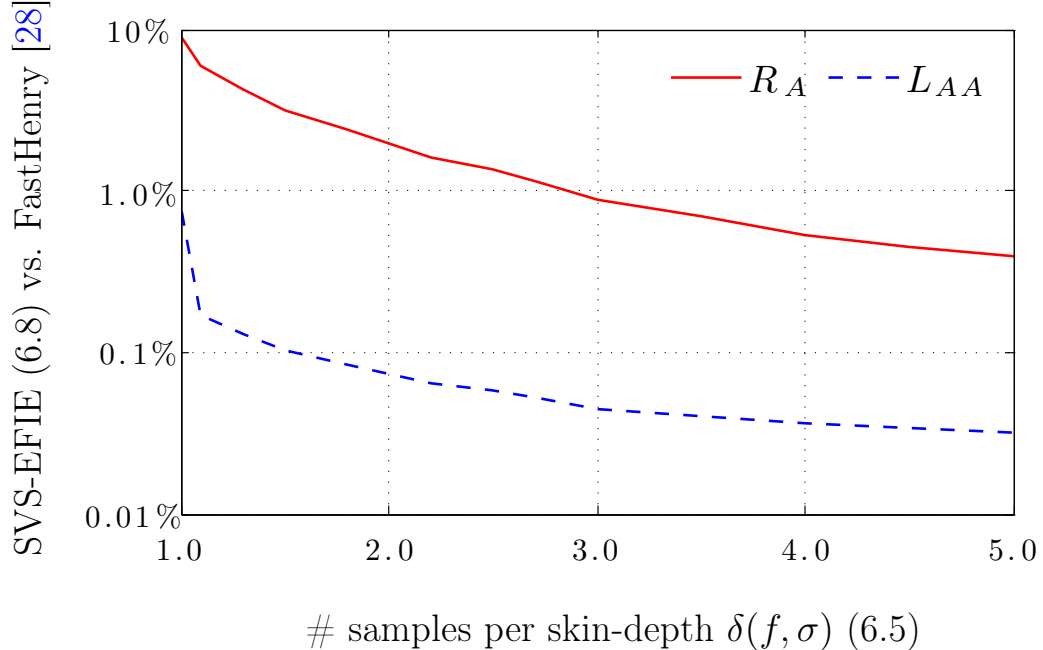


Figure 6.4: Relative error of the MoM solution (6.38) of the novel SVS-EFIE (6.8) with respect to the FastHenry reference solution [28] for resistance R_A and self-inductance L_{AA} in the twelve-conductor package depicted in Fig. 6.2 as a function of mesh refinement – number of samples per skin-depth (6.5) at 1 GHz. © 2014 IEEE.

Table 6.1: Computational Time and Memory for the Solution of the V-EFIE and SVS-EFIE for the twelve-conductor package. © 2014 IEEE.

	V-EFIE (6.1)	SVS-EFIE (6.8)
$f = 0.5 \text{ GHz}$, $M = 720$ linear elements, $N = 2,916$ filaments		
Total Time	312 s	175 s
Fill Time	258 s	173 s
SLAE Solve Time	54 s	2 s
Memory	1.7 Gb	0.44 Gb
$f = 1.0 \text{ GHz}$, $M = 2,880$ linear elements, $N = 12,996$ filaments		
Total Time	1,742 s	550 s
Fill Time	1,219 s	544 s
SLAE Solve Time	523 s	6 s
Memory	7.7 Gb	1.2 Gb
$f = 1.5 \text{ GHz}$, $M = 3,456$ linear elements, $N = 19,044$ filaments		
Total Time	4,128 s	999 s
Fill Time	2,515 s	989 s
SLAE Solve Time	1,613 s	11 s
Memory	12.8 Gb	1.97 Gb

6.5 Conclusion

The paper presented a new rigorous single-source surface-volume-surface integral equation for resistance and inductance extraction in 3-D interconnects of an arbitrary cross-section. The new equation is derived from the classical volume electric field integral equation via representation of the electric field inside the conductor volume as a superposition of the cylindrical waves emanating from its boundary. Being derivative free, the novel equation features only a single unknown on the conductor boundary and is shown to produce an error-controllable solution with a significant reduction of the computational time in comparison to the Method of Moments solution of the traditional volume electric field integral equation.

Bibliography

- [1] L. M. Wedepohl, D. J. Wilcox, “Transient analysis of underground power-transmission systems. System-model and wave-propagation characteristics,” *Proceedings of the Institution of Electrical Engineers*, Vol. 120, No. 2, pp. 253–260, Feb 1973.
- [2] S. Bonyadi-ram, B. Kordi, G. E. Bridges, “Buried cable parameter extraction using a full-space unbounded conformal mapping technique,” *13th International Symposium on Antenna Technology and Applied Electromagnetics and the Canadian Radio Science Meeting (ANTEM/URSI)*, pp. 1–4, Feb. 2009.
- [3] B. Young, *Digital Signal Integrity*, New York: McGraw-Hill, 2001.
- [4] D. M. Pozar, *Microwave Engineering*, 2nd Ed., New York: Wiley, 1997.
- [5] R. Achar, M. S. Nakhla, “Simulation of High-Speed Interconnects,” *Proc. IEEE*, Vol. 89, No. 5, pp. 693–728, May 2001.
- [6] K. G. Nickols, T. J. Kazmierski, M. Zwolinski, A. D. Brown, “Overview of SPICE-like circuit simulation algorithms,” *Circuits, Devices and Systems, IEE Proc.*, Vol. 141, No. 4, pp. 242–250, Aug 1994.

- [7] Manitoba HVDC Research Centre, *PSCAD/EMTDC Power System Simulation Software Users' Guide*, Version 4.2.1, Winnipeg, Manitoba, Canada, 2010.
- [8] B. M. Notaros, *Electromagnetics*, Pearson Prentice Hall, 2010.
- [9] W. C. Chew, J.-M. Jin, E. Michielssen, and J. Song, (ed.) *Fast and Efficient Algorithms in Computational Electromagnetics*, Norwood: Artech House, 2001.
- [10] J.-M. Jin, *The Finite Element Method in Electromagnetics*, 2nd Ed., New York: Wiley, 2002.
- [11] A. Peterson, S. Ray, and R. Mittra, *Computational Methods for Electromagnetics*, IEEE Press, 1998.
- [12] C. Müller, *Foundations of the Mathematical Theory of Electromagnetic Waves*, Berlin, Heidelberg, New York: Springer-Verlag, 1969.
- [13] J. R. Mautz, R. F. Harrington, “H-field, E-field, and Combined-field solutions for conducting bodies of revolution,” *AEÜ*, Vol. 32, No. 4, pp. 157–164, 1978.
- [14] R. E. Kleinman, P. A. Martin, “On the single integral equation for the transmission problem of acoustics,” *SIAM J. Appl. Math.*, Vol. 48(2), pp. 307–325, 1988.
- [15] Z. G. Qian, W. C. Chew, and R. Suaya, “Generalized impedance boundary condition for conductor modeling in surface integral equation,” *IEEE Trans. Microw. Theory Techn.*, Vol. 55, No. 11, pp. 2354–2364, Nov. 2007.

- [16] David Swatek, "Investigation of Single Source Surface Integral Equation for Electromagnetic Wave Scattering by Dielectric Bodies," *Ph.D. Thesis, Univ. of Manitoba, 1999.*
- [17] D. R. Swatek, I. R. Ceric, "A recursive single source integral equation analysis for wave scattering by heterogeneous dielectric bodies," *IEEE Trans. Antennas Propag.*, Vol. 48, No. 8, pp. 1175–1185, Aug. 2000.
- [18] M. S. Yeung, "Single integral equation for electromagnetic scattering by three-dimensional homogeneous dielectric objects," *IEEE Trans. Antennas Propag.*, Vol. 47, No. 10, pp. 1615–1622, Oct. 1999.
- [19] W. C. Chew, *Waves and Field in Inhomogeneous Media*, IEEE Press, 1995.
- [20] A. C. Cangellaris, J. L. Prince, and L. P. Vakanas, "Frequency-dependent inductance and resistance calculation for three-dimensional structures in high-speed interconnect systems," *IEEE Trans. Compon. Packag. Manuf. Technol.*, Vol. 13, No. 1, pp. 154–159, 1990.
- [21] A. Menshov and V. Okhmatovski, "Method of moment solution of Surface-Volume-Surface Electric Field Integral Equation for two-dimensional transmission lines of complex cross-sections," *IEEE Workshop on Signal and Power Integrity (SPI)*, pp. 31–34, May 2012.
- [22] A. Menshov and V. Okhmatovski, "New Single-Source Surface Integral Equations for Scattering on Penetrable Cylinders and Current Flow Modeling in 2-D Conductors," *IEEE Trans. Microw. Theory Techn.*, Vol. 61, No. 1, pp. 341-350, Jan. 2013.

- [23] M. Abramovitz and I. Stegun, (ed.) *Handbook of Mathematical Functions*, Dover, 1964.
- [24] D. Colton and R. Kress, (ed.) *Integral Equation Methods in Scattering Theory*, Malabar, Florida: Krieger Publishing Company, 1992.
- [25] R. Harrington, *Field Computation by Moment Methods*, IEEE Press, 1993.
- [26] W. H. Press, et. al. *Numerical Recipes: The Art of Scientific Computing*, Cambridge University Press, 2007.
- [27] D. Wilton, A. Glisson, D. Schaubert, O. Al-Bundak, C. Butler, “Potential integrals for uniform and linear source distributions on polygonal and polyhedral domains,” *IEEE Trans. Antennas Propag.*, Vol. 32, No. 3, pp. 276–281, Mar. 1984.
- [28] M. Kamon, M. J. Tsuk, and J. White, “FASTHENRY: A Multipole Accelerated 3-D Inductance Extraction Program,” *IEEE Trans. Microw. Theory Techn.*, Vol. 42, No. 9, pp. 1750–1758, 1994.
- [29] V. Fraysse, L. Giraud, and S. Gratton, “A set of GMRES routines for real and complex arithmetics,” *CERFACS Tech. Rep. TR/PA/97/49*, www.cerfacs.fr
- [30] C. H. Smith, A. F. Peterson, and R. Mitra, “The biconjugate gradient method for electromagnetic scattering,” *IEEE Trans. Antennas Propag.*, Vol. 38, No. 6, pp. 938–940, June 1990.

Chapter 7

Application of the Novel Surface-Volume-Surface EFIE to Power Cables Parameter Extraction

As the result of the research collaboration with Manitoba Hydro, a significant part of this M.Sc. project (Chapters 3, 4) is devoted to the current flow modeling and parameter extraction for 2-D power cables. Within the scope of the research, numerical implementation of the Method of Moments solution of the proposed SVS-EFIE was done using C++ programming language. Such implementation allows for OpenMP [Ope11] shared-memory parallelization and takes advantage of highly optimised Intel Math Kernel Library (MKL) [Int13] for matrix operations. The Method of Moments discretization is performed using the frequency adaptive mesh obtained via open-source finite element mesh generator GMSH [GR09].

To demonstrate the proper parameter extraction for cables of different cross-sections, we present several numerical results and benchmarks of the C++ implementation of the novel SVS-EFIE formulation. The simulations were performed on a computer with an four-core Intel Core i7 processor running at 2.7 GHz and having 16 GB of DDR3 1600 MHz operating memory. The solutions were generated using the five-triangles per skin-depth frequency adaptive mesh with the aid of both OpenMP shared-memory parallelization and the help of Intel MKL.

In the first numerical example, we consider a co-axial cable of a circular cross-section depicted in Fig. 7.1. The inner conductor (2) is made of copper ($\sigma = 5.96 \cdot 10^7$ S/m) and has the radius of 0.022 m. The cable sheath (1) is made of lead ($\sigma = 4.55 \cdot 10^6$ S/m) and has the inner and outer radii of 0.0395 m and 0.044 m, respectively. At 60 Hz frequency, the contour mesh consists of 172 linear elements and the volumetric mesh — 1,636 triangles. The obtained matrix fill time was 76 ms, and the solution of the set of linear algebraic equations required about 1 ms. The per-unit-length resistance R and inductance L of the co-axial cable were extracted using the differential line pair formulas [Pau07], as follows

$$R = R_{1,1} + R_{2,2}, \quad (7.1)$$

$$L = L_{1,1} - 2L_{1,2} + L_{2,2}, \quad (7.2)$$

where $R_{1,1}$ is the resistance of the lead sheath, $R_{2,2}$ is the resistance of the copper inner conductor, $L_{1,1}$ is the self-inductance of the sheath, $L_{2,2}$ is the self-inductance of the inner conductor, and $L_{1,2}$ is the mutual inductance between the sheath and inner conductor.

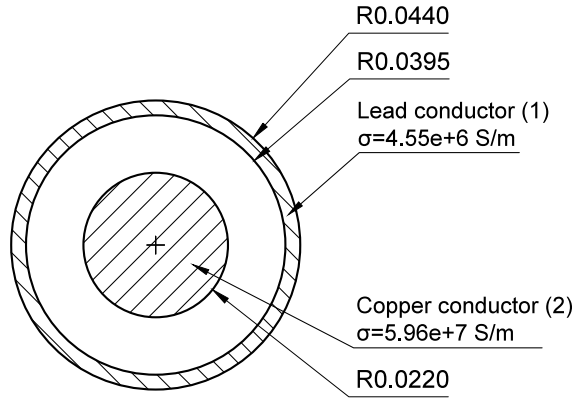


Figure 7.1: Circular co-axial cable with lead sheath (1) and copper inner conductor (2).

The values of the per-unit-length resistance R and inductance L for 60 Hz were initially extracted via SVS-EFIE and further compared to those from PSCAD [Man10] as shown in Table 7.1. For the frequency sweep from 10 mHz to 10 kHz the comparison of the R and L values obtained via PSCAD and SVS-EFIE is depicted in Fig. 7.2 and Fig. 7.3, respectively. The maximum relative error with respect to PSCAD does not exceed 3% in resistance and 1% in inductance for all frequencies of the analysis.

The computational time for the extraction of resistance and inductance grows with the number of elements in both contour and volume meshes. The increase in the mesh density is dictated by skin-effect, so the behaviour of the current density inside the conductor cross-section is properly captured. The parameter extraction for 26 frequencies (logarithmic distribution) between 10 mHz and 100 Hz required less than 1 s, while the extraction for 32 frequencies between 10 mHz and 1 kHz — about 5 s, and the extraction for 38 frequencies between 10 mHz and 10 kHz — about 74 s.

Table 7.1: Extracted resistance (7.1) and inductance (7.2) of the circular co-axial cable depicted in Fig. 7.1 at 60 Hz.

	SVS-EFIE Solver	PSCAD	Relative error w.r.t. PSCAD
Resistance, R (p. u. l.)	0.2043 mΩ/m	0.2035 mΩ/m	0.39%
Inductance, L (p. u. l.)	0.1621 μH/m	0.1627 μH/m	0.36%

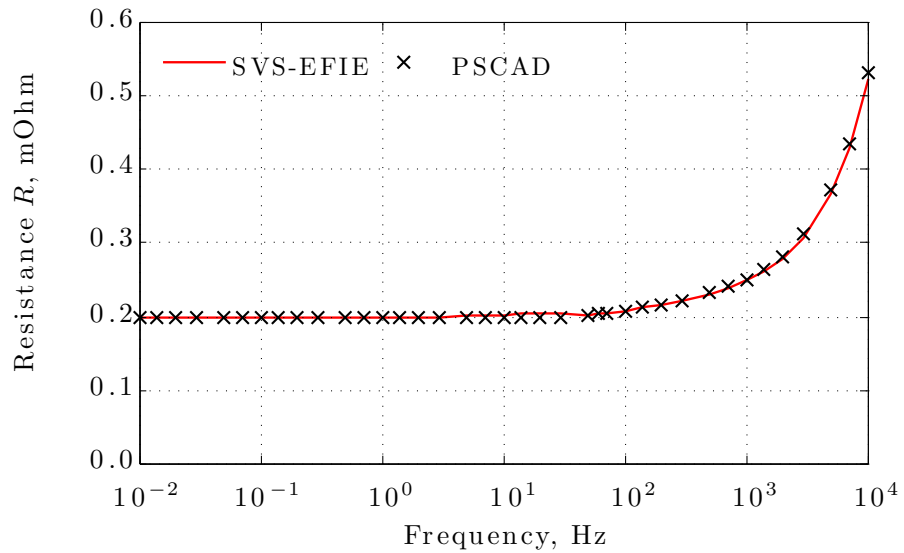


Figure 7.2: Extracted resistance (7.1) of the circular co-axial cable depicted in Fig. 7.1 for the frequency sweep from 10 mHz to 10 kHz.

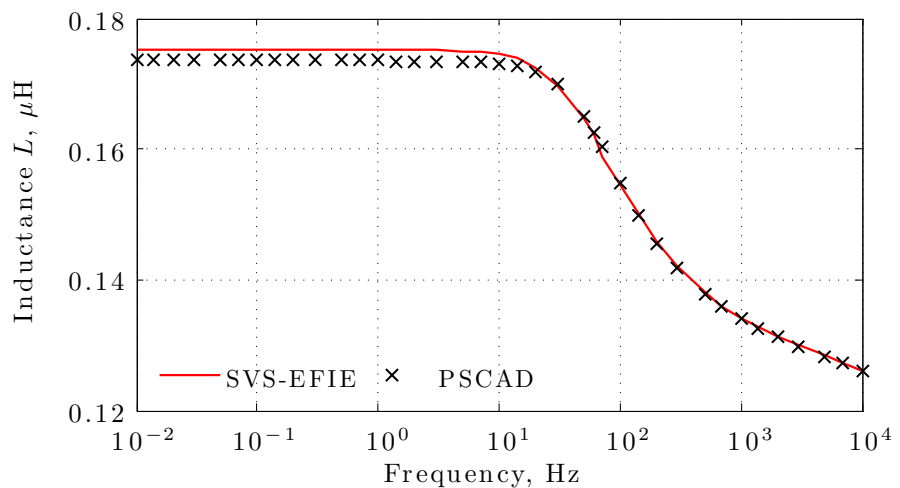


Figure 7.3: Extracted inductance (7.2) of the circular co-axial cable depicted in Fig. 7.1 for the frequency sweep from 10 mHz to 10 kHz.

In the next numerical example, we consider a co-axial cable of a square cross-section (depicted in Fig. 7.4). The per-unit-length resistance R and inductance L of the co-axial cable are extracted using the differential line pair formulas [Pau07] similar to those of the circular co-axial cable. The comparison of the extracted values of R and L to those obtained via V-EFIE (2.20) for the frequency sweep from 10 mHz to 10 kHz is depicted in Fig. 7.5 and Fig. 7.6, respectively. The maximum relative error with respect to the V-EFIE (2.20) does not exceed 3% in resistance and 1% in inductance for all frequencies of the analysis. The comparison is performed with respect to the V-EFIE, since the current versions of PSCAD cannot handle such cable cross-sections.

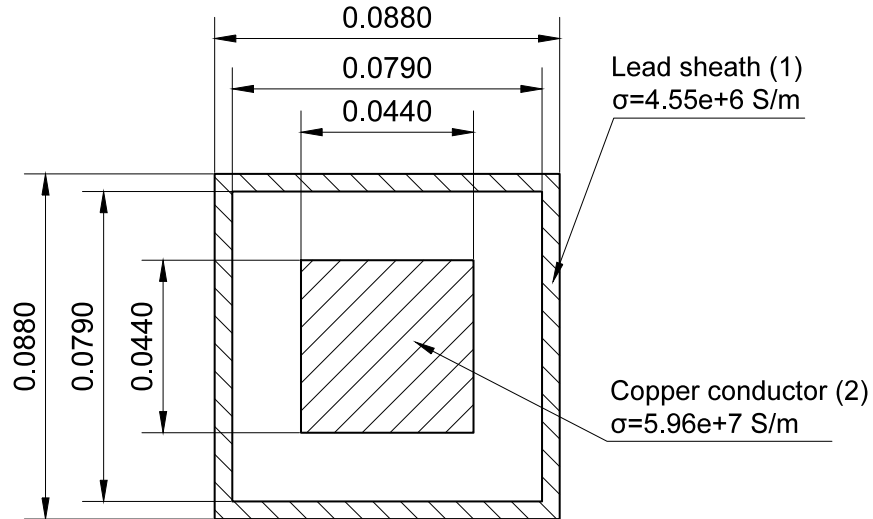


Figure 7.4: Square co-axial cable with lead sheath (1) and copper inner conductor (2).

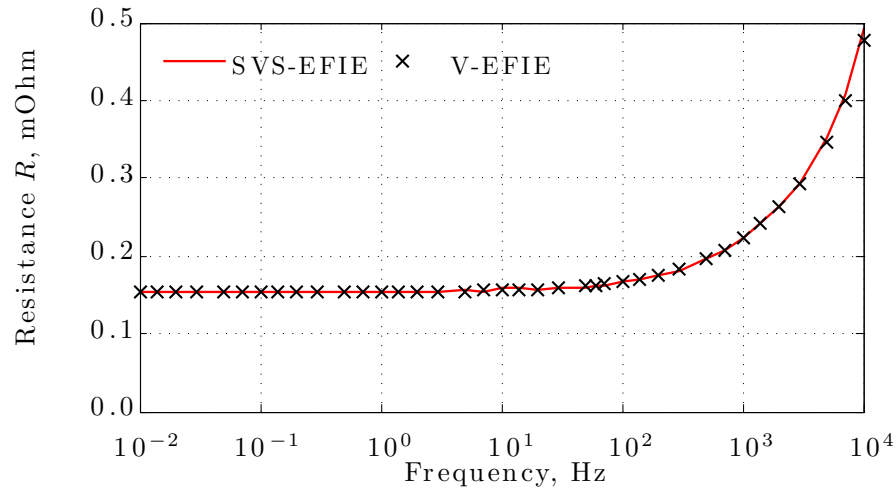


Figure 7.5: Extracted resistance (7.1) of the square co-axial cable depicted in Fig. 7.4 for the frequency sweep from 10 mHz to 10 kHz.

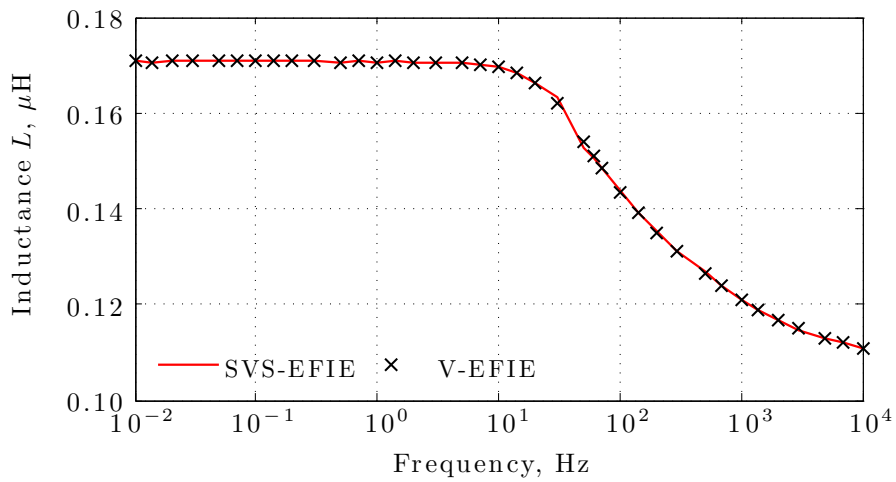


Figure 7.6: Extracted inductance (7.2) of the square co-axial cable depicted in Fig. 7.4 for the frequency sweep from 10 mHz to 10 kHz.

In the last two studies, we examine the extracted parameters for the complicated three-conductor co-axial cables depicted in Fig. 7.7 and Fig. 7.8. The values of the per-unit-length resistance and inductance at 60 Hz were initially obtained via SVS-EFIE and further compared to those from the V-EFIE (2.20) as shown in Table 7.2 and Table 7.3, respectively. Again, these cables cannot be simulated using current versions of PSCAD.

For the three-conductor round co-axial cable (Fig. 7.7), the parameter extraction for 26 frequencies (logarithmic distribution) between 10 mHz and 100 Hz required less than 4 s, the extraction for 32 frequencies between 10 mHz and 1 kHz — about 6 s, and the extraction for 38 frequencies between 10 mHz and 10 kHz — about 26 s. The maximum relative error with respect to V-EFIE (2.20) does not exceed 2.5% in resistance and 0.5% in inductance for all frequencies of the analysis.

For the three-conductor sectorial co-axial cable (Fig. 7.8), the parameter extraction for 26 frequencies (logarithmic distribution) between 10 mHz and 100 Hz required about 1 s, the extraction for 32 frequencies between 10 mHz and 1 kHz — about 3 s, and the extraction for 38 frequencies between 10 mHz and 10 kHz — about 31 s. The maximum relative error with respect to V-EFIE (2.20) does not exceed 5% in resistance and 0.1% in inductance for all frequencies of the analysis.

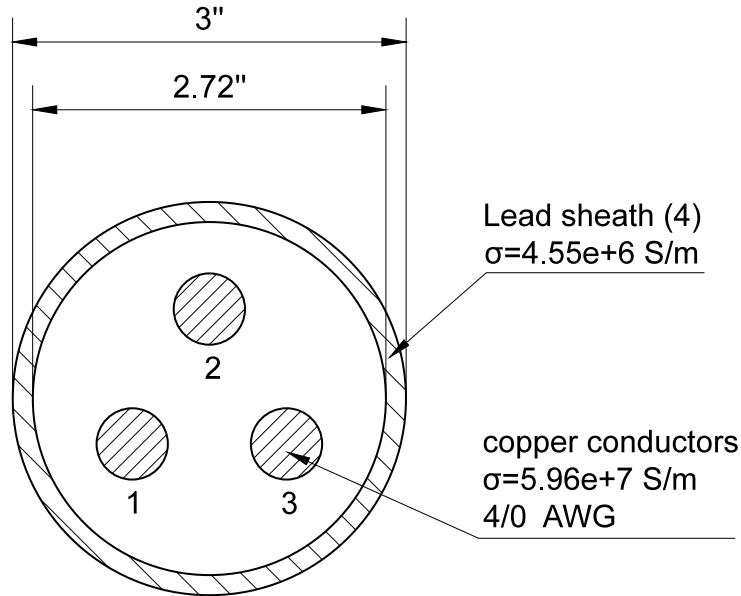


Figure 7.7: Three-conductor round co-axial cable with lead sheath and copper inner conductors (Pirelli 35 KV 3 conductor round paper insulated cable 4/0 American Wire Gauge (AWG)).

Table 7.2: Extracted resistance and inductance of the three-conductor round co-axial cable depicted in Fig. 7.7 at 60 Hz.

	SVS-EFIE Solver	V-EFIE	Relative error w.r.t. V-EFIE
Resistance, $R_{1,1}$ (p. u. l.)	0.1611 mΩ/m	0.1699 mΩ/m	0.07%
Resistance, $R_{4,4}$ (p. u. l.)	0.2681 mΩ/m	0.2714 mΩ/m	1.21%
Inductance, $L_{1,1}$ (p. u. l.)	1.0782 μH/m	1.0778 μH/m	0.04%
Inductance, $L_{1,2}$ (p. u. l.)	0.7071 μH/m	0.7071 μH/m	0.01%
Inductance, $L_{1,4}$ (p. u. l.)	0.6635 μH/m	0.6634 μH/m	0.01%

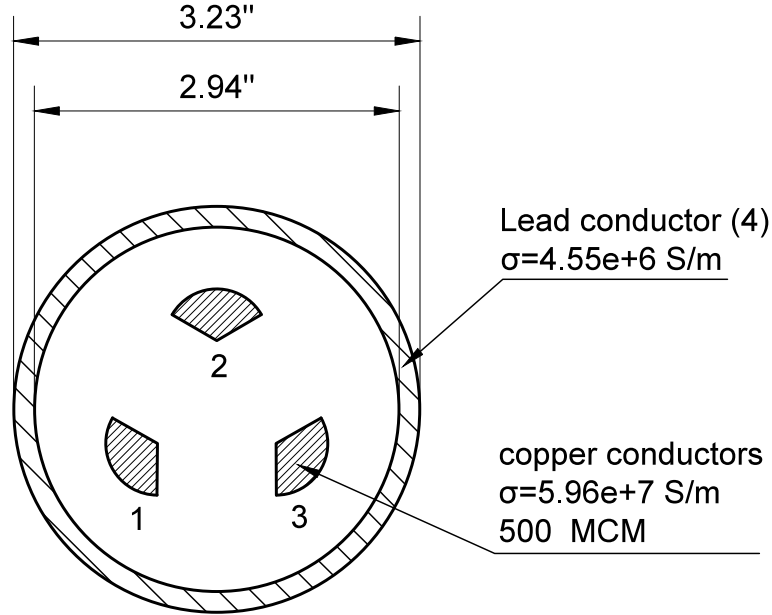


Figure 7.8: Three-conductor sectorial co-axial cable with lead sheath and copper inner conductors (Pirelli 35 KV 3 conductor sectorial paper insulated cable 500 MCM).

Table 7.3: Extracted resistance and inductance of the three-conductor sectorial co-axial cable depicted in Fig. 7.8 at 60 Hz.

	SVS-EFIE Solver	V-EFIE	Relative error w.r.t. V-EFIE
Resistance, $R_{1,1}$ (p. u. l.)	0.1379 mΩ/m	0.1370 mΩ/m	0.65%
Resistance, $R_{4,4}$ (p. u. l.)	0.2427 mΩ/m	0.4240 mΩ/m	0.13%
Inductance, $L_{1,1}$ (p. u. l.)	1.0521 μH/m	1.0521 μH/m	0.01%
Inductance, $L_{1,2}$ (p. u. l.)	0.7141 μH/m	0.7141 μH/m	0.01%
Inductance, $L_{1,4}$ (p. u. l.)	0.6482 μH/m	0.6482 μH/m	0.01%

Chapter 8

Conclusions and Future Work

8.1 Conclusions

In this thesis, a new rigorous single-source surface-volume-surface integral equation has been derived for full-wave scattering on 2-D homogeneous penetrable cylinders and current flow modeling in 2-D and 3-D conductors of an arbitrary cross-section. The novel integral equation is derived from the classical volume electric field integral equation via representation of the electric field at any point inside the homogeneous subregion as a superposition of the elementary cylindrical waves emanating from its boundary. Being derivative free, the novel formulation features only a single unknown on the conductor boundary and involves only a few simple integral operators. These advantages come at the cost of having more complicated field translation integral operators: surface-to-surface, volume-to-surface, and surface-to-volume. We provide a detailed derivation of the matrices in the Method of Moment discretization of the novel surface-volume-surface integral equation for 2-D and 3-D magneto-quasi-statics and 2-D transverse magnetic polarised wave scattering.

Several numerical examples ranging from isolated single-conductor lines and 2-D power cables of an arbitrary cross-section to 3-D interconnects have been used to demonstrate the accuracy of the method and its computational benefits vs. the traditional solution based on the volume integral equation for current flow modeling and inductance extraction [Che95, KTW94]. The solution of the full-wave surface-volume-surface integral equation is compared against that of the traditional surface and volume integral equations [PRM98, Ric65].

The surface-volume-surface integral equation is shown to produce an error-controllable solution with a significant reduction in computational time as opposed to the Method of Moments solution of the volume electric field integral equation. Specifically, the proposed formulation can extend the capabilities of PSCAD/EMTDC [Man10] software to handle cable cross-sections of an arbitrary shape, which further allows to increase the accuracy of transient simulations of power delivery systems.

8.2 Future Work

- To take the advantage of the matrix sparsity in Method of Moments solution of the surface-volume-surface integral equation for magneto-quasi-statics.

(The author of the thesis plans to submit the journal paper on that topic in early 2014)

- To extend the proposed 2-D full-wave formulation of the surface-volume-surface integral equation for the scattering under transverse electric polarization.
- To investigate and implement the acceleration of matrix-vector and matrix-matrix multiplies in the Method of Moment solution of the novel surface-volume-surface integral equation using fast Fourier transform [CTB95], fast multipole method [GR87], and matrix decomposition [Bor09, MB96] methods.
- To implement the Method of Moments solution of the surface-volume-surface integral equation in the presence of a layered medium. As the proposed integral equation formulation is derivative free, it can be particularly suitable for the analysis in multilayered media.
- To derive the surface-volume-surface formulation for the solution of 3-D full-wave scattering problems.

Bibliography

- [AS64] M. Abramovitz and I. Stegun, (ed.) *Handbook of Mathematical Functions*, Dover, 1964.
- [AN01] R. Achar, M. S. Nakhla, “Simulation of High-Speed Interconnects,” *Proc. IEEE*, Vol. 89, No. 5, pp. 693–728, May 2001.
- [BKB09] S. Bonyadi-ram, B. Kordi, G. E. Bridges, “Buried cable parameter extraction using a full-space unbounded conformal mapping technique,” *13th International Symposium on Antenna Technology and Applied Electromagnetics and the Canadian Radio Science Meeting (ANTEM/URSI)*, pp. 1–4, Feb. 2009.
- [Bor09] S. Börm, “ \mathcal{H}^2 -matrices — multilevel methods for the approximation of integral operators,” *Comput. Visual. Sci.*, Vol. 7, pp. 173–181, 2004.
- [Cad09] Serdar Cadirci, “RF Stealth and Counter-RF Stealth Technologies,” *M.Sc. Thesis, Naval Postgraduate School, 2009*.
- [Che95] W. C. Chew, *Waves and Field in Inhomogeneous Media*, IEEE Press, 1995.
- [CJMS01] W. C. Chew, J.-M. Jin, E. Michielssen, and J. Song, (ed.) *Fast and Efficient Algorithms in Computational Electromagnetics*, Norwood: Artech House, 2001.
- [CK92] D. Colton and R. Kress, (ed.) *Integral Equation Methods in Scattering Theory*, Malabar, Florida: Krieger Publishing Company, 1992.

- [Col92] R. Collin *Field Theory of Guided Waves*, IEEE Press, 1990.
- [CTB95] M. F. Catedra, R. F. Torres, J. Basterrechea, E. Cago, *The CG-FFT Method: Application of Signal Processing Techniques to Electromagnetics*, Artech House, 1995.
- [Gli84] A. Glisson, “An integral equation for electromagnetic scattering from homogeneous dielectric bodies,” *IEEE Trans. Antennas Propag.*, Vol. 32, No. 2, pp. 173–175, Feb. 1984.
- [GR09] C. Geuzaine and J.-F. Remacle, “Gmsh: a three-dimensional finite element mesh generator with built-in pre- and post-processing facilities,” *Int. J. Num. Meth. in Eng.*, Vol. 79, No. 11, pp. 1309–1331, 2009.
- [GR87] L. Greengard and V. Rokhlin, “The fast algorithm for particle simulations,” *J. Comp. Phys.*, Vol. 73, No. 2, pp. 325–348, Dec. 1987.
- [IMS12] A. Menshov and V. Okhmatovski, “Novel surface integral equation formulation for accurate broadband RL extraction in transmission lines of arbitrary cross-section,” Microwave Symposium Digest (MTT), 2012 IEEE MTT-S International, pp. 1-3, 17–22 June 2012.
- [Int13] Intel Corporation, *Intel Math Kernel Library Reference Manual Version 11.1*, Sep. 2013.
- [Jin02] J. - M. Jin, *The Finite Element Method in Electromagnetics*, 2nd Ed., New York: Wiley, 2002.
- [KM88] R. E. Kleinman, P. A. Martin, “On the single integral equation for the transmission problem of acoustics,” *SIAM J. Appl. Math.*, Vol. 48(2), pp. 307–325, 1988.
- [KS86] A. Kishk and L. Shafai, “Different formulations for numerical solutions of single or multibodies of revolution with mixed boundary conditions,” *IEEE Trans. Antennas Propag.*, Vol. 34, No. 5, pp. 666–673, May 1986.

- [KTW94] M. Kamon, M. J. Tsuk, and J. White, “FASTHENRY: A Multipole Accelerated 3-D Inductance Extraction Program,” *IEEE Trans. Microw. Theory Techn.*, Vol. 42, No. 9, pp. 1750–1758, 1994.
- [Man10] Manitoba HVDC Research Centre, *PSCAD/EMTDC Power System Simulation Software Users’ Guide*, Version 4.2.1, Winnipeg, Manitoba, Canada, 2010.
- [MB96] E. Michielssen, A. Boag, “A multilevel matrix decomposition algorithm for analysing scattering from large structures,” *IEEE Trans. Antennas Propag.*, Vol. 44, No. 8, pp. 1086–1093, Aug. 1996.
- [MH78] J. R. Mautz, R. F. Harrington, “H-field, E-field, and Combined-field solutions for conducting bodies of revolution,” *AEÜ*, Vol. 32, No. 4, pp. 157–164, 1978.
- [ML10] P. Mojabi and J. LoVetri “Comparison of TE and TM inversions in the framework of the Gauss-Newton Method,” *IEEE Trans. Antennas Propag.*, Vol. 58, No. 4, pp. 1336–1348, 2010.
- [MO13] A. Menshov and V. Okhmatovski, “New Single-Source Surface Integral Equations for Scattering on Penetrable Cylinders and Current Flow Modeling in 2-D Conductors,” *IEEE Trans. Microw. Theory Techn.*, Vol. 61, No. 1, pp. 341–350, Jan. 2013.
- [MF53] P. M. Morse, H. Feshbach, *Methods of theoretical physics*, New York: McGraw-Hill, 1953.
- [Mor04] Jason Morsey, “Integral Equation Methodologies for the Signal Integrity Analysis of PCB and Interconnect Structures in Layered Media from DC to Multi-GHz Frequencies,” *Ph.D. Thesis, Univ. of Illinois at U.-C.*, 2004.
- [Mul69] C. Müller, *Foundations of the Mathematical Theory of Electromagnetic Waves*, Berlin, Heidelberg, New York: Springer-Verlag, 1969.

- [Not10] B. M. Notaros, *Electromagnetics*, Pearson Prentice Hall, 2010.
- [Ope11] OpenMP Architecture Review Board, *OpenMP Application Program Interface, Version 3.1*, July 2011, available from <http://www.openmp.org>.
- [Pau07] C. R. Paul, *Analysis of Multiconductor Transmission Lines*, New York: Wiley, 2007.
- [Poz97] D. M. Pozar, *Microwave Engineering*, 2nd Ed., New York: Wiley, 1997.
- [PRM98] A. Peterson, S. Ray, and R. Mittra, *Computational Methods for Electromagnetics*, IEEE Press, 1998.
- [QCS07] Z. G. Qian, W. C. Chew, and R. Suaya, “Generalized impedance boundary condition for conductor modeling in surface integral equation,” *IEEE Trans. Microw. Theory Techn.*, Vol. 55, No. 11, pp. 2354–2364, Nov. 2007.
- [RWD84] S. Ramo, J. R. Whinnery, T. Van Duzer, *Fields and Waves in Communication Electronics*, 2nd Ed., New York, Wiley, 1984.
- [Ric65] J. Richmond, “Scattering by a dielectric cylinder of arbitrary cross section shape,” *IEEE Trans. Antennas Propag.*, Vol. 13, No. 3, pp. 334–341, 1965.
- [SC00] D. R. Swatek, I. R. Ceric “A recursive single source integral equation analysis for wave scattering by heterogeneous dielectric bodies,” *IEEE Trans. Antennas Propag.*, Vol. 48, No. 8, pp. 1175–1185, Aug. 2000.
- [Ser03] Kibilay Sertel, “Multilevel Fast Multipole Method for Modeling Permeable Structures Using Conformal Finite Elements,” *Ph.D. Thesis, University of Michigan, 2003*.
- [SPI12] A. Menshov and V. Okhmatovski, “Method of moment solution of Surface-Volume-Surface Electric Field Integral Equation for two-dimensional transmission lines of complex cross-sections,” Signal and Power Integrity (SPI), 2012 IEEE 16th Workshop on, pp. 31–34, 13–16 May 2012.

- [Str41] J. A. Stratton, *Electromagnetic Theory*, New Yourk: McGraw-Hill, 1941.
- [Swa99] David Swatek, “Investigation of Single Source Surface Integral Equation for Electromagnetic Wave Scattering by Dielectric Bodies,” *Ph.D. Thesis, Univ. of Manitoba, 1999.*
- [VABM08] F. Valdes, F. P. Andriulli, H. Bagci, and E. Michielssen, “On the discretization of single source integral equations for analyzing scattering from homogeneous penetrable objects,” *IEEE Antennas and Propag. Soc. Int. Symp.*, pp. 1–4, July 2008.
- [WW73] L. M. Wedepohl, D. J. Wilcox, “Transient analysis of underground power-transmission systems. System-model and wave-propagation characteristics,” *Proceedings of the Institution of Electrical Engineers*, Vol. 120, No. 2, pp. 253–260, Feb 1973.
- [Yeu99] M. S. Yeung, “Single integral equation for electromagnetic scattering by three-dimensional homogeneous dielectric objects,” *IEEE Trans. Antennas Propag.*, Vol. 47, No. 10, pp. 1615–1622, Oct. 1999.
- [You01] B. Young, *Digital Signal Integrity*, New York: McGraw-Hill, 2001.